ABSTRACT

Title of dissertation: UNSTEADY AERODYNAMIC MODELING WITH TIME-VARYING FREE-STREAM MACH NUMBERS

Arun Isaac Jose, Master of Science, 2005

Dissertation directed by: Professor J. Gordon Leishman
Department of Aerospace Engineering

The development of a reduced-order unsteady airfoil theory is described for application to non-steady, subsonic compressible flows with variable free-stream Mach number. The airfoil theory, which is suitable for application to most types of comprehensive helicopter rotor analyses, is developed for arbitrary, time-dependent combined variations in angle of attack and Mach number. The approach is validated using CFD solutions based on the Euler equations. The new model is developed using the indicial theory as a basis, and shows excellent agreement with direct CFD solutions for a wide range of practical flows. For supercritical flows, nonlinearities associated with the formation and movement of shock waves are observed in the CFD solutions, which the unsteady airfoil theory proves inadequate. Overall, this study shows that the reduced-order unsteady aerodynamic theory provides significant improvements in sectional airloads predictions over existing methods that might be used in various types of comprehensive helicopter rotor analyses.

UNSTEADY AERODYNAMIC MODELING WITH TIME-VARYING FREE-STREAM MACH NUMBERS

by

Arun Isaac Jose

Thesis submitted to the Faculty of the Graduate School of the
University of Maryland, College Park in partial fulfillment
of the requirements for the degree of
Master of Science
2005

Advisory Committee:

Professor J. Gordon Leishman, Chair/Advisor
Professor James D. Baeder, Co-Advisor
Professor Roberto Celi

ACKNOWLEDGMENTS

I owe my gratitude to all the people who have made this thesis possible and who have made my graduate experience one that I will cherish forever. First and foremost I would like to thank my advisor, Professor Gordon Leishman for giving me an opportunity to work at the rotorcraft center at the University of Maryland. I am grateful to him for being patient and understanding with me on several occasions and for his support and encouragement. He has always made himself available for help and has taken great pains to go through my work and suggest improvements. His wide experience and knowledge of helicopters and his dedication and hardwork have inspired me a lot.

I would also like to thank my co-advisor, Dr. James Baeder for his suggestions and advice on various occasions during my graduate life. His sharp intellect and grasp over computational issues has greatly inspired me. Thanks are also due to Dr. Chopra and Dr. Celi with whom I have interacted through courses and discussions and who have provided valuable inputs and support to my research.

My colleagues at the graduate research office of the rotorcraft center have made my graduate life a most enriching experience. In particular, I would like to express my deep gratitude to Shreyas and Sandeep whose help and support has been invaluable to my academics and research. Special thanks are also due to Jaina and Karthik, who have guided me in the CFD component of my research. I would also like to thank Abhishek, Anne, Nitin, Moble, Vinod and all the others at the rotorcraft center whose presence

has made my graduate experience all the more lively and enjoyable. I would also like to express my gratitude to Arun Kota and Vamsee Yerramilli for being such wonderful friends and house-mates.

I owe my deepest thanks to my family - my mother and father who have always stood by me and laid the foundation for my academic, personal and spiritual life. Words cannot express the gratitude I owe them. I shall always remain indebted to them for the many sacrifices they have made to make me what I am.

TABLE OF CONTENTS

LIST OF TABLES

LIST OF FIGURES

Nomenclature

A_n	coefficients of indicial response functions
a	sonic velocity, ft/s
b_n	exponents of indicial response functions
c	airfoil chord, m
C_m	pitching moment coefficient about 1/4-chord
C_n	normal force coefficient
C_{n_α}	lift curve slope for compressible flows $= 2\pi/\beta$
C_p	coefficient of pressure $= (p - p_\infty)/\frac{1}{2}\rho V_\infty^2$
I	integral term
k	reduced frequency $= \omega c/2V$
f	generic flow variable
M	Mach number
M_{cr}	critical Mach number
$M_{\Omega R}$	hover tip Mach number
N	number of coefficients in indicial response function
s	distance traveled by airfoil in semi-chords $= \frac{2}{c}\int_0^t V\,dt$
R	radius of rotor
r	non-dimensional radial location of a rotor blade-section
t	time,
T	noncirculatory time constant
V	free-stream (or local) velocity, ft/s

w velocity normal to the chord, ft/s

$\bar{x}_{ac}$ non-dimensional aerodynamic center

X, Y deficiency functions

α angle of attack, deg.

$\dot{\alpha}$ pitch rate, deg/s

α_m mean angle of attack, deg.

$\overline{\alpha}$ amplitude of α oscillations, deg.

β Glauert factor $= \sqrt{1 - M^2}$

ε generic forcing function

λ velocity perturbation ratio

σ dummy time variable of integration

ϕ indicial response function

Ω Rotational speed of rotor, rad/s

ω circular frequency, rad/s

Superscripts

c circulatory part

nc noncirculatory part

qs quasi-steady

Subscripts

f generic force component

m pitching moment component

n normal force component

α	angle of attack component
$\dot{\alpha}$	pitch rate component
M	Mach number component
0	Value at $t = 0$

Abbreviations

AoA	angle of attack
CFD	computational fluid dynamics

Chapter 1

Introduction

Helicopter rotors operate in a highly unsteady flow field (see Fig. 1.1). The non-uniform inflow produced by the rotor wake combined with the pitching, flapping and lagging motion of the rotor blades produce highly non-steady changes in the angles of attack and aerodynamic forces acting on the blades. Other important sources of unsteadiness at the blade element include fluctuations in the local free-stream velocity (and Mach number) in forward flight (see Ref. 1). Overall, unsteady aerodynamic effects contribute to determining rotor performance, the aeroelastic behavior of the rotor system, the vibratory loads, and also to rotor noise. The ultimate goal for the rotor analyst is to be able to model unsteady aerodynamic effects more accurately and more efficiently within the context of the entire integrated rotor analysis. Because of the computationally intensive nature of this problem, there are constraints on the computational requirements, accuracy and allowable mathematical representation of the aerodynamic model. The task of predicting the aerodynamic loads on the rotor blades is, therefore, extremely challenging because it involves a balance between numerical accuracy and computational cost. One powerful tool for high-fidelity aerodynamic predictions is computational fluid dynamics (CFD). Besides providing good estimates of the aerodynamic forces acting on the rotor blade in almost any condition, it also gives valuable insight into the physics of the flow, albeit at extremely high computational cost. Because the rotor analyst is faced with the problem of

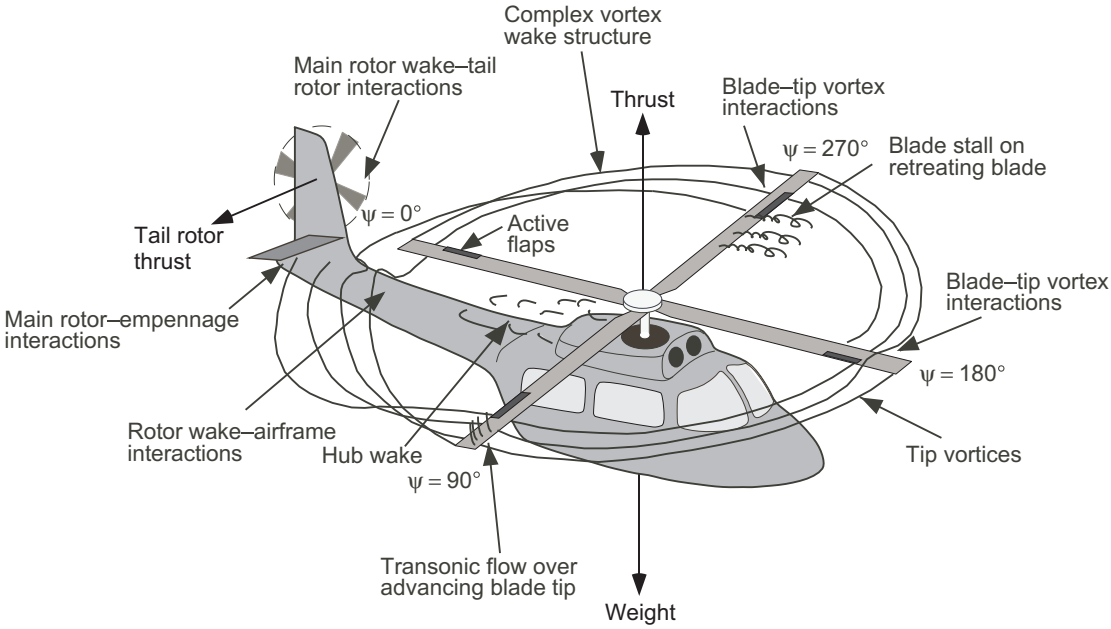

Figure 1.1: Unsteady aerodynamic phenomena in helicopter rotor environment (Courtesy Dr. Gordon Leishman, Ref. 1).

tightly coupling the aerodynamic model into the structural dynamic response model of the rotor, the mathematical representation for the aerodynamics may have to be formulated in a specific computational form. These efficiency and mathematical form constraints usually make the direct use of CFD unsuitable for use in comprehensive rotor design and analysis codes. Nevertheless, CFD methods can help form a basis to develop and validate reduced-order unsteady aerodynamic models that retain all the appropriate mathematical structures and computational efficiency necessary for helicopter applications. This is one goal of the current work.

A quasi-steady analysis may be used to obtain a first estimate of the aerodynamic forces in helicopter rotor applications. However, depending on the flow conditions and degree of unsteadiness, the actual airloads can differ significantly from their quasi-steady

values, both in magnitude and in phase. The practical limitations of CFD and the inadequacy of the quasi-steady approach necessitates the use of intermediate levels of aerodynamic modeling that retain the high fidelity of CFD while being of appropriate mathematical form and also being computationally less expensive. The indicial method (Refs. 2–6) is one such tool, which provides high fidelity solutions at low computational cost; it offers at least three or four orders of magnitude reduction in computational time over direct CFD solutions. This makes the indicial method highly suitable for use in routine rotor analysis, if its use can be properly justified.

In the indicial method, the general motion of a body can be expressed as a sum of discrete step motions. If the indicial (step) response to a step input can be determined, the aerodynamic response for arbitrary motion of the body can be calculated using superposition principles (Duhamel superposition). The indicial responses have been determined exactly for thin airfoils operating in unsteady incompressible flows, mainly by Wagner (Ref. 7), Küssner (Ref. 8), von Kármán & Sears (Ref. 9) and Sears (Ref. 10).

Exact solutions for an oscillating airfoil in a steady, incompressible free-stream flow was first obtained by Theodorsen (Ref. 11). The problem of non-steady free-stream velocity fluctuations, such as those found at the blade element of a helicopter rotor, raises considerably the complexity of the problem. This is mainly because of the non-uniform convection velocity of the downstream wake. Nevertheless, solutions for the additional effects of unsteady free-stream were given by Greenberg (Ref. 12) and Kottapalli (Ref. 13). However, these theories make certain simplifying assumptions that restrict their range of validity to low free-stream velocity amplitudes. This is not useful for helicopter problems. A more comprehensive theory was given by Isaacs (Ref. 14) and later generalized

for arbitrary pitch axis location by Van der Wall & Leishman (Ref. 15). However, Isaacs model has certain practical limitations because the solution is expressed in the frequency domain. This makes it difficult to implement it for arbitrary types of forcing (angle of attack and Mach number). A time domain solution for arbitrary variations in pitch angle and free-stream velocity was developed by Van der Wall & Leishman (Ref. 15). It was shown that by using an exponential approximation to the Wagner function, the lift variation for arbitrary forcing can be solved using Duhamel integration to a numerical accuracy comparable to the exact solutions. Comparisons with Isaacs (Ref. 15) theory showed that any small differences were partly dependent on the temporal discretization used in the superposition scheme and partly on the quality of the exponential function used to approximate the Wagner indicial function.

Helicopter rotors operate at high subsonic Mach numbers, especially in the outboard regions of the advancing side, rendering incompressible flow assumptions invalid. This means that all the theories considered by Van der Wall & Leishman (Ref. 15) become less effective. Not only that, but the use of a strictly incompressible flow theory may produce erroneous results if applied for problems involving compressibility effects. For compressible flows, the pressure disturbances travel at a finite speed and there are greater lags in the aerodynamic response compared to incompressible flow. No exact solutions for the time-varying free-stream problem can be obtained, and alternate approaches must be used. The issues of modeling compressibility effects on unsteady airfoil behavior using linear indicial theory has been studied for many years, first by Mazelsky, Beddoes and others (Refs. 3, 16–18), and then by Leishman and co-workers (Refs. 19–23). Efficient mathematical models have been developed to determine the forces acting on an airfoil

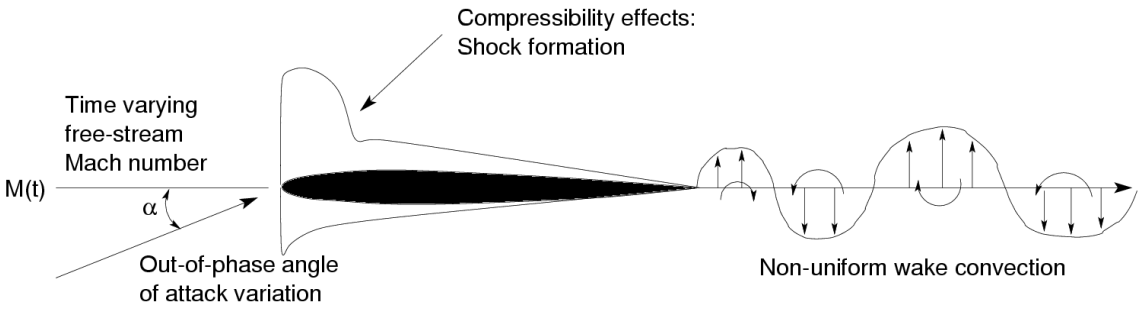

Figure 1.2: Schematic of the flow problem.

undergoing oscillations in angle of attack and plunge motion at constant Mach number. However, indicial based models to predict lift and pitching moment for combined angle of attack and free-stream Mach number oscillations need further development.

In the present work a method is proposed to model subsonic flows involving combined angle of attack and free-stream Mach number variations. The new theory is validated for a NACA 0006 airfoil using CFD. Figure 1.2 shows a schematic of the basic flow problem. The goal of the work is to predict the lift and pitching moment for non-steady variations in angle of attack and Mach number. All the calculations were carried out with the Mach number and angle of attack varying at the same reduced frequency, i.e.

$$M(t) = M_0(1+\lambda\sin\omega t)$$

$$\alpha(t) = \alpha_m + \overline{\alpha}\sin\omega t$$

For a helicopter with a hover tip Mach number, $M_{\Omega R}$, advance ratio μ and a chord to radius ratio of c/R, this would correspond to

$$\omega = \Omega \tag{1.1}$$

$$M_0 = xM_{\Omega R} \tag{1.2}$$

$$\lambda = \frac{\mu}{x} \tag{1.3}$$

$$k = \frac{\Omega c}{2V} = \frac{c}{2Rx} \tag{1.4}$$

where $x = r/R$ and Ω is the rotational speed. From these expressions it is seen that for a given blade section, M_0, λ and k are fixed. For a high speed helicopter with an advance ratio, $\mu = 0.4$, a hover tip Mach number, $M_{\Omega R} = 0.65$, and a chord to radius ratio, $c/R = 1/15$, the following values of M_0, λ and k are obtained at different radial stations of the rotor:

x	M_0	λ	k
0.3	0.195	1.33	0.1111
0.4	0.26	1.0	0.0833
0.5	0.325	0.8	0.0666
0.8	0.52	0.5	0.0416
1.0	0.65	0.4	0.03

Table 1.1: Values of M_0, λ and k at different radial locations of the rotor for a helicopter with a hover tip Mach number, $M_{\Omega R} = 0.65$, $\mu = 0.4$ and $c/R = 1/15$.

From these results it is clear that the reduced frequencies associated with Mach number changes are not high. However, most of the calculations in this work were carried out at a reduced frequency of 0.2 because it was felt that the unsteady aerodynamic models could be better contrasted and evaluated under more unsteady conditions (i.e., higher reduced frequencies) rather than for nearly quasi-steady conditions (i.e., low reduced frequencies). Also, it must be borne in mind that while the reduced frequencies associated with free-stream Mach number changes are not high, those associated with pitching motion are high because besides the collective and cyclic pitch, it includes vi-

bration effects and is, therefore, associated with several frequencies. It is also important to note that in the inboard sections of the rotor, flow reversal occurs on the retreating side ($\lambda > 1$) and this makes it difficult to predict the unsteady airloads accurately for these blade-sections.

It is shown in this work that all existing indicial models for subsonic flows effectively adopt a quasi-steady approach to incorporate the effect of changing Mach number. One improvement made to these theories in the present work is the inclusion of the appropriate noncirculatory terms resulting from changes in Mach number. The new theory uses the incompressible indicial theory of van der Wall & Leishman (Ref. 15) as a basis for developing a more generalized theory capable of handling compressible flows that involve combined angle of attack and free-stream Mach number variations.

The thesis has been divided into four chapters: *Introduction*, *Methodology*, *Results and Discussion* and *Conclusions*. The chapter on methodology describes the theory and implementation of various unsteady aerodynamic models, namely, CFD, the incompressible indicial method, the existing compressible indicial method and the new indicial method. Because the primary advantage of the indicial method lies in its computational efficiency, a detailed analysis of different numerical approaches is performed and an improved algorithm is proposed, which provides a good balance between computational efficiency and numerical accuracy. The *Results and Discussion* chapter compares the results obtained using the different unsteady aerodynamic models for a wide range of flow conditions. The various unsteady aerodynamic theories are validated against CFD results. An attempt is also made to understand the physics behind certain flow nonlinearities that occur at higher Mach numbers. The effect of viscosity and airfoil thickness are also briefly

discussed. Finally, the conclusions are presented along with some possible directions for future work, which would extend the application of the indicial method to include a wider range of flow conditions and airfoils.

Chapter 2

Methodology

This chapter describes the different unsteady aerodynamic models that have been used to develop and validate the new compressible indicial model for time-varying free-stream Mach numbers. An overview of the CFD model, the unsteady incompressible indicial model and the existing compressible indicial model is given. This is followed by a detailed description of the new indicial model along with numerical algorithms to efficiently implement it.

2.1 The CFD Method

Computational fluid dynamics (CFD) is a valuable tool for unsteady aerodynamic predictions. All CFD calculations were made using an extension of the TURNS code (Ref. 25). This is a single block Navier-Stokes solver that has been used to study a variety of unsteady airfoil and rotor flow problems. The calculations were performed in the Euler mode on a 241×53 structured C-grid (see Fig. 2.1). A finite difference upwind numerical algorithm was used to solve the governing equations, with the evaluation of the inviscid fluxes being based on Roe's upwind-biased flux-difference scheme. In this work, CFD has been used to :

- Obtain the unsteady indicial response to a step change in forcing. This is used to extract the indicial coefficients that are used to specify the indicial response function.

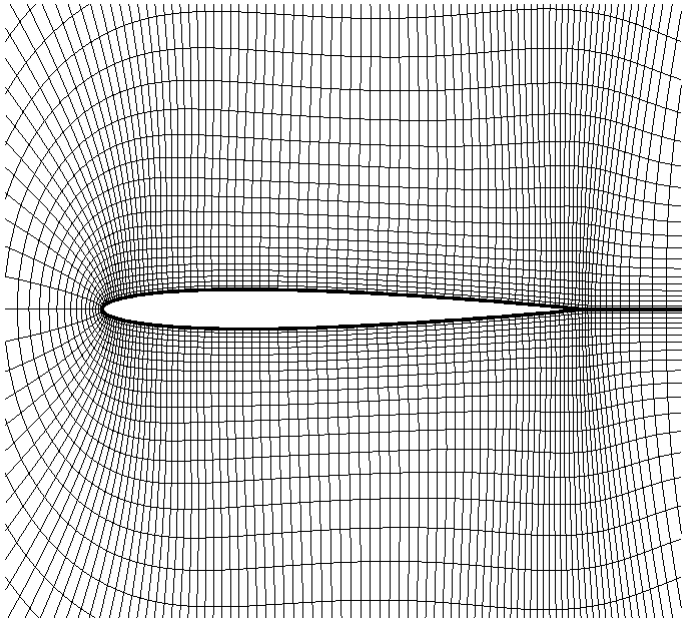

Figure 2.1: C-grid used for CFD computations on the NACA0006 airfoil.

This approach has been followed by Lee et al. (Ref. 24).

- To obtain the unsteady lift and pitching moment variation on the airfoil for arbitrary forcing in angle of attack, Mach number and pitch rate.

- To validate the new indicial theory for a wide range of flow conditions that would be relevant to helicopters.

- To understand the physics behind nonlinear phenomena that occur at high angles of attack and Mach number.

All the CFD calculations were performed for a NACA 0006 airfoil in Euler mode using the field velocity approach (Ref. 26).

2.1.1 The Governing Equations

The Conservative form of the Navier-Stokes equations can be written as :

$$\frac{\partial Q}{\partial t} + \frac{\partial (E - E_v)}{\partial x} + \frac{\partial (F - F_v)}{\partial y} = 0 \tag{2.1}$$

$$Q = \begin{bmatrix} \rho \\ \rho u \\ \rho v \\ \rho E_t \end{bmatrix}, E = \begin{bmatrix} \rho u \\ \rho u^2 + p \\ \rho uv \\ (\rho E_t + p)u \end{bmatrix}, F = \begin{bmatrix} \rho v \\ \rho vu \\ \rho v^2 + p \\ (\rho E_t + p)v \end{bmatrix}, \tag{2.2}$$

$$E_v = \begin{bmatrix} 0 \\ \tau_{xx} \\ \tau_{xy} \\ u\tau_{xx} + v\tau_{xy} - q_x \end{bmatrix}, F_v = \begin{bmatrix} 0 \\ \tau_{xy} \\ \tau_{yy} \\ u\tau_{xy} + v\tau_{yy} - q_y \end{bmatrix}$$

where

$$\begin{aligned} E_t &= C_v T + \frac{1}{2}\left(u^2 + v^2\right), \\ q_x &= -k\frac{\partial T}{\partial x}, \\ \tau_{xx} &= \frac{2}{3}\mu\left(2\frac{\partial u}{\partial x} - \frac{\partial v}{\partial y}\right), \\ \tau_{xy} &= \mu\left(\frac{\partial u}{\partial y} + \frac{\partial v}{\partial x}\right) \end{aligned}$$

To have well conditioned matrices during the solution process, the equations need to be normalized. For the above equations, the various flow parameters are non-dimensionalized

using reference parameters in the following manner

$$x^* = \frac{x}{L}, \quad y^* = \frac{y}{L}, \quad t^* = \frac{ta_\infty}{L}, \quad \rho^* = \frac{\rho}{\rho_\infty},$$
$$u^* = \frac{u}{a_\infty}, \quad v^* = \frac{v}{a_\infty}, \quad T^* = \frac{T}{T_\infty}, \quad p^* = \frac{p}{\rho a_\infty^2},$$
$$E_t^* = \frac{E_t}{a_\infty^2}, \quad \mu^* = \frac{\mu}{\mu_\infty}$$

and

$$\tau_{xx}^* = \frac{2\mu^*}{3Re_L}\left(2\frac{\partial u^*}{\partial x^*} - \frac{\partial v^*}{\partial y^*}\right) q_x^* = \frac{-\mu^*}{(\gamma-1)M_\infty^2 Re_L Pr}\frac{\partial T^*}{\partial x^*}$$

where L is taken as the chord length, a_∞ is the velocity of sound far away from the airfoil, ρ_∞ is taken to be the density of the free-stream, T_∞ is taken to be the static temperature of the free-stream. The Reynolds number and Prandtl number are given by

$$Re_L = \frac{\rho_\infty a_\infty L}{\mu_\infty}, \; Pr = \frac{\mu C_p}{k}$$

2.1.2 Transformation From the Physical Domain to the Computational Domain

The physical domain is mapped on to a computational domain where the grid lines are orthogonal and equal-spaced. The governing equations can then be solved on the computational domain by determining the metrics of the transformation. The transformed equations can be written as

$$\frac{\partial \overline{Q}}{\partial t} + \frac{\partial \overline{E}}{\partial \xi} + \frac{\partial \overline{F}}{\partial \eta} = \frac{\partial \overline{E}_v}{\partial \xi} + \frac{\partial \overline{F}_v}{\partial \eta} \tag{2.3}$$

Where the barred vectors are the vectors in the transformed $(\xi - \eta)$ coordinate system. These can be expressed in terms of the Cartesian vectors as follows:

$$\overline{Q} = \frac{1}{J}[Q] \tag{2.4}$$

$$\overline{E} = \frac{1}{J}[\xi_x E + \xi_y F] \tag{2.5}$$

$$\overline{F} = \frac{1}{J}[\eta_x E + \eta_y F] \tag{2.6}$$

$$\overline{E_v} = \frac{1}{J}[\xi_x E_v + \xi_y F_v] \tag{2.7}$$

$$\overline{F_v} = \frac{1}{J}[\eta_x E_v + \eta_y F_v] \tag{2.8}$$

where J is the Jacobian of the inverse coordinate transformation (i.e., $J = \det\left(\frac{\partial(x,y)}{\partial(\varepsilon,\eta)}\right)$).

2.1.3 Modes of Operation

The TURNS code is designed to compute the solution for a wide range of steady and unsteady flow problems. In the present work, the code was used for the following purposes:

1. To calculate the steady-state lift for a given angle of attack and Mach number. Also, the final-state of a steady calculation is used as input to an unsteady computation with the same initial conditions (i.e., at the same initial angle of attack and Mach number). Figure 2.2 shows a typical lift transient for a steady CFD calculation. Note that the initial oscillations do not matter as long as the final solution converges to the steady-state value.

2. To calculate the unsteady lift response to a step change in angle of attack. This is used to determine the indicial coefficients that specify the indicial response functions. Figure 2.3 shows a typical indicial (step) normal force response for a step change in angle of attack.

3. To calculate the lift and pitching moment for combined variations in angle of attack and Mach number. This is used to validate the indicial theory for a wide range of flow conditions. Figure 2.4 shows a typical unsteady lift response for combined

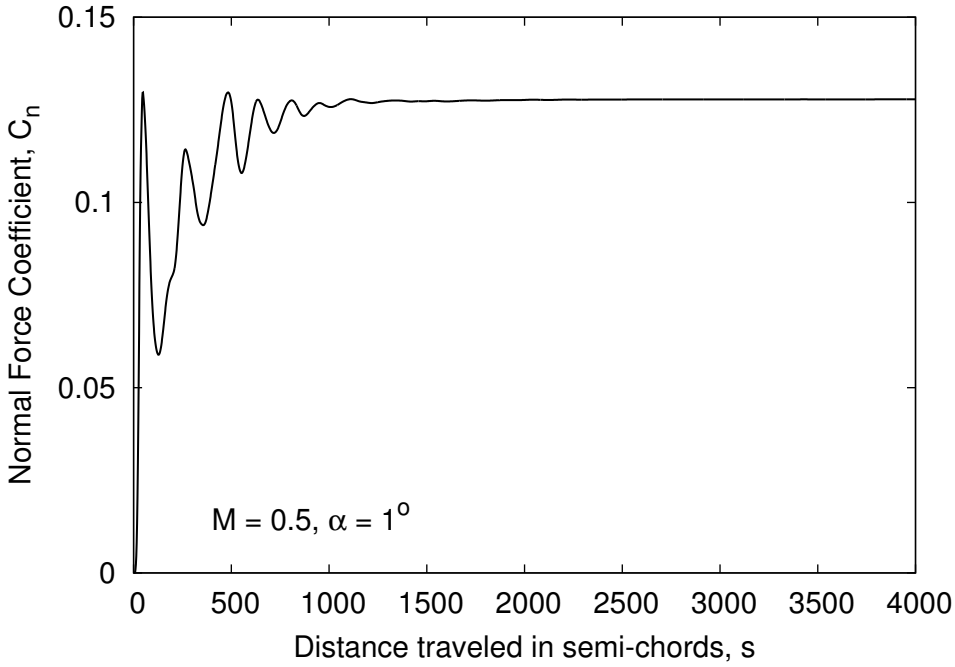

Figure 2.2: Typical lift transient for steady CFD computation ($M = 0.5$, $\alpha = 1^\circ$).

variations in angle of attack and Mach number.

2.2 The Indicial Method

The indicial approach is based on the concept that an aerodynamic response $f(t)$, can be linearized with respect to its boundary condition (or forcing function), $\varepsilon(t)$, if $f(t)$ is a smooth, non-discontinuous function of $\varepsilon(t)$. This allows the representation of $f(t)$ in a Taylor series about some value of $\varepsilon = \varepsilon_0$, i.e.,

$$f(t) = f(0) + \Delta\varepsilon \frac{\partial f}{\partial \varepsilon}\Big|_{\varepsilon=\varepsilon_0} + \cdots \tag{2.9}$$

If the response $\partial f/\partial\varepsilon$ depends only on the elapsed time from the perturbation $\Delta\varepsilon$ (i.e., a linear time-invariant response), then it may be shown that the formal solution for $f(t)$ is the well-known Duhamel integral

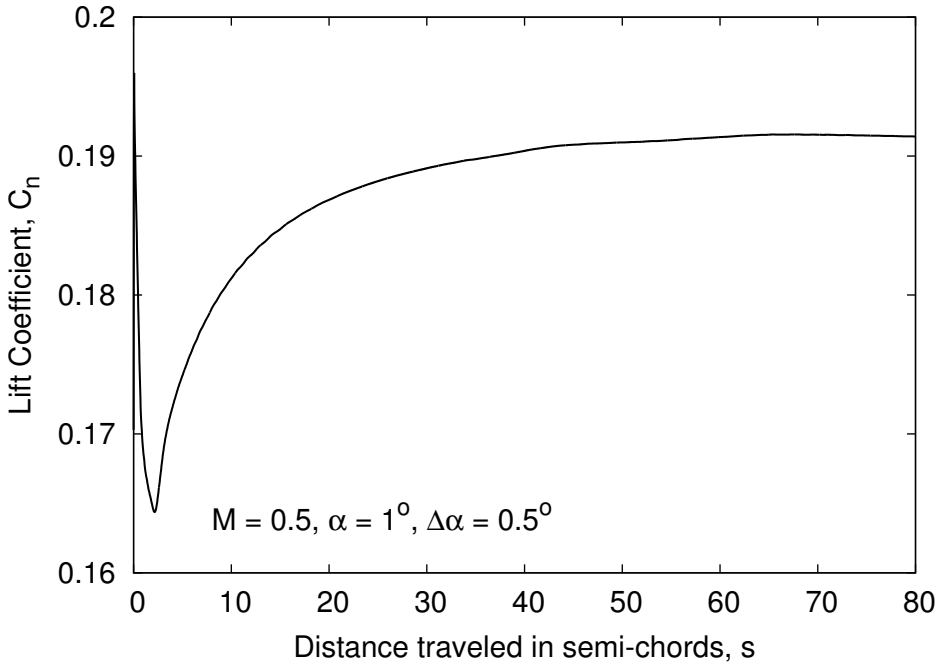

Figure 2.3: Typical unsteady lift response for a step change in angle of attack ($M = 0.5$, $\alpha = 1^\circ$, $\Delta\alpha = 0.5^\circ$).

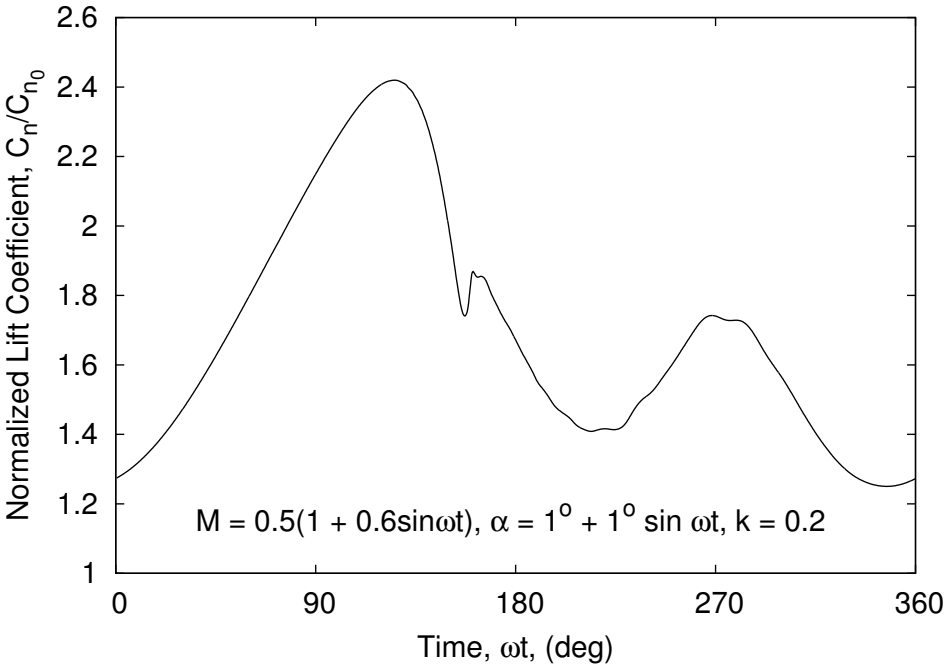

Figure 2.4: Typical unsteady lift variation for arbitrary forcing in angle of attack and Mach number ($M = 0.5(1 + \sin\omega t)$, $\alpha = 1^\circ + 1^\circ \sin\omega t$, $k = 0.2$).

$$f(t) = f(0) + \int_0^t \frac{d\varepsilon}{d\sigma}(\sigma)\phi(t-\sigma)\,d\sigma \tag{2.10}$$

where $\phi(t) = \frac{\partial f}{\partial \varepsilon}|_{\varepsilon=\varepsilon_0}$. Hence, if the forcing function ε is known and if $\phi(t)$ (the indicial response) is also known (say, from computation or experiment), then the Duhamel integral in Eq. (2.10) gives the value of $f(t)$ for any arbitrary changes in $\varepsilon(t)$.

2.2.1 Incompressible Method

Before describing the reduced-order model for compressible flows, the incompressible flow approach must be reviewed. The incompressible flow theory forms a rigorous basis from which to extend the modeling to consider the treatment of compressibility effects.

Lift Coefficient

The lift response to changes in angle of attack α and free-stream velocity V consists of clearly separable circulatory and noncirculatory components, i.e., it can be assumed that

$$C_n(t) = C_n^c(t) + C_n^{nc}(t) \tag{2.11}$$

The circulatory part is associated with the formation of circulation around the airfoil section. The noncirculatory part is associated with apparent mass effects (i.e., flow inertia effects). Van der Wall & Leishman (Ref. 15) show that the unsteady incompressible circulatory lift equation is given by

$$C_n^c(t) = \frac{1}{V}\left[2\pi w_{3/4}(s=0)\phi_W(s) + \int_0^s \frac{d(2\pi w_{3/4})}{d\sigma}(\sigma)\,\phi_W(s-\sigma)\,d\sigma\right] \tag{2.12}$$

where $w_{3/4}$ is the normal velocity at the $3/4$ chord point. For an airfoil oscillating about

its $1/4$-chord point, $w_{3/4}$ is given by

$$w_{3/4} = V\alpha + \frac{\dot{\alpha}c}{2} \tag{2.13}$$

The parameter s is the distance traveled by the airfoil in semi-chords, and for a non-steady free-stream it is given by

$$s = \frac{2}{c}\int_0^t V(t)\,dt \tag{2.14}$$

The Wagner function, $\phi_W(s)$, is known exactly (Ref. 7) but is usually represented approximately in exponential form for use in the Duhamel integral. One approximation to the Wagner function, which is attributed to R. T. Jones (Ref. 27, 28), is written as a two-term exponential series with four coefficients (see Fig. 2.5), i.e.,

$$\phi_W(s) = 1 - 0.165e^{-0.0455s} - 0.335e^{-0.3s} \tag{2.15}$$

Notice that $\phi_W(\infty) = 1$, so that in the absence of any forcing, the result reduces to the quasi-steady result, which is given by

$$C_n^c(s \to \infty) = \frac{1}{V}\left(2\pi w_{3/4}\right) = 2\pi\left(\alpha + \frac{\dot{\alpha}c}{2V}\right) \tag{2.16}$$

and for steady flow where $\dot{\alpha} = 0$,

$$C_n^c(s \to \infty) = 2\pi\alpha \tag{2.17}$$

For an airfoil oscillating about the 1/4-chord point, the noncirculatory component of the lift response is given by

$$C_n^{nc}(t) = \frac{\pi c}{2V^2}\left(\frac{d(V\alpha)}{dt} + \frac{\ddot{\alpha}c}{4}\right) \tag{2.18}$$

where c is the chord length of the airfoil. Notice that unlike the circulatory component, the noncirculatory component is dependent only on the *instantaneous* rate of change in the

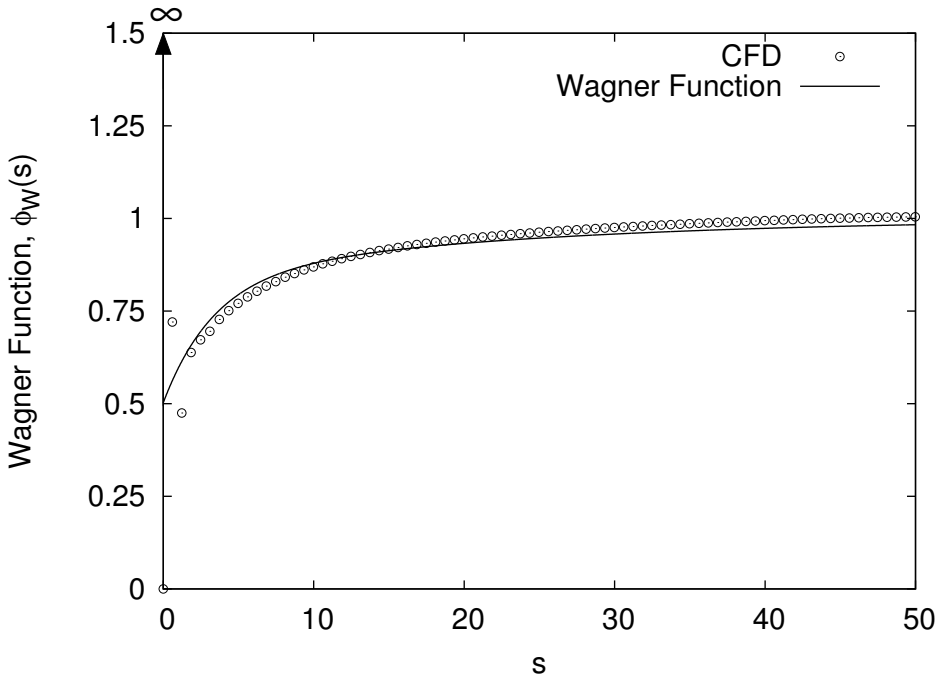

Figure 2.5: The Wagner function for incompressible flow compared to CFD solution for the normalized lift for a step change in angle of attack.

forcing. This, as will be seen later, is an important difference between the compressible and incompressible indicial methods.

Pitching Moment Coefficient

To determine the pitching moment coefficient about the 1/4-chord, the unsteady pressure distribution over the airfoil needs to be determined. From Wagner's theory (Ref. 7), the circulatory part of the pressure distribution is given by

$$\Delta C_p(x,t) = \frac{4\Delta w_{3/4}}{V}\sqrt{\frac{c-x}{x}}\phi_W(s) + \frac{4\Delta\dot{\alpha}c}{V}\left(\frac{x}{c}-\frac{1}{4}\right)\sqrt{\frac{c-x}{x}} \qquad (2.19)$$

where x is the chordwise coordinate, starting at the leading edge. The first term in the above equation is the usual thin airfoil result combined with the Wagner function and is, therefore, an unsteady term. The second term is also a circulatory term, albeit a quasi-

steady term. By integrating Eq. (2.19) in space, it can be shown that the quasi-steady term does not contribute to the total lift but affects the pitching moment. It can be shown that the lift resulting from the first term passes through 1/4-chord point and consequently, it does not contribute to the pitching moment about the 1/4-chord. The pitching moment can be obtained from Eq. (2.19) by evaluating the moment about the $1/4$ chord-point, i.e.,

$$C_{m_{1/4}}(t) = \int_0^1 \Delta C_p\,(0.25-\overline{x})\,d\overline{x} = -\frac{\pi}{8}\left(\frac{\dot{\alpha}c}{V}\right) \tag{2.20}$$

However, for a general airfoil the center of pressure of the circulatory forces does not coincide with the 1/4-chord point. Consequently, the first term in Eq. (2.19) also contributes to the pitching moment about the 1/4-chord. The modified pitching moment equation is then given by

$$\begin{aligned} C_{m_{1/4}}(t) &= \frac{1}{V}\Big[2\pi w_{3/4}(0.25-x_{\rm cp})(s=0)\phi_W(s) \\ &\quad + \int_0^s \frac{d(2\pi w_{3/4}(0.25-x_{\rm cp}))}{d\sigma}(\sigma)\,\phi_W(s-\sigma)\,d\sigma\Big] - \frac{\pi}{8}\left(\frac{\dot{\alpha}c}{V}\right) \end{aligned} \tag{2.21}$$

where

$$x_{\rm cp} = x_{\rm cp}(\alpha_{\rm eff}) \tag{2.22}$$

$$\alpha_{\rm eff} = \alpha + \frac{\dot{\alpha}c}{2V} \tag{2.23}$$

The center of pressure, $x_{\rm cp}$, can be obtained as a function of the angle of attack from steady state computational or experimental data. If $x_{\rm cp}$ is assumed to be constant and coincident with the aerodynamic center, then the equation reduces to

$$C_{m_{1/4}}(t) = C_n^c(t)(0.25-x_{\rm ac}) - \frac{\pi}{8}\left(\frac{\dot{\alpha}c}{V}\right) \tag{2.24}$$

2.2.2 Compressible Flow Equations

For an incompressible flow Laplace's equation applies, but for a linearized compressible flow a form of the wave equation applies (Ref. 29). In this case, closed form solutions for the unsteady airloads are much more involved and cannot, in general, be found for all values of time. There are low- and high-frequency approximations available, which are good check cases for any theory, but these results are not particularly useful for helicopter rotor applications, in general.

Lift Coefficient

The lift response for the compressible flow has the same basic form as the incompressible indicial model but with important differences. The indicial response for compressible flows also involves circulatory and noncirculatory terms such that the total can be assumed to be decomposed as

$$C_n(t) = C_n^c(t) + C_n^{nc}(t) \tag{2.25}$$

One important difference between the incompressible and compressible theories lies in the treatment of the noncirculatory terms. For compressible flows, the velocity of sound is finite, which has two important consequences. First, the initial value of the circulatory part of the indicial response is zero. Second, the noncirculatory component of the indicial lift is finite (it is infinite for incompressible flow) and is also influenced by the forcing at prior time. Consequently, like the circulatory term, the hereditary effects in the noncirculatory airloads must be solved for using the Duhamel integral.

Circulatory Part

From small perturbation theory, the quasi-steady lift for subsonic compressible flows can be obtained from the corresponding incompressible lift by introducing the Glauert factor, $\beta = \sqrt{1-M^2}$, i.e.,

$$C_n^{qs}(t) = \frac{1}{V}\left(\frac{2\pi w_{3/4}}{\beta}\right) = \frac{2\pi}{\beta}\left(\alpha + \frac{\dot{\alpha}c}{2V}\right) \tag{2.26}$$

Noting the difference between the quasi-steady results for the incompressible and compressible cases (Eqs. (2.16) and (2.26), respectively), the same result can be used in the unsteady equation by replacing $2\pi w_{3/4}$ in Eq. (2.12) by $2\pi w_{3/4}/\beta$. This gives

$$\begin{aligned} C_n^c(t,M) &= \frac{1}{V}\left[\left(\frac{2\pi w_{3/4}}{\beta}\right)(s=0)\phi_n^c(s,M) + \int_0^s \frac{d}{d\sigma}\left(\frac{2\pi w_{3/4}}{\beta}\right)(\sigma)\phi_n^c(s-\sigma,M)\,d\sigma\right] \\ &= \frac{1}{V}\left[C_{n_\alpha} w_{3/4}(s=0)\phi_n^c(s,M) + \int_0^s \frac{d(C_{n_\alpha} w_{3/4})}{d\sigma}(\sigma)\phi_n^c(s-\sigma,M)\,d\sigma\right] \end{aligned} \tag{2.27}$$

where $\phi_n^c(s,M)$ is the analogous circulatory lift response function for compressible flows and $C_{n_\alpha} = 2\pi/\beta$ is the static lift curve slope from Glauert rule. The functional representation of the indicial response functions in this case are more complicated and will be described later.

Because the term $C_{n_\alpha} w_{3/4}$ itself is a function of α, M and $\dot{\alpha}$, the above equation can be rewritten in the form

$$\begin{aligned} C_n^c(t,M) &= \frac{1}{V}\Big[C_{n_\alpha} w_{3/4}(\alpha_0, M_0, \dot{\alpha_0})\phi_n^c(s,M) + \\ &\int_0^s \left(\frac{\partial C_{n_\alpha} w_{3/4}}{\partial \alpha}\frac{d\alpha}{d\sigma} + \frac{\partial C_{n_\alpha} w_{3/4}}{\partial M}\frac{dM}{d\sigma} + \frac{\partial C_{n_\alpha} w_{3/4}}{\partial \dot{\alpha}}\frac{d\dot{\alpha}}{d\sigma}\right)(\sigma)\,\phi_n^c(s-\sigma,M)\,d\sigma\Big] \end{aligned} \tag{2.28}$$

where α_0, M_0 and $\dot{\alpha}_0$ correspond to the initial values of α, M and $\dot{\alpha}$, respectively. The parameter $C_{n_\alpha} w_{3/4}$ may be rewritten as

$$C_{n_\alpha} w_{3/4} = \frac{2\pi w_{3/4}}{\beta}$$

$$
\begin{aligned}
&= \frac{2\pi}{(1-M^2)^{1/2}}\left(V\alpha+\frac{1}{2}\dot{\alpha}c\right) \\
&= 2\pi\left(\frac{aM\alpha+\dot{\alpha}c/2}{(1-M^2)^{1/2}}\right) \qquad (2.29)
\end{aligned}
$$

where a is the sonic velocity. From the above equation, the partial derivatives of $C_{n_\alpha}w_{3/4}$ are

$$\frac{\partial(C_{n_\alpha}w_{3/4})}{\partial\alpha} = \frac{2\pi aM}{\beta} \qquad (2.30)$$

$$\frac{\partial(C_{n_\alpha}w_{3/4})}{\partial M} = \frac{2\pi a\alpha+\pi Mc\dot{\alpha}}{\beta^3} \qquad (2.31)$$

$$\frac{\partial(C_{n_\alpha}w_{3/4})}{\partial\dot{\alpha}} = \frac{\pi c}{\beta} \qquad (2.32)$$

The above results can now be substituted into Eq. (2.28) to obtain

$$
\begin{aligned}
C_n^c(t,M) &= \frac{1}{aM}\Bigg[\frac{2\pi\left(aM_0\alpha_0+\frac{1}{2}c\dot{\alpha}_0\right)}{\beta_0}\phi_n^c(s,M)+ \\
&\int_0^s\left(\frac{2\pi aM}{\beta}\frac{d\alpha}{d\sigma}+\frac{(2\pi a\alpha+\pi Mc\dot{\alpha})}{\beta^3}\frac{dM}{d\sigma}+\frac{\pi c}{\beta}\frac{d\dot{\alpha}}{d\sigma}\right)(\sigma)\phi_n^c(s-\sigma,M)\,d\sigma\Bigg] \qquad (2.33)
\end{aligned}
$$

Notice that velocity, V, has been replaced by aM. Rearranging Eq. (2.33) gives

$$
\begin{aligned}
C_n^c(t,M) &= \frac{1}{M}\Bigg[\frac{2\pi\left(M_0\alpha_0+\dot{\alpha_0}c/2a\right)}{\beta_0}\phi_n^c(s,M)+ \\
&\int_0^s\left(\frac{2\pi M}{\beta}\frac{d\alpha}{d\sigma}+\frac{(2\pi\alpha+\pi Mc\dot{\alpha}/a)}{\beta^3}\frac{dM}{d\sigma}+\frac{\pi c/a}{\beta}\frac{d\dot{\alpha}}{d\sigma}\right)(\sigma)\phi_n^c(s-\sigma,M)\,d\sigma\Bigg] \qquad (2.34)
\end{aligned}
$$

The foregoing equation gives the circulatory lift response to arbitrary forcing in α, $\dot{\alpha}$ and M. It retains the same form as the equation used for incompressible flow (c.f. Eq. (2.12)) but now accounts for compressibility effects.

Noncirculatory Effects

The noncirculatory components, which are not associated with the formation of circulation around the airfoil, also contribute significantly to the lift and pitching moment, especially at high reduced frequencies. It is, therefore, important to include noncirculatory

effects into the aerodynamic model. The noncirculatory terms are modeled by using the semi-analytical approach described by Lomax (Ref. 29), Beddoes (Ref. 3) and Leishman (Ref. 1), and is based on linear theory. From one-dimensional piston theory (Refs. 29, 30) it is known that for the initial value of the indicial response then

$$\Delta C_p(x,t=0) = \frac{2\rho a \Delta w(x)}{\frac{1}{2}\rho V^2} = \left(\frac{4}{M}\right)\frac{\Delta w(x)}{V} \tag{2.35}$$

For forcing about the 1/4-chord point, the distribution of $w(x)$ over the chord is given by

$$w(x) = V\alpha + \left(\frac{x}{c} - \frac{1}{4}\right)\dot{\alpha}c \tag{2.36}$$

Therefore,

$$\Delta w(x) = \alpha\Delta V + V\Delta\alpha + \left(\frac{x}{c} - \frac{1}{4}\right)\Delta\dot{\alpha}c \tag{2.37}$$

This latter result can be used to derive the initial value of the noncirculatory component of the lift coefficient as

$$\begin{aligned} C_n^{nc}(t=0) &= \frac{1}{c}\int_0^c \Delta C_p\, dx \\ &= \frac{4}{MV}\frac{1}{c}\int_0^c \left(\Delta(V\alpha) + \left(\frac{x}{c} - \frac{1}{4}\right)c\Delta\dot{\alpha}\right) dx \\ &= \frac{4}{MV}\left(\alpha\Delta V + V\Delta\alpha + \frac{c\Delta\dot{\alpha}}{4}\right) \\ &= \frac{4}{M}\Delta\alpha + \frac{4\alpha}{M^2}\Delta M + \frac{c}{aM^2}\Delta\dot{\alpha} \end{aligned}$$

This is the *initial* value of the noncirculatory lift response at $t = 0$ for any change in α, M or $\dot{\alpha}$. The noncirculatory airloads subsequently decay from these initial values in the absence of any other forcing. This decay is represented by the noncirculatory response functions $\phi_{n_\alpha}^{nc}(s,M)$, $\phi_{n_M}^{nc}(s,M)$, $\phi_{n_{\dot{\alpha}}}^{nc}(s,M)$, i.e., it can be written in general that

$$C_n^{nc}(t,M) = \frac{4}{M}\Delta\alpha\,\phi_{n_\alpha}^{nc}(s,M) + \frac{4\alpha}{M^2}\Delta M\,\phi_{n_M}^{nc}(s,M) + \frac{c}{aM^2}\Delta\dot{\alpha}\,\phi_{n_{\dot{\alpha}}}^{nc}(s,M)$$

The total value of noncirculatory lift can now be obtained by summing the individual responses to the indicial forcing at each instant of time by using the Duhamel integral, i.e., by using

$$\begin{aligned} C_n^{nc}(t) &= \int_0^s \frac{4}{M}\frac{d\alpha}{d\sigma}(\sigma)\phi_{n_\alpha}^{nc}(s-\sigma,M)\,d\sigma + \int_0^s \frac{4\alpha}{M^2}\frac{dM}{d\sigma}(\sigma)\phi_{n_M}^{nc}(s-\sigma,M)\,d\sigma \\ &\quad + \int_0^s \frac{c}{aM^2}\frac{d\dot{\alpha}}{d\sigma}(\sigma)\phi_{n_{\dot{\alpha}}}^{nc}(s-\sigma,M)\,d\sigma \end{aligned} \tag{2.38}$$

Pitching Moment Coefficient

Following a similar approach, the indicial equations for the pitching moment can also be obtained. One difference however, is that the quasi-steady term in the incompressible indicial equation is now treated as an unsteady term with an associated indicial response function $\phi_m^c(s,M)$. As will be shown later, however, the unsteady component of $\phi_m^c(s,M)$ diminishes rapidly and the term essentially behaves like a quasi-steady term for all but very high rates of change. The pitching moment about the 1/4-chord can be written as

$$\begin{aligned} C_{m_{1/4}}^c(t,M) &= \frac{1}{V}\Big[(C_{n_\alpha} w_{3/4}(0.25-x_{\text{cp}})(\alpha_0,M_0)\phi_n^c(s,M) \\ &+ \int_0^s \frac{d(C_{n_\alpha} w_{3/4}(0.25-x_{\text{cp}}))}{d\sigma}\phi_n^c(s-\sigma,M)\,d\sigma\Big] \\ &- \frac{1}{V}\left[\frac{\pi\dot{\alpha}_0 c}{8\beta_0}\phi_m^c(s,M) + \int_0^s \frac{d}{d\sigma}\left(\frac{\pi\dot{\alpha}c}{8\beta}\right)\phi_m^c(s-\sigma,M)\,d\sigma\right] \end{aligned} \tag{2.39}$$

where

$$x_{\text{cp}} = x_{\text{cp}}(M,\alpha_{\text{eff}}) \tag{2.40}$$

$$\alpha_{\text{eff}} = \alpha + \frac{\dot{\alpha}c}{2V} \tag{2.41}$$

In the above equations, the center of pressure of the circulatory forces x_{cp} is expressed as a function of Mach number and angle of attack based on steady-state data obtained

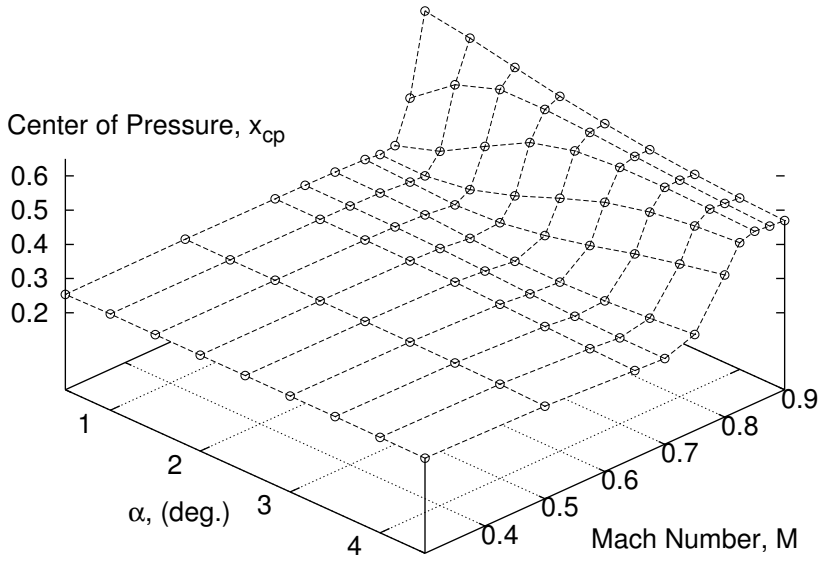

Figure 2.6: Variation in the steady-state center of pressure as a function of free-stream Mach number and angle of attack for the NACA 0006 airfoil.

using CFD for a wide range of angles of attack and Mach numbers. In the present work, the steady-state center of pressure, x_{cp}, was calculated using CFD for all combinations of angles of attack (0.5, 1.0, 1.5, 2.0, 2.5, 3.0, 3.5, 4.0, 4.5) and Mach numbers (0.1, 0.2, ..., 0.9) (see Fig. 2.6).

For the noncirculatory part, the initial pitching moment at $t = 0$ can be obtained by following a similar approach that was described for the lift response. It can be shown that

$$\begin{aligned} C_m^{nc}(t=0) &= \frac{1}{c^2}\int_0^c \Delta C_p(\frac{c}{4}-x)\,dx \\ &= \frac{4}{MV}\frac{1}{c^2}\int_0^c \left(\Delta(V\alpha)+(x-\frac{c}{4})\Delta\dot{\alpha}\right)(\frac{c}{4}-x)\,dx \\ &= \frac{4}{MV}\left(-\frac{\alpha\Delta V}{4}-\frac{V\Delta\alpha}{4}-\frac{7c\Delta\dot{\alpha}}{48}\right) \\ &= -\frac{1}{M}\Delta\alpha-\frac{\alpha}{M^2}\Delta M-\frac{7c}{12aM^2}\Delta\dot{\alpha} \end{aligned}$$

This equation provides the noncirculatory pitching moment response at $t = 0$. For $t > 0$,

the noncirculatory response functions $\phi^{nc}_{m_\alpha}(s,M)$, $\phi^{nc}_{m_M}(s,M)$ and $\phi^{nc}_{m_{\dot\alpha}}(s,M)$ are used, i.e.,

$$C^{nc}_m(t,M) = -\frac{1}{M}\Delta\alpha\phi^{nc}_{m_\alpha}(s,M) - \frac{\alpha}{M^2}\Delta M\phi^{nc}_{m_M}(s,M) - \frac{7c}{12aM^2}\Delta\dot\alpha\phi^{nc}_{m_{\dot\alpha}}(s,M) \qquad (2.42)$$

The total response can now be obtained using the Duhamel integral to get

$$\begin{aligned} C^{nc}_m(t,M) &= -\int_0^s \frac{1}{M}\frac{d\alpha}{d\sigma}(\sigma)\phi^{nc}_{m_\alpha}(s-\sigma,M)\,d\sigma \\ &- \int_0^s \frac{\alpha}{M^2}\frac{dM}{d\sigma}(\sigma)\phi^{nc}_{m_M}(s-\sigma,M)\,d\sigma \\ &- \int_0^s \frac{7c}{12aM^2}\frac{d\dot\alpha}{d\sigma}(\sigma)\phi^{nc}_{m_{\dot\alpha}}(s-\sigma,M)\,d\sigma \end{aligned} \qquad (2.43)$$

Indicial Response Functions

The unsteady equations described in the earlier sections involve the use of circulatory and noncirculatory indicial response functions. Representation of these response functions in a suitable form and determination of the coefficients describing them is explained in this section.

Similar to the Wagner function, the compressible indicial response function $\phi^c_n(s,M)$ can be expressed using the Beddoes two term exponential series as

$$\phi^c_n(s,M) = 1 - A_1 e^{-b_1\beta^2 s} - A_2 e^{-b_2\beta^2 s} \qquad (2.44)$$

In this case, the coefficients A_1, A_2, b_1 and b_2 were obtained from CFD results for simulated step changes in angle of attack and fitting the form of Eq. (2.44) to the computed results at each Mach number (see also Lee et al. Ref. 24). Strictly speaking, the linearized indicial coefficients are a function of Mach number, M, and angle of attack, α, at the instant of forcing. This issue is of particular significance at high Mach numbers and angles of attack where the indicial coefficients are more sensitive to changes in the

forcing (M and/or α). However, for most conditions it is reasonable to assume the indicial coefficients to be constant. In the present work, the indicial coefficients were assigned the values $A_1 = 0.3493$, $A_2 = 0.6507$, $b_1 = 0.0984$, $b_2 = 0.7759$ based on results obtained by Lee et al. (Ref. 24). This was found to give good results for a wide range of flow conditions, although further discussion of the nonlinear aspects of this problem are given in Chapter 4. It is important to note the following differences between the Wagner function and its compressible counterpart:

- $A_1 + A_2 = 0.5$ for the Wagner function whereas for the compressible response function, $A_1 + A_2 = 1$. This means that at $\phi_W(t = 0) = 0.5$ and $\phi_W(t \to \infty) = 1$ while $\phi_n^c(M, t = 0) = 0$ and $\phi_n^c(M, t \to \infty) = 1$.

- There is a compressibility scaling factor β^2 in the exponential terms. This factor modifies the indicial response as a function of Mach number and reflects the increased aerodynamic lags in the flow resulting from compressibility effects.

The circulatory pitching moment response function for pitch rate is expressed as

$$\phi_m^c(s, M) = 1 - A_5 e^{-b_5 \beta^2 s} \tag{2.45}$$

where $A_5 = 1$, $b_5 = 5.0$. Notice that b_5 is large in comparison with b_1 or b_2. This means that the exponential term decays to zero very fast (i.e., the steady state is reached almost immediately).

The noncirculatory response for compressible flows has a finite initial value which decays quickly to zero as time progresses. This is modeled by the indicial functions

$$\phi_{n_\alpha}^{nc}(s, M) = \exp\left(\frac{-s}{T_{n_\alpha}}\right) \tag{2.46}$$

$$\phi^{nc}_{n_M}(s,M) = \exp\left(\frac{-s}{T_{n_M}}\right) \tag{2.47}$$

$$\phi^{nc}_{n_{\dot\alpha}}(s,M) = \exp\left(\frac{-s}{T_{n_{\dot\alpha}}}\right) \tag{2.48}$$

$$\phi^{nc}_{m_\alpha}(s,M) = A_3 \exp\left(\frac{-s}{b_3 T_{m_\alpha}}\right) + A_4 \exp\left(\frac{-s}{b_4 T_{m_\alpha}}\right) \tag{2.49}$$

$$\phi^{nc}_{m_M}(s,M) = A_3 \exp\left(\frac{-s}{b_3 T_{m_M}}\right) + A_4 \exp\left(\frac{-s}{b_4 T_{m_M}}\right) \tag{2.50}$$

$$\phi^{nc}_{m_{\dot\alpha}}(s,M) = \exp\left(\frac{-s}{T_{m_{\dot\alpha}}}\right) \tag{2.51}$$

The exact linearized solutions to the subsonic indicial response in the initial stages can be obtained analytically as a function of time (following Ref. 29), i.e.,

$$\begin{aligned} C_{n_w}(s,M) &= \frac{4}{M}\frac{\Delta w}{V}\left[1-\frac{1-M}{2M}s\right] \\ &= \frac{4\Delta\alpha}{M}\left[1-\frac{1-M}{2M}s\right] + \frac{4\alpha\Delta M}{M^2}\left[1-\frac{1-M}{2M}s\right] \end{aligned} \tag{2.52}$$

$$C_{n_{\dot\alpha}}(s,M) = -\frac{1}{M}\frac{c\Delta\dot\alpha}{V}\left[1-\frac{1-M}{2M}s+\frac{2-M}{4M}\frac{s^2}{2M}\right] \tag{2.53}$$

$$\begin{aligned} C_{m_w}(s,M) &= -\frac{1}{M}\frac{\Delta w}{V}\left[1-\frac{1-M}{2M}s+\frac{M-2}{4M}\frac{s^2}{2M}\right] \\ &= -\frac{\Delta\alpha}{M}\left[1-\frac{1-M}{2M}s+\frac{M-2}{4M}\frac{s^2}{2M}\right] - \\ &\quad \frac{\alpha\Delta M}{M^2}\left[1-\frac{1-M}{2M}s+\frac{M-2}{4M}\frac{s^2}{2M}\right] \end{aligned} \tag{2.54}$$

$$\begin{aligned} C_{m_{\dot\alpha}}(s,M) &= \frac{1}{M}\frac{c\Delta\dot\alpha}{V}\left[-\frac{7}{12}+\frac{5(1-M)}{8M}s-\right. \\ &\quad \left.\frac{1-M^2}{8M^2}s^2+\frac{(1-M)^3+4M}{64M^2}s^3\right] \end{aligned} \tag{2.55}$$

However, these results are valid only for a short period, namely $0 \le s \le 2M/(1+M)$.

The coefficients T_{n_α}, T_{n_M}, $T_{n_{\dot\alpha}}$, etc. (in Eqs. 2.46–2.51) can be obtained by matching the slopes of the assumed combined (circulatory and noncirculatory) response to a given forcing (α, M, $\dot\alpha$) at $t = 0$ with the results obtained from linear theory. Using this approach

it can be shown that

$$T_{n_\alpha} = \frac{4Mk_\alpha}{2(1-M)+2\pi M^2\beta(A_1b_1+A_2b_2)} \tag{2.56}$$

$$T_{n_M} = \frac{4Mk_M}{2(1-M)+2\pi M^2\beta^{-1}(A_1b_1+A_2b_2)} \tag{2.57}$$

$$T_{n_{\dot\alpha}} = \frac{2Mk_{\dot\alpha}}{(1-M)+2\pi M^2\beta(A_1b_1+A_2b_2)} \tag{2.58}$$

$$T_{m_\alpha} = \frac{2Mk_{m_\alpha}(A_3b_4+A_4b_3)}{b_3b_4(1-M)} \tag{2.59}$$

$$T_{m_M} = \frac{2Mk_{m_\alpha}(A_3b_4+A_4b_3)}{b_3b_4(1-M)} \tag{2.60}$$

$$T_{m_{\dot\alpha}} = \frac{14Mk_{m_{\dot\alpha}}}{15(1-M)+3\pi M^2\beta A_5b_5} \tag{2.61}$$

The coefficients k_α, k_M, etc. are modifiers that represent variations in the initial values of the indicial response because of two-dimensional effects (piston theory is a one-dimensional theory). Normally, the values are set to 0.75. The indicial coefficients associated with the noncirculatory pitching moment response were assigned the values $A_3 = 1.5$, $A_4 = -0.5$, $b_3 = 0.25$, $b_4 = 0.1$ based on results obtained by Lee et al. (Ref. 24).

Now that the circulatory and noncirculatory indicial responses are completely defined, the lift and pitching moment can be obtained for any arbitrary forcing. Figure 2.7 shows the indicial response to a step change in angle of attack ($\alpha_m = 0^\circ$, $\Delta\alpha = 1^\circ$) for Mach numbers of $M = 0.3$ and 0.5. It is seen that for low to moderate subsonic Mach numbers, there is very good agreement between the CFD and the indicial results. For the higher (supercritical) Mach number of 0.8, there are some differences between CFD and indicial model in its present form (see Fig. 2.8). These differences arise because of the limitations of the steady linear compressible theory as well as because of nonlinear effects at supercritical Mach numbers. This can be corrected by modifying the indicial method so that the lift curve slope is obtained directly from steady-state CFD predictions instead

of steady linear compressible theory. This issue is discussed in greater detail in Chapter 4.

2.2.3 Existing (Old) Indicial Model

The previous sections have described the new indicial model involving changes in Mach number. Previously, compressible flow calculations involving Mach number variations were performed using an approach similar to the one proposed, but with some important differences. The circulatory lift response was previously obtained by introducing the Glauert factor *outside* the Duhamel integral, i.e., by writing

$$\begin{aligned} C_n^c(t,M) &= \frac{1}{V\beta}\Big[\left(2\pi w_{3/4}\right)(s=0)\phi_n^c(s,M) + \\ &\quad \int_0^s \frac{d}{d\sigma}\left(2\pi w_{3/4}\right)(\sigma)\phi_n^c(s-\sigma,M)\,d\sigma\Big] \end{aligned} \tag{2.62}$$

The circulatory response function $\phi_n^c(s,M)$ is identical for the new and existing models. For the noncirculatory component of the lift, however, the old model does not have the additional forcing term resulting from changes in Mach number. In the latter case

$$C_n^{nc}(t) = \int_0^s \frac{4}{M}\frac{d\alpha}{d\sigma}(\sigma)\phi_{n_\alpha}^{nc}(s-\sigma,M)\,d\sigma + \int_0^s \frac{c}{aM^2}\frac{d\dot{\alpha}}{d\sigma}(\sigma)\phi_{n_{\dot{\alpha}}}^{nc}(s-\sigma,M)\,d\sigma \tag{2.63}$$

Comparing Eq. (2.63) with Eq. (2.38), it is seen that the old model has only two terms as compared to the three terms that are used in the new model. The indicial response functions and the time constants are identical for the two models.

2.3 Numerical Solution Methodology

The primary motivation behind using the indicial method is that it provides orders of magnitude reduction in computational time as compared to CFD. Therefore, it becomes

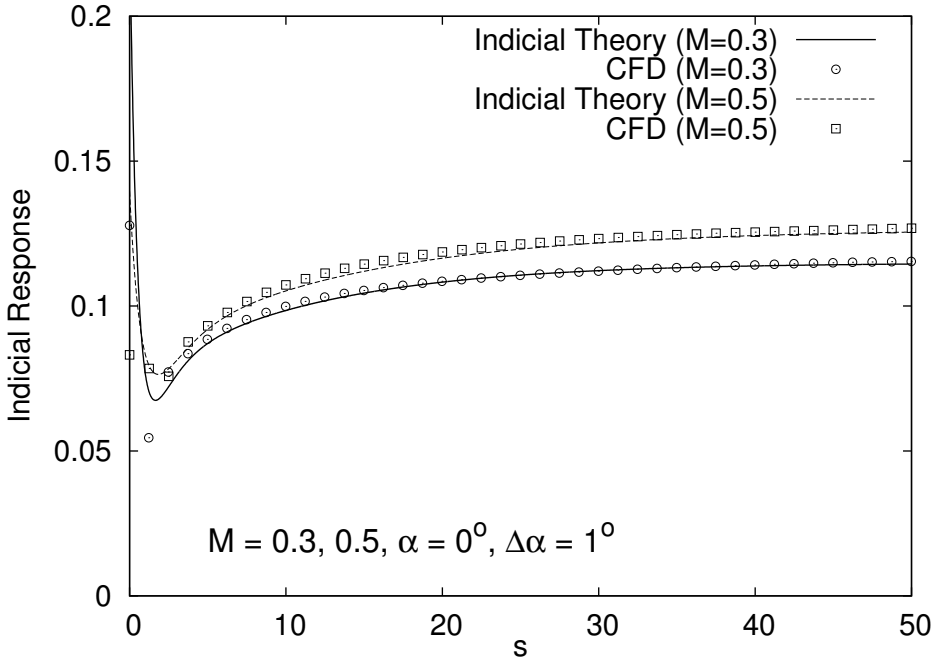

Figure 2.7: Comparison of the indicial response to change in α for $\alpha_m = 0^\circ$ and $M = 0.3$, 0.5.

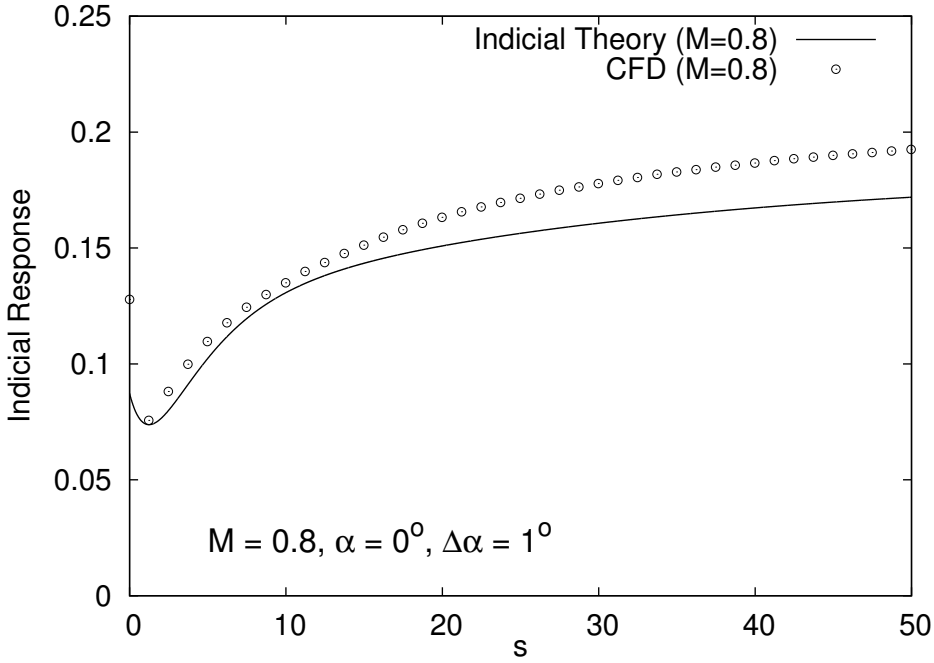

Figure 2.8: Comparison of the indicial response to change in α for $\alpha_m = 0^\circ$, $\Delta\alpha = 1^\circ$, $M = 0.8$.

important to use efficient numerical algorithms to reduce the computational cost, while at the same time maintaining a good level of accuracy. The following sections describe the numerical issues involved in implementing the indicial method.

2.3.1 The Duhamel Integral

The indicial method involves the evaluation of the Duhamel integral for calculating the circulatory and noncirculatory airloads. An exact analytical solution to the Duhamel integral is possible only for trivial flows, and numerical techniques have to be used for solving more general problems. Because the solution procedure is the same for both circulatory and noncirculatory terms, only the circulatory part is discussed here. Depending on whether the Mach number is constant or varying with time, different approaches need to be used. For constant Mach number flows, the recurrence algorithms developed by Beddoes & Leishman (Refs. 1, 3) are adequate, providing significant reductions in the computational time. When the Mach number is not constant, alternate algorithms must be used, and the solution process becomes computationally more expensive. However, the indicial method still remains at least three orders of magnitude faster than the corresponding CFD computation.

From Eq. (2.27) the circulatory lift was shown to be of the form

$$\begin{aligned} C_n^c(t,M) &= \frac{1}{V}\left[C_{n_\alpha} w_{3/4}(0)\phi_n^c(s) + \int_0^s \frac{dC_{n_\alpha} w_{3/4}}{d\sigma}(\sigma)\phi_n^c(s-\sigma)\right] \\ &= \frac{1}{V}\left[(C_{n_\alpha} w_{3/4})_{\text{eff}}(s)\right] \end{aligned} \tag{2.64}$$

where the notation $(C_{n_\alpha} w_{3/4})_{\text{eff}}(s)$ is used for ease of representation. If a two term exponentially growing indicial response function is used in the form

$$\phi_n^c(s) = 1 - A_1 e^{-b_1 \beta^2 s} - A_2 e^{-b_2 \beta^2 s} \tag{2.65}$$

then the expression within square brackets in Eq. (2.64) can be written as

$$\begin{aligned}
(C_{n_\alpha} w_{3/4})_{\text{effective}}(s) &= C_{n_\alpha} w_{3/4}(0)\phi_n^c(s) + \int_0^s \frac{dC_{n_\alpha} w_{3/4}}{d\sigma}(\sigma)\phi_n^c(s-\sigma)d\sigma \\
&= C_{n_\alpha} w_{3/4}(0)\left(1 - A_1 e^{-b_1\beta^2 s} - A_2 e^{-b_2\beta^2 s}\right) + \\
&\quad \int_0^s \frac{dC_{n_\alpha} w_{3/4}}{d\sigma}(\sigma)\left(1 - A_1 e^{-b_1\beta^2(s-\sigma)} - A_2 e^{-b_2\beta^2(s-\sigma)}\right)d\sigma \\
&= C_{n_\alpha} w_{3/4}(0) - A_1 C_{n_\alpha} w_{3/4}(0) e^{-b_1\beta^2 s} - A_2 C_{n_\alpha} w_{3/4}(0) e^{-b_2\beta^2 s} + \\
&\quad \int_0^s dC_{n_\alpha} w_{3/4}(s) - \int_0^s A_1 \frac{dC_{n_\alpha} w_{3/4}}{d\sigma}(\sigma) e^{-b_1\beta^2(s-\sigma)}d\sigma - \\
&\quad \int_0^s A_2 \frac{dC_{n_\alpha} w_{3/4}}{d\sigma}(\sigma) e^{-b_2\beta^2(s-\sigma)}d\sigma
\end{aligned} \tag{2.66}$$

The terms $A_1 C_{n_\alpha} w_{3/4}(0) e^{-b_1\beta^2 s}$ and $A_2 C_{n_\alpha} w_{3/4}(0) e^{-b_2\beta^2 s}$, which contain the initial value of $C_{n_\alpha} w_{3/4}$, are short term transients and can be neglected. Therefore, the Duhamel integral can be rewritten as

$$\begin{aligned}
(C_{n_\alpha} w_{3/4})_e(s) &= C_{n_\alpha} w_{3/4}(0) + C_{n_\alpha} w_{3/4}(s) - C_{n_\alpha} w_{3/4}(0) - X(s) - Y(s) \\
&= C_{n_\alpha} w_{3/4}(s) - X(s) - Y(s)
\end{aligned} \tag{2.67}$$

where the X and Y terms are given by

$$X(s) = \int_0^s A_1 \frac{dC_{n_\alpha} w_{3/4}}{d\sigma}(\sigma) e^{-b_1\beta^2(s-\sigma)}d\sigma \tag{2.68}$$

$$Y(s) = \int_0^s A_2 \frac{dC_{n_\alpha} w_{3/4}}{d\sigma}(\sigma) e^{-b_2\beta^2(s-\sigma)}d\sigma \tag{2.69}$$

The X and Y terms are often called "deficiency" functions. They may take on either positive or negative values.

2.3.2 Recurrence Algorithm (M = constant)

Consider the manipulation of the $X(s)$ term. The $Y(s)$ term can be treated likewise. Assuming a continuously sampled system with time step Δs (which may be non-uniform), then at the next time step

$$X(s+\Delta s) = \int_0^{s+\Delta s} A_1 \frac{dC_{n_\alpha} w_{3/4}}{d\sigma}(\sigma) e^{-b_1\beta^2(s+\Delta s-\sigma)} d\sigma \tag{2.70}$$

Splitting the integral into two parts gives

$$\begin{aligned} X(s+\Delta s) &= \int_0^{s} A_1 \frac{dC_{n_\alpha} w_{3/4}}{d\sigma}(\sigma) e^{-b_1\beta^2(s+\Delta s-\sigma)} d\sigma + \\ &\quad \int_s^{s+\Delta s} A_1 \frac{dC_{n_\alpha} w_{3/4}}{d\sigma}(\sigma) e^{-b_1\beta^2(s+\Delta s-\sigma)} d\sigma \\ &= \int_0^{s} A_1 \frac{dC_{n_\alpha} w_{3/4}}{d\sigma}(\sigma) e^{-b_1\beta^2(s-\sigma)} e^{-b_1\beta^2\Delta s} d\sigma + \\ &\int_s^{s+\Delta s} A_1 \frac{dC_{n_\alpha} w_{3/4}}{d\sigma} e^{b_1\beta^2\sigma} e^{-b_1\beta^2(s+\Delta s)} d\sigma \end{aligned} \tag{2.71}$$

Because the indicial coefficients, A_1, b_1, A_2, b_2 and β are constant (linear indicial method with constant Mach number), the term $e^{-b_1\beta^2\Delta s}$ can be taken outside the integral

$$\begin{aligned} X(s+\Delta s) &= e^{-b_1\beta^2\Delta s} \int_0^{s} A_1 \frac{dC_{n_\alpha} w_{3/4}}{d\sigma}(\sigma) e^{-b_1\beta^2(s-\sigma)} d\sigma \\ &\quad + \int_s^{s+\Delta s} A_1 \frac{dC_{n_\alpha} w_{3/4}}{d\sigma} e^{-b_1\beta^2(s+\Delta s-\sigma)} d\sigma \\ &= X(s) e^{-b_1\beta^2\Delta s} + I \end{aligned} \tag{2.72}$$

Notice that this new value, $X(s+\Delta s)$, is a one-step recurrence formula in terms of the previous value, $X(s)$, and a new increment, I, over the new period. No information at earlier time steps need be saved to evaluate this expression.

Consider now the evaluation of the I term. Again, because the indicial coefficients (A_1, b_1, A_2, b_2) and β are constant, the term $A_1 e^{-b_1\beta^2(s+\Delta s)}$ can be taken outside the

integral

$$
\begin{aligned}
I &= \int_s^{s+\Delta s} A_1 \frac{dC_{n_\alpha} w_{3/4}}{d\sigma}(\sigma) e^{-b_1\beta^2(s+\Delta s-\sigma)} d\sigma \\
&= \int_s^{s+\Delta s} A_1 \frac{dC_{n_\alpha} w_{3/4}}{d\sigma}(\sigma) e^{b_1\beta^2\sigma} e^{-b_1\beta^2(s+\Delta s)} d\sigma \\
&= A_1 e^{-b_1\beta^2(s+\Delta s)} \int_s^{s+\Delta s} \frac{dC_{n_\alpha} w_{3/4}}{d\sigma}(\sigma) e^{b_1\beta^2\sigma} d\sigma \\
&= A_1 e^{-b_1\beta^2(s+\Delta s)} \int_s^{s+\Delta s} \frac{dC_{n_\alpha} w_{3/4}}{d\sigma}(\sigma) f(\sigma) d\sigma
\end{aligned} \tag{2.73}
$$

with $f(\sigma) = e^{b_1\beta^2\sigma}$ in this case. At this point, several simplifying assumptions can be made. Introducing a simple backward-difference approximation for $d(C_{n_\alpha} w_{3/4})/ds$ at time $s+\Delta s$ gives

$$
\begin{aligned}
\left.\frac{dC_{n_\alpha} w_{3/4}}{d\sigma}\right|_{s+\Delta s} &= \frac{C_{n_\alpha} w_{3/4}(s+\Delta s) - C_{n_\alpha} w_{3/4}(s)}{\Delta s} \\
&= \frac{\Delta(C_{n_\alpha} w_{3/4})_{s+\Delta s}}{\Delta s}
\end{aligned} \tag{2.74}
$$

which has an error of order $(C_{n_\alpha} w_{3/4})''(s+\Delta s)\Delta s$. The remaining part of the integral involving $f(\sigma)$ can be evaluated exactly and I becomes

$$
I = A_1 \left(\frac{\Delta(C_{n_\alpha} w_{3/4})_{s+\Delta s}}{\Delta s} \right) \left(\frac{1 - e^{-b_1\beta^2\Delta s}}{b_1\beta^2} \right) \tag{2.75}
$$

$$
= A_1 \left(\frac{\Delta(C_{n_\alpha} w_{3/4})_{s+\Delta s}}{\Delta s} \right) \left(\frac{1 - e^{-b_1\beta^2\Delta s}}{b_1\beta^2\Delta s} \right) \Delta s \tag{2.76}
$$

$$
\approx A_1 \Delta(C_{n_\alpha} w_{3/4})_{s+\Delta s} \tag{2.77}
$$

Notice that the recurrence functions X and Y contain all the time-history information of the unsteady aerodynamics, and are simply updated once at each time step. This approach, thereby provides numerically efficient solutions to the unsteady aerodynamics for arbitrary variations in forcing. Obviously, the results can be extended to any mode of

forcing and to any number of exponential terms that may be used to represent the indicial response function.

2.3.3 Exact Algorithm ($M \neq$ constant)

The recurrence algorithm discussed above is valid only when the indicial coefficients and β are constant (i.e., the free-stream Mach number is constant). When the indicial coefficients and/or β are not constant, the above algorithm is no longer accurate. The exact analytical expression for $X(s)$ is given by

$$X(s) = \int_0^s A_1 \frac{dC_{n_\alpha} w_{3/4}}{d\sigma}(\sigma) e^{-b_1 \beta^2(s)(s-\sigma)} d\sigma \tag{2.78}$$

Notice that β has been replaced by $\beta(s)$ to indicate that it is dependent on time. Because β is no longer constant, the manipulations in Eq. (2.72) and Eq. (2.73) can no longer be made, and $X(s)$ has to be calculated by evaluating the Duhamel integral repeatedly for each instant of time. This is done using

$$\begin{aligned} X(s) &= \int_0^s \frac{dC_{n_\alpha} w_{3/4}}{d\sigma}(\sigma) A_1 e^{-b_1 \beta^2(s)(s-\sigma)}\, d\sigma \\ &= \sum_{i=1}^{N} \Delta(C_{n_\alpha} w_{3/4})_i A_1 e^{-b_1 \beta_N^2 (s-\sigma_i)} \\ &= \Delta(C_{n_\alpha} w_{3/4})_1 A_1 e^{-b_1 \beta_N^2 (s-\sigma_1)} + \Delta(C_{n_\alpha} w_{3/4})_2 A_1 e^{-b_1 \beta_N^2 (s-\sigma_2)} + \cdots \\ &\quad \Delta(C_{n_\alpha} w_{3/4})_{N-1} A_1 e^{-b_1 \beta_N^2 (s-\sigma_{N-1})} + \Delta(C_{n_\alpha} w_{3/4})_N A_1 e^{-b_1 \beta_N^2 (s-\sigma_N)} \end{aligned} \tag{2.79}$$

In the above equation, $\sigma_1, \sigma_2, \ldots, \sigma_N$ correspond to the reduced time at the various instants of forcing. Notice that β^2 in the exponent is always evaluated at time t or s (i.e., at the instant when the lift is calculated) and not at the instant when the forcing is applied (i.e., at σ_1, σ_2, etc.). From the above equation it is seen that the entire time history of the forcing has to be stored and summed to obtain the airloads at any given time. This

makes the exact algorithm an O(N^2) algorithm, compared to the recurrence algorithm which is O(N), where N is the total number of time-steps. While this involves additional computational overhead, it is still at least three orders of magnitude faster than CFD, as long as the computation does not involve several cycles of oscillation (or equivalently, a large number of time-steps). Figures 2.9 and 2.10 show two cases where the recurrence algorithm gives rise to errors in the lift prediction. The advantage of using the exact algorithm is clearly evident from these examples.

However, one drawback of the exact algorithm is that if the problem involves several cycles of oscillation (say hundreds of cycles), then the cost of storing the entire time history of the forcing and computing the contribution of each forcing event separately can get prohibitively expensive, rendering the computational advantage of the indicial method invalid. For example, consider a case where the airfoil undergoes 100 cycles of oscillation. If it is assumed that there are 500 time-steps per cycle then this would involve a total of $500 \times 100 = 5 \times 10^4$ time-steps. This means that the exact algorithm would be 5×10^4 times more expensive than the recurrence algorithm (O(N^2) versus O(N)). Figure 2.11 clearly shows that the computational cost increases rapidly as the number of cycles increases (i.e., as the computation is performed for extended periods of time). It is, therefore, essential to develop an alternative numerical scheme that combines the computational efficiency of the recurrence algorithm while retaining the accuracy of the exact algorithm.

The following section describes a modified approach to solve the Duhamel integral involving a combination of the recurrence and exact approaches, which is shown to give the same degree of accuracy of the exact method but at a lower computational cost. It is

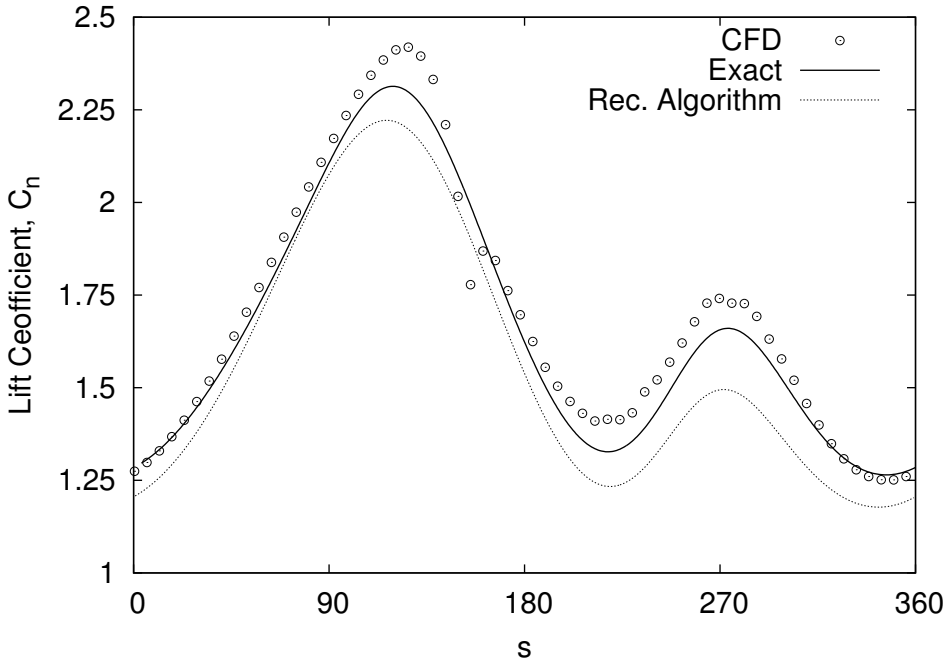

Figure 2.9: Lift predictions using the exact and the recurrence algorithms for combined variations in angle of attack and Mach number, $M_0 = 0.5$, $\lambda = 0.6$, $\alpha = 1^\circ + 1^\circ \sin \omega t$.

based on the fact that the indicial response is nearly constant (or varies very gradually) after about 15 to 20 chord lengths of reduced time after the forcing is applied. Therefore only those forcing events (such as a change in α, $\dot{\alpha}$ or M) that are less than 15 to 20 chord lengths (of reduced time) old, need to be calculated exactly. The contribution of the remaining forcing events to the total lift can be computed approximately using the recurrence algorithm.

2.3.4 Modified Algorithm

This approach combines the positive features of both the recurrence and the exact algorithms. Here, the recurrence algorithm is used to compute the contribution to the total lift from events (forcing) that occurred a long time back, while the exact algorithm is used to

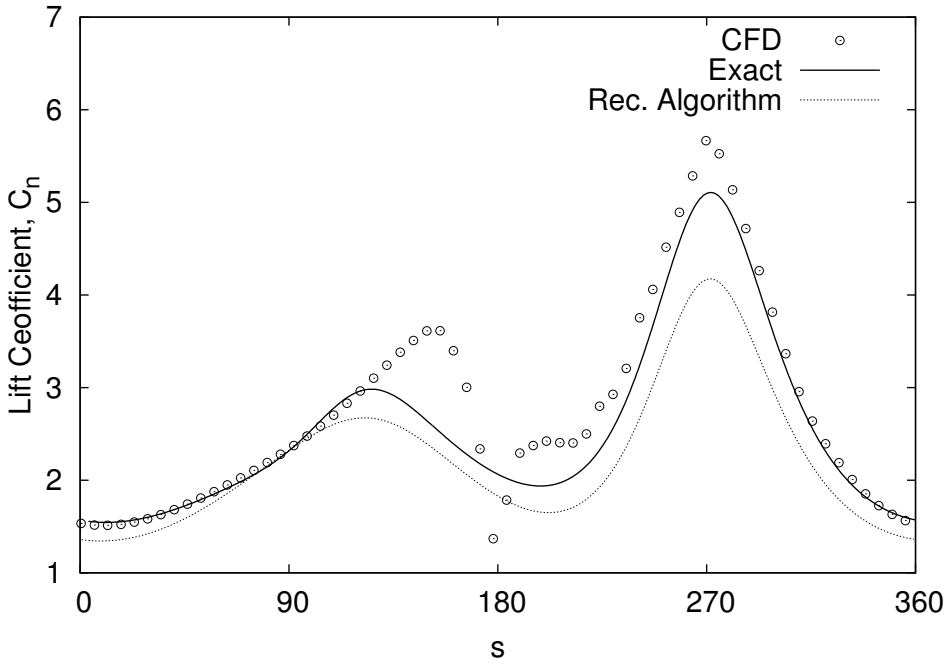

Figure 2.10: Lift predictions using the exact and the recurrence algorithms for combined variations in angle of attack and Mach number, $M_0 = 0.5$, $\lambda = 0.8$, $\alpha = 1^\circ + 1^\circ \sin \omega t$.

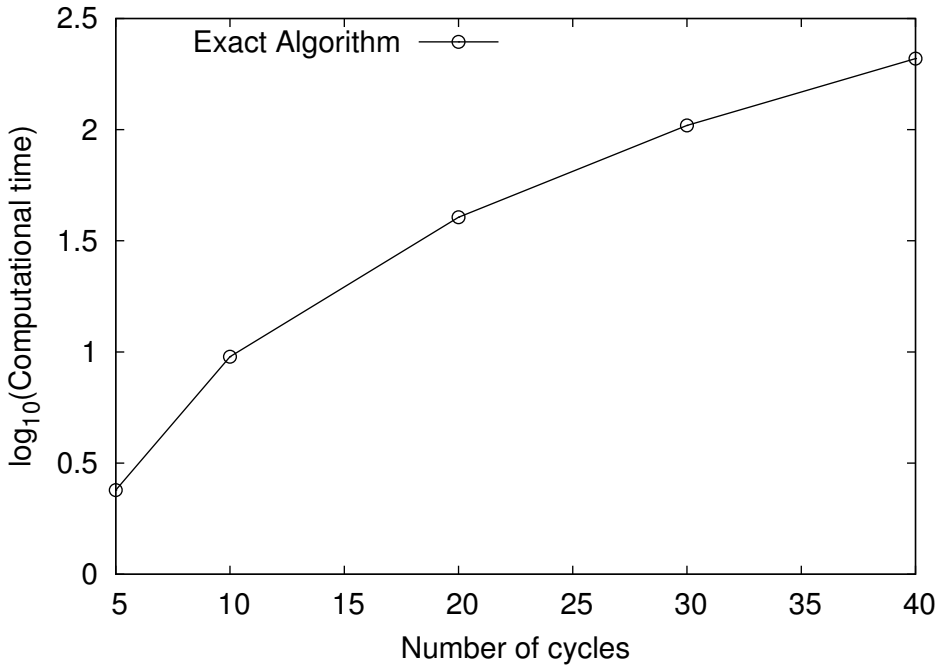

Figure 2.11: Semilog plot of the computational time vs the number of cycles using the exact algorithm (Total number of cycles = 30).

compute the contribution from recent events. The $X(s)$ term is split into two parts where,

$$\begin{aligned} X(s) &= \int_0^s A_1 \frac{d(C_{n_\alpha} w_{3/4})}{d\sigma}(\sigma) e^{-b_1 \beta^2(s)(s-\sigma)}\, d\sigma \\ &= \int_0^{s^*} A_1 \frac{d(C_{n_\alpha} w_{3/4})}{d\sigma}(\sigma) e^{-b_1 \beta^2(s)(s-\sigma)}\, d\sigma + \int_{s^*}^s A_1 \frac{d(C_{n_\alpha} w_{3/4})}{d\sigma}(\sigma) e^{-b_1 \beta^2(s)(s-\sigma)}\, d\sigma \\ &= X_1(s) + X_2(s) \end{aligned} \tag{2.80}$$

In the above equation, the first integral, $X_1(s)$, contains the contribution to $X(s)$ of the events (forcing) that occurred a long time back (corresponding to $s < s^*$). It is relatively small in comparison with $X_2(s)$, which contains the contribution of forcing events that took place recently ($s > s^*$). Because the contribution of $X_1(s)$ to $X(s)$ is relatively small, it is reasonable to permit some errors in its calculation. $X_1(s)$ can therefore be calculated using the recurrence algorithm, without any significant loss in the overall accuracy of $X(s)$. The value of the integral $X_2(s)$ is significant because it represents the sum of the indicial responses from recent forcing events. The exact algorithm is, therefore, used to evaluate the $X_2(s)$ integral. The quantity $X(s+\Delta s)$ can be written as

$$\begin{aligned} X(s+\Delta s) &= X_1(s+\Delta s) + X_2(s+\Delta s) \\ X_1(s+\Delta s) &= X_1(s) e^{-b_1 \beta^2(s)\Delta s} + A_1 \Delta (C_{n_\alpha} w_{3/4})_{N-m} e^{-b_1 \beta^2(s)(s-s^*)} \\ X_2(s+\Delta s) &= \sum_{i=N-m+1}^{N} A_1 \Delta (C_{n_\alpha} w_{3/4})_i e^{-b_1 \beta^2(s)(s-\sigma_i)} \end{aligned} \tag{2.81}$$

where m is the time-step corresponding to $s = s^*$ measured backwards in time (i.e., if Δs is constant, then $m\Delta s = s - s^*$) and N is the total number of time-steps ($N =$ time-steps per cycle $\times$ number of cycles). The value of m can, therefore, be viewed as an accuracy factor; $m = 1$ yields the recurrence algorithm while $m = N$ yields the exact algorithm. For intermediate values of m, a modified (and improved) recurrence algorithm is produced

that is both computationally efficient and numerically accurate. The choice of s^* (or equivalently, the choice of m) depends on the range of variation of the Mach number. At higher Mach numbers, the exact algorithm has to be used for a longer period of time (i.e., higher m) because the indicial response asymptotes to the steady-state value more slowly (as modeled by the β^2 factor in the exponential terms of the indicial response function). If the range of Mach numbers is not high, or if the flow is largely in the incompressible range, then the recurrence algorithm is usually adequate. The modified algorithm gives greater flexibility to the analyst, enabling a balance between the accuracy and computational efficiency to suit the specific needs of the problem.

2.3.5 Performance Comparison

Figures 2.12 and 2.13 show the results obtained for a mean Mach number of 0.5, $\lambda = 0.4$ and $\lambda = 0.6$. The runs were performed using 500 time-steps per cycle for 30 cycles of oscillation. The unsteady lift variation is shown for different values of m expressed in terms of number of cycles (i.e., 2.0 cycles would correspond to $m = 2.0 \times 500 = 1000$). For $\lambda = 0.4$ (see Fig. 2.12) it is seen that the differences between the recurrence and the exact algorithms are not significant. This is mainly because the Mach numbers involved are not too high and consequently the time-lags associated with the indicial response are not substantially different from the incompressible case (i.e., β is close to unity). It is seen that when two cycles of oscillation are calculated exactly and the remaining three are calculated using the recurrence algorithm, the results are nearly identical to the the exact algorithm (where all 30 cycles are computed exactly). For $\lambda = 0.6$ (see Fig. 2.13), it is seen that there are significant differences between the exact and the recurrence algorithms.

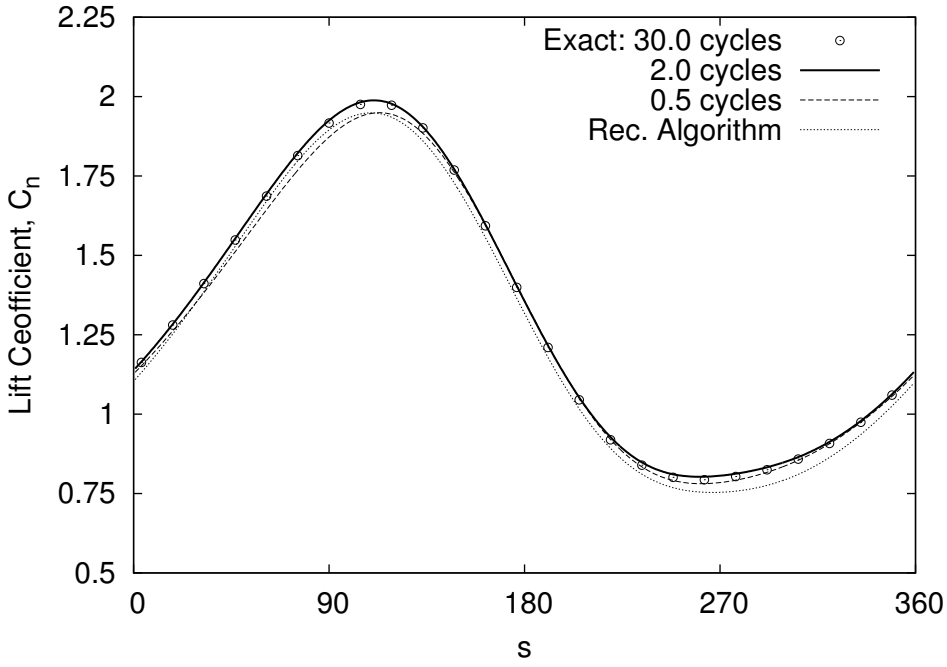

Figure 2.12: Lift predictions using the exact and the modified algorithm for combined variations in angle of attack and Mach number, $M_0 = 0.5$, $\lambda = 0.4$, $\alpha = 1^\circ + 1^\circ \sin \omega t$.

The modified algorithm is shown to provide nearly the same degree of accuracy as the exact algorithm when 2.5 cycles are calculated exactly.

Figure 2.14 shows log-log plot of the computational time versus the number of cycles using the exact and the modified algorithms. From the slope of the lines, notice that the exact algorithm is a second order method of O(N^2) while the modified algorithm is a first order method of O(Nm). Clearly, the modified algorithm offers a significant reduction in the computational time.

Figure 2.15 compares the relative computational time involved in computing the unsteady airloads using the CFD and the different numerical algorithms. It is evident that the recurrence algorithm is computationally nearly five orders of magnitude faster than an equivalent CFD computation. However, it is not numerically accurate for flows

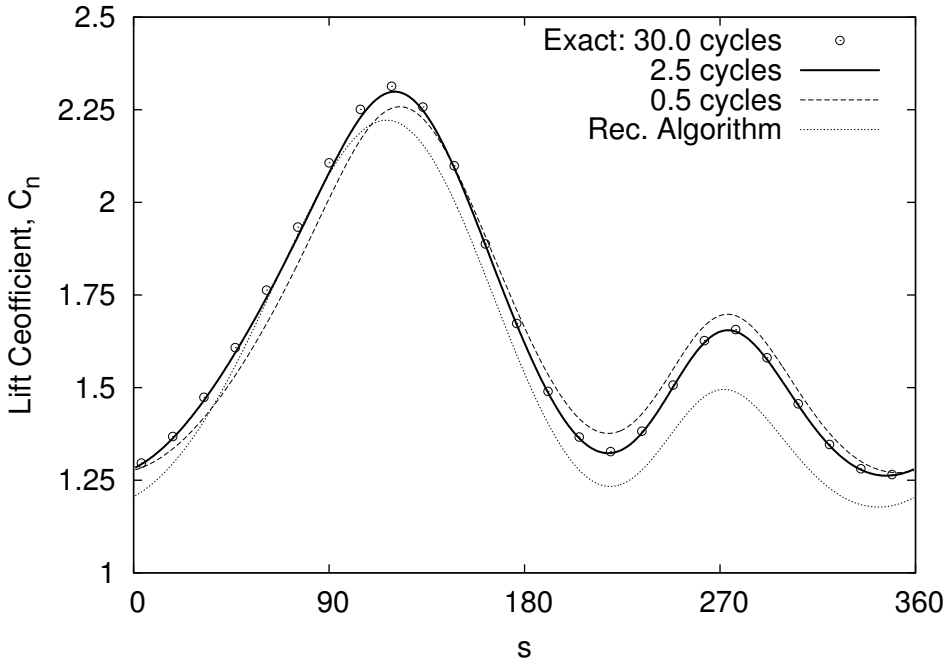

Figure 2.13: Lift predictions using the exact and the modified algorithm for combined variations in angle of attack and Mach number, $M_0 = 0.5$, $\lambda = 0.6$, $\alpha = 1^\circ + 1^\circ \sin \omega t$.

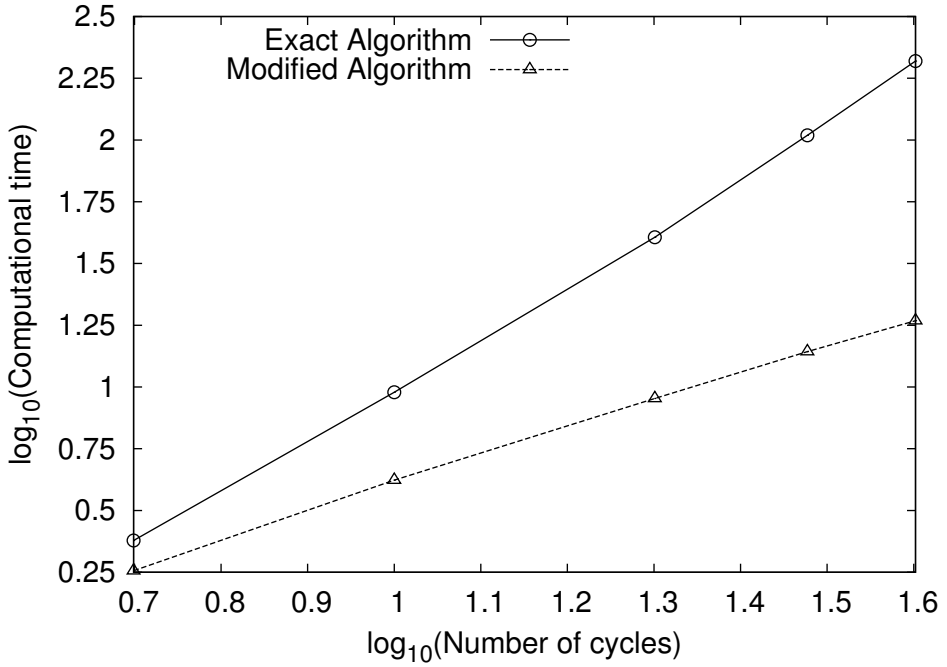

Figure 2.14: Log-log plot of the computational time versus the number of cycles, using the exact and the modified algorithms.

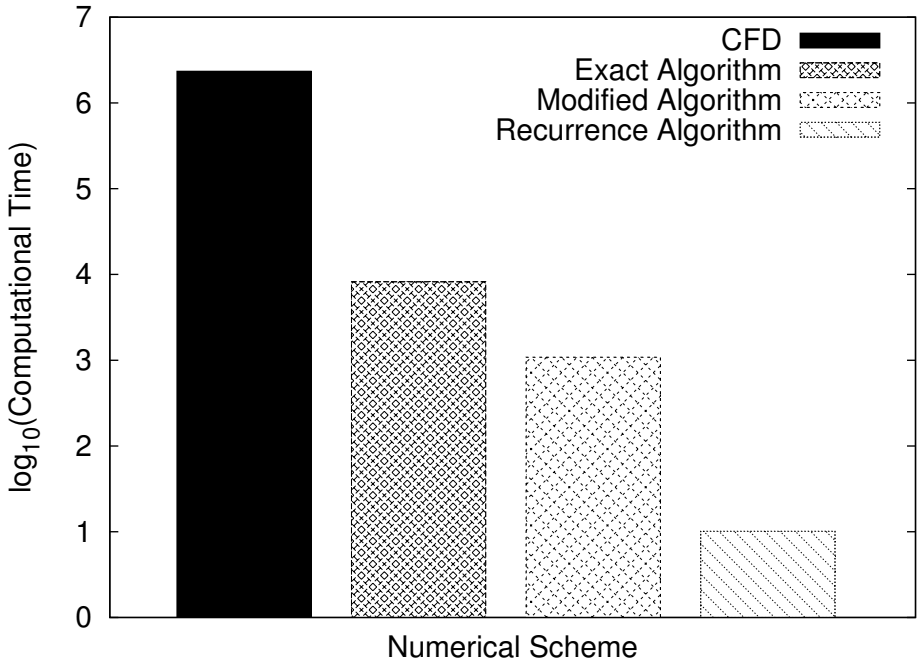

Figure 2.15: Comparison of computational times using different numerical schemes for a test case involving 30 cycles of oscillation.

with time-varying free-stream Mach numbers. The exact algorithm is computationally more expensive than the recurrence algorithm, but provides accurate solutions for the indicial formulation. The modified algorithm provides a computationally less expensive alternative that has the same accuracy as the exact algorithm. The computational expense of using the modified algorithm depends on the actual flow problem. For example in the inboard regions where the flow operates in the low subsonic regime, the recurrence algorithm is adequate. The modified algorithm is needed only in the far-outboard regions of the blade where the Mach numbers are higher.

Chapter 3

Results and Discussion

This chapter compares the results obtained using the incompressible indicial theory, the existing compressible theory, and the revised compressible theory against CFD results for a wide range of flow conditions. Based on the indicial models described in the earlier sections, results have been computed for various non-steady, periodic flow conditions. The parameters of importance are: M_0 (mean value of the Mach number), λ (perturbation velocity ratio), α_m (mean angle of attack), $\overline{\alpha}$ (amplitude of pitch oscillations), and k (reduced frequency). In each case, the forcing is assumed to be of the form

$$M = M_0(1+\lambda\sin\omega t)$$

$$\alpha = \alpha_m + \overline{\alpha}\sin(\omega t+\psi)$$

where ψ is the phase difference between the Mach number and angle of attack oscillations. In all cases, the normal force coefficient has been normalized by the linearized steady-state lift; the incompressible lift coefficient is normalized by $2\pi\alpha_0$, and the compressible lift coefficient is normalized by $2\pi\alpha_0/\beta$. The CFD and indicial codes were executed for five cycles of oscillation so that the initial transients were completely removed. The last cycle was used to show the results. A CFD run usually involved 6286 time steps with six Newton sub-iterations per time step. The indicial method was run using 500 time-steps per cycle. It was seen that the indicial method reduces the computational time by nearly three to four orders of magnitude. This is the primary computational advantage of the

indicial method that makes it suitable for routine rotor analysis codes. The CFD results were normalized by using the steady-state lift obtained at M_0 and α_0. The results are discussed for three separate conditions (cases):

1. Constant free-stream Mach number with oscillatory variations in angle of attack.

2. Constant angle of attack with an oscillating free-stream Mach number.

3. Combined angle of attack and free-stream Mach number oscillations.

3.1 Case 1: Constant Free-Stream Mach Number with Oscillatory Pitch Motion

Figures 3.1, 3.2, 3.3, 3.4 show the normalized lift and pitching moment variation for constant Mach number and oscillating angle of attack for different Mach numbers (0.3, 0.5, 0.65 and 0.8). Figures 3.1 and 3.2 show results for $\alpha = 1^\circ + 1^\circ \sin \omega t$. There is excellent agreement in the lift predictions between the indicial model and CFD for all free-stream Mach numbers. The pitching moment predictions also agree well with the CFD results. This is because at low angles of attack nonlinear effects associated with the compressibility of the flow are small.

If the amplitude of the pitch oscillations is increased further to $\alpha = 2^\circ + 2^\circ \sin \omega t$ (see Figs. 3.3 and 3.4), it is seen that the results for $M = 0.8$ begin to differ in magnitude and phase (especially for the pitching moment). The reason behind this can be better understood by viewing the pressure distribution over the airfoil at various instants of time (see Fig. 3.5). It is observed that at all times, a shock wave is present on the upper surface

of the airfoil. The shock wave moves back and forth as the airfoil oscillates, affecting the pressure distribution over the airfoil. Because the indicial model does not explicitly account for the presence or movement of shock waves, it is less capable in predicting the unsteady airloads. The pitching moment is particularly affected because it is very sensitive to any phenomena that can change the distribution of chordwise pressure (and hence the aerodynamic center and center of pressure) over the airfoil. Notice also that when the Mach number is constant, the predictions from the existing indicial model and the new indicial model are identical in all respects. This follows from the fact that β is constant and there are no additional noncirculatory terms arising from variations in the Mach number.

3.2 Case 2: Constant Angle of Attack with Varying Free-Stream Mach Number

Figures 3.6, 3.7, 3.8 and 3.9 show the normalized lift and pitching moment variation for constant angle of attack and varying free-stream Mach number for perturbation velocity ratios of 0.2, 0.4, 0.6 and 0.8. From the results in Figs. 3.6 and 3.7, it is seen that for a mean Mach number of 0.3 there is very good agreement between CFD and the indicial models. However, the new compressible indicial model yields better results than both the incompressible theory and the existing indicial theory for all values of λ. The indicial pitching moment predictions follow the CFD results in phase, but differ slightly in magnitude in the low Mach number region. This is because of the slight differences in the prediction of the unsteady lift, as well as uncertainties in the estimation of the center of

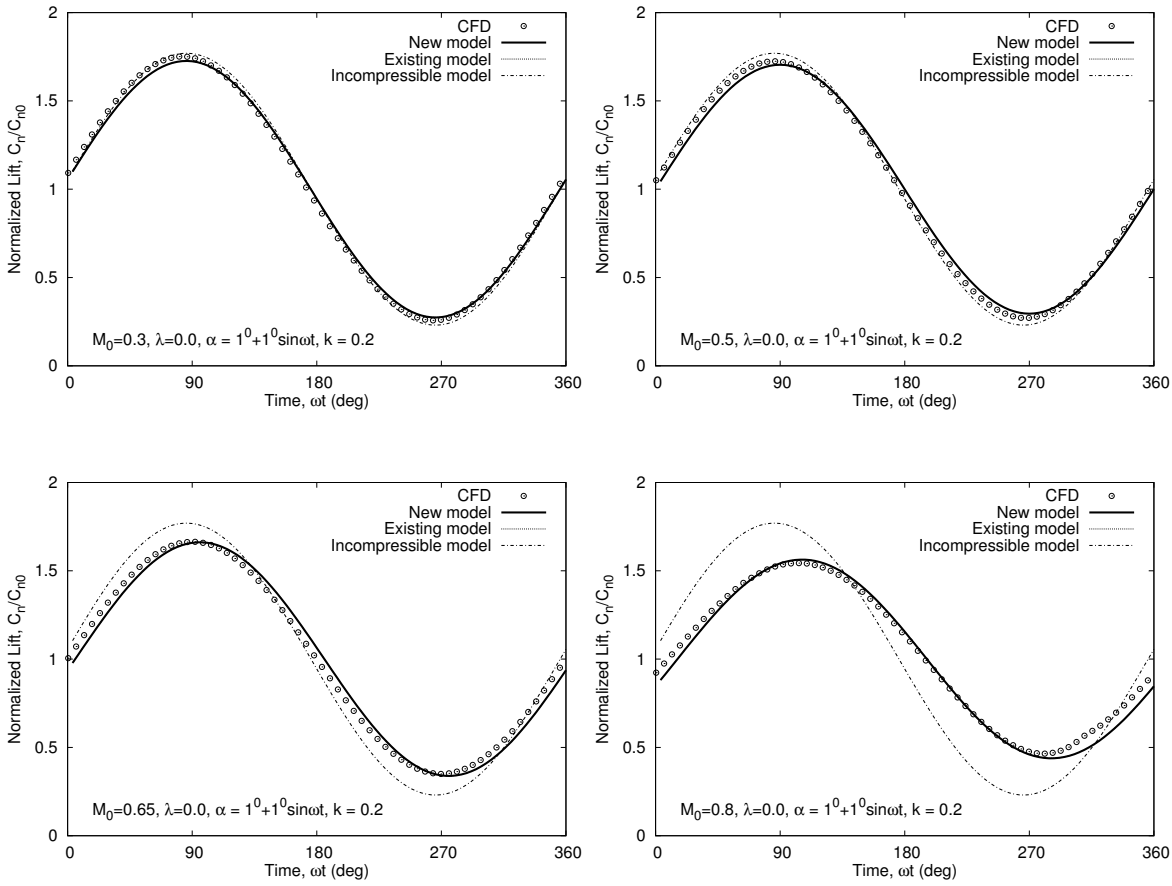

Figure 3.1: Variation of lift coefficient for constant Mach number and oscillating angle of attack for $\alpha = 1^\circ + 1^\circ \sin \omega t, k = 0.2$.

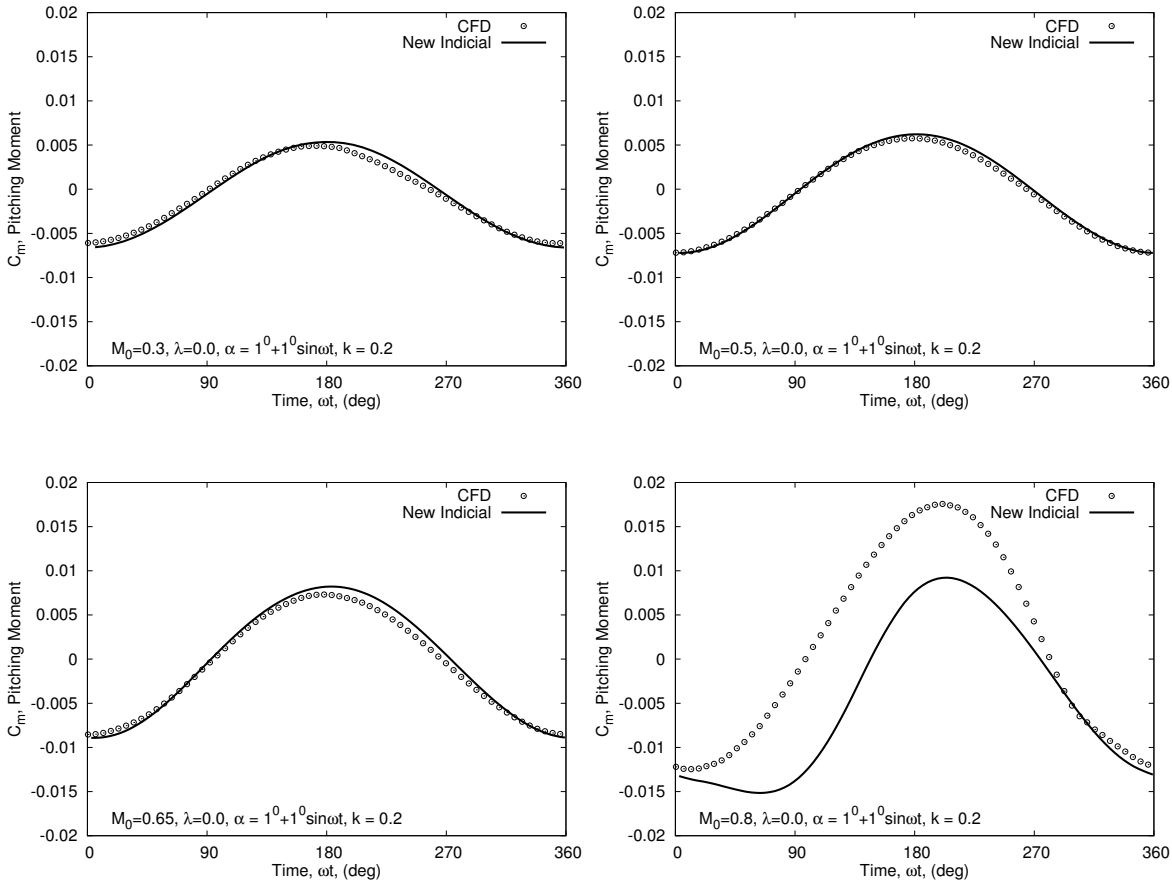

Figure 3.2: Variation of pitching moment for constant Mach number and oscillating angle of attack for $\alpha = 1^\circ + 1^\circ \sin \omega t, k = 0.2$.

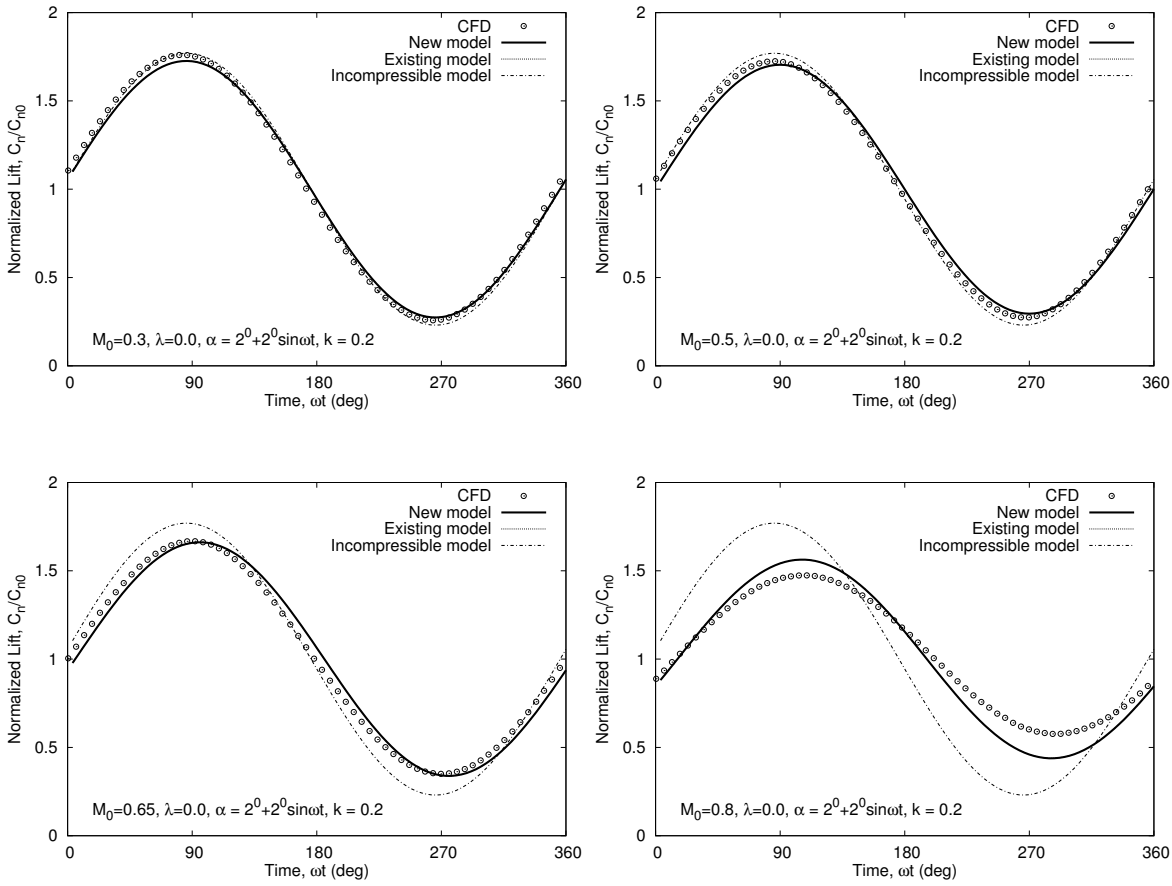

Figure 3.3: Variation of lift coefficient for constant Mach number and oscillating angle of attack for $\alpha = 2^\circ + 2^\circ \sin \omega t, k = 0.2$.

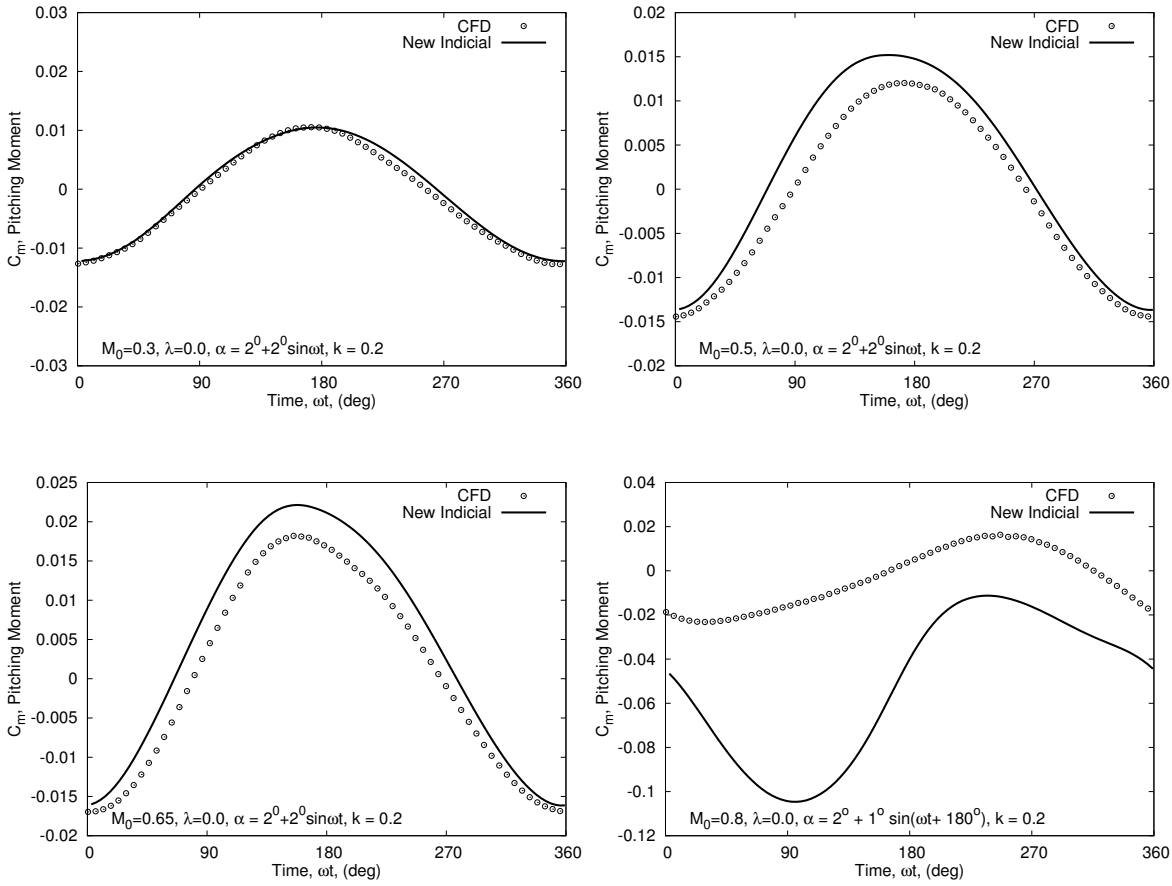

Figure 3.4: Variation of pitching moment for constant Mach number and oscillating angle of attack for $\alpha = 2^\circ + 2^\circ \sin \omega t, k = 0.2$.

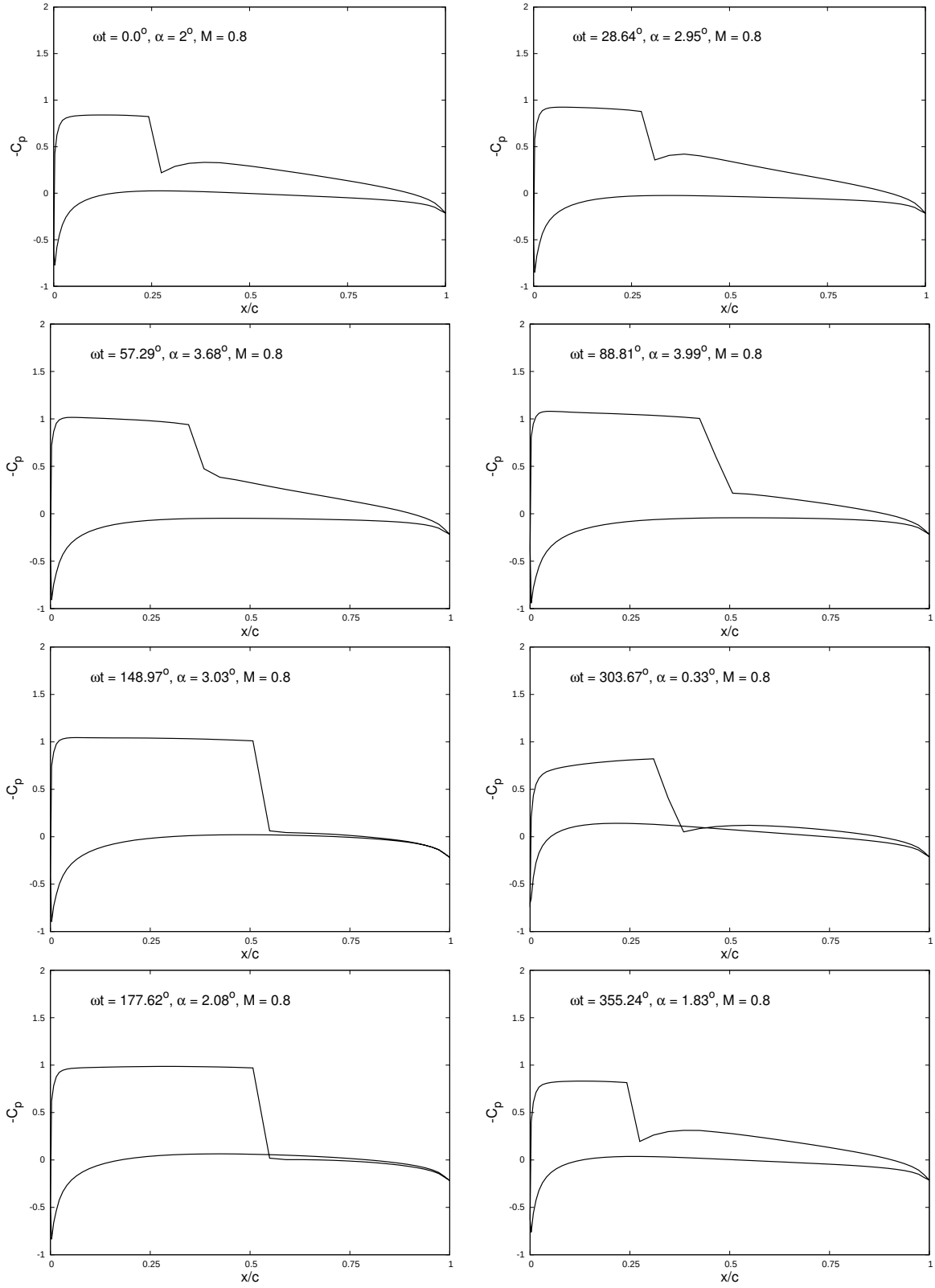

Figure 3.5: Pressure distribution over the airfoil at different times for $M = 0.8$, $\alpha = 2^\circ + 2^\circ \sin\omega t$, $k = 0.2$.

pressure.

For a higher mean Mach number of 0.5 (Figs. 3.8 and 3.9), the incompressible indicial method and the existing compressible indicial method differ from the CFD results in both magnitude and in phase. Initially, as the Mach number increases, there is an increase in the lift because of compressibility effects. This behavior is obviously not captured by the incompressible indicial model but it is well-captured by both the existing and new compressible indicial models. However, while the existing compressible model captures the general behavior, it is associated with discrepancies in magnitude and phase. The new model on the other hand shows good agreement with the CFD; it gives very good agreement for $\lambda = 0.2$ and $\lambda = 0.4$. For $\lambda = 0.6$ and $\lambda = 0.8$, certain nonlinearities are observed beyond $\omega t = 90^\circ$ (i.e., after the maximum Mach number is reached in the oscillatory cycle). These are not captured by any of the reduced-order models because the flow physics behind these nonlinearities involves the formation of shock waves, which are very difficult to account for within the limitations imposed by a linear model.

A study of the variation of chordwise pressure distribution with time (see Figs. 3.14 and 3.15) for $\lambda = 0.6$ reveals the flow physics behind these nonlinearities. Figure 3.14 shows the pressure distribution for $0^\circ < \omega t < 137^\circ$ and Fig. 3.15 shows the pressure distributions for $143.24^\circ < \omega t < 164.43^\circ$. Although the results in Figs. 3.14 and 3.15 involve changes in α as well, the basic phenomenon of shock formation and movement is the same as for the constant angle of attack case. Initially, there is a phase lag between the Mach number and the lift response. As the Mach number increases beyond the maximum Mach number of 0.8 and starts decreasing, a strong pressure gradient begins to build up. This pressure gradient gradually develops into a shock, which then moves

over the upper surface of the airfoil. With the formation of the shock, the indicial lift predictions begin to deviate from the CFD results. As the Mach number decreases further, the shock wave approaches the leading edge and finally vanishes. The point where the shock reaches the leading edge and leaves the airfoil is associated with a sudden jump in the lift curve at $\omega t \approx 164^\circ$. The same behavior is responsible for the sudden jump in the curve at $\omega t \approx 170^\circ$ for the $\lambda = 0.8$ case in Fig. 3.12. The formation and movement of the shock wave has a significant effect on the pressure distribution over the airfoil, and is responsible for the differences between the CFD and the indicial results. Accurate prediction of the pitching moment coefficient is all the more challenging because it is dependent on an accurate estimate of both the lift and the center of pressure of the circulatory forces. Because the formation and movement of shock wave over the airfoil surface has a significant effect on the pressure distribution, it is very difficult to make accurate predictions of their effects without increasing the mathematical and numerical complexity of the reduced-order model.

3.3 Case 3: Combined Angle Of Attack and Free-Stream Mach Number Oscillations

Figures 3.10, 3.11, 3.12 and 3.13 show the results for combined pitching and free-stream Mach number oscillations. When the Mach numbers involved are relatively low ($M < 0.4$), there is very good agreement between CFD and both the incompressible and compressible flow models. For low perturbation velocity ratios ($\lambda = 0.2$ and $\lambda = 0.4$), the incompressible model offers reasonably good predictions. For higher values of λ, how-

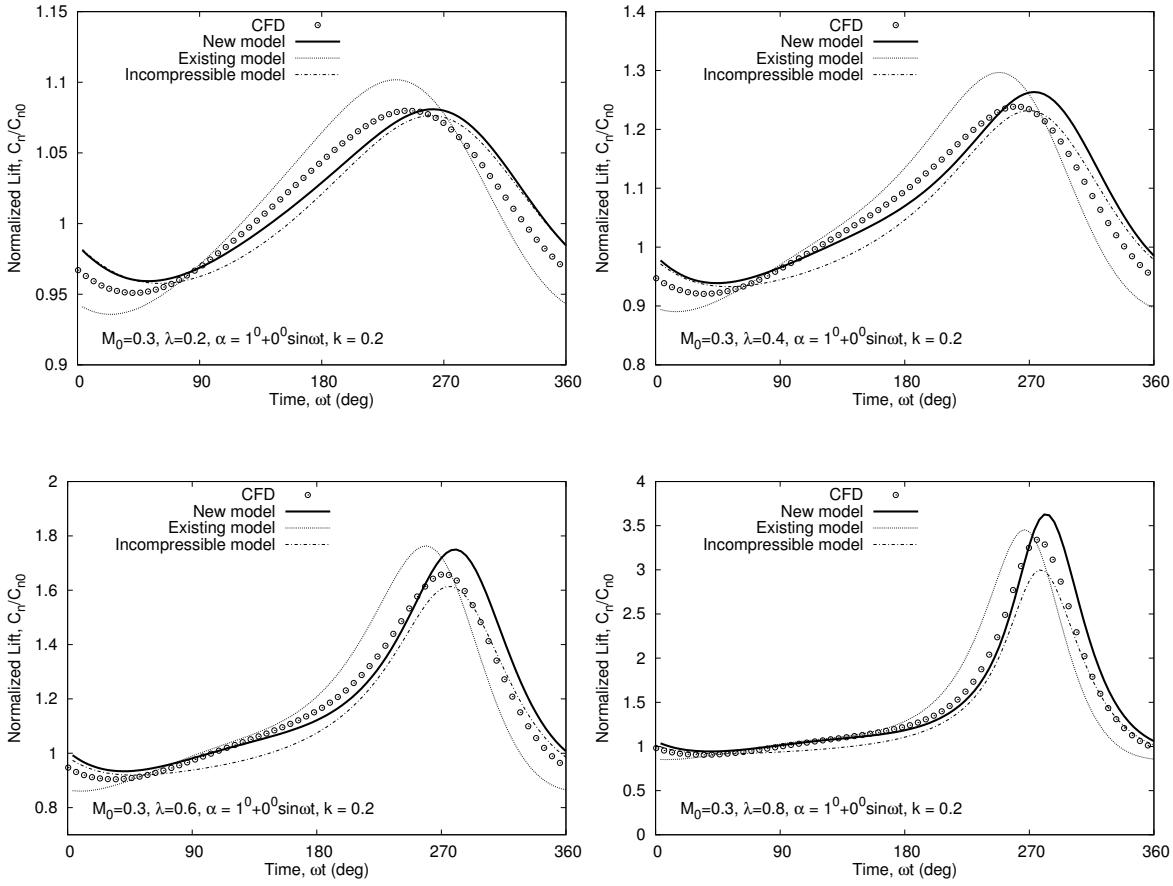

Figure 3.6: Variation of lift coefficient for constant angle of attack and oscillating free-stream Mach number for $M = 0.3(1+\lambda\sin\omega t)$, $k = 0.2$, $\alpha = 1^\circ$.

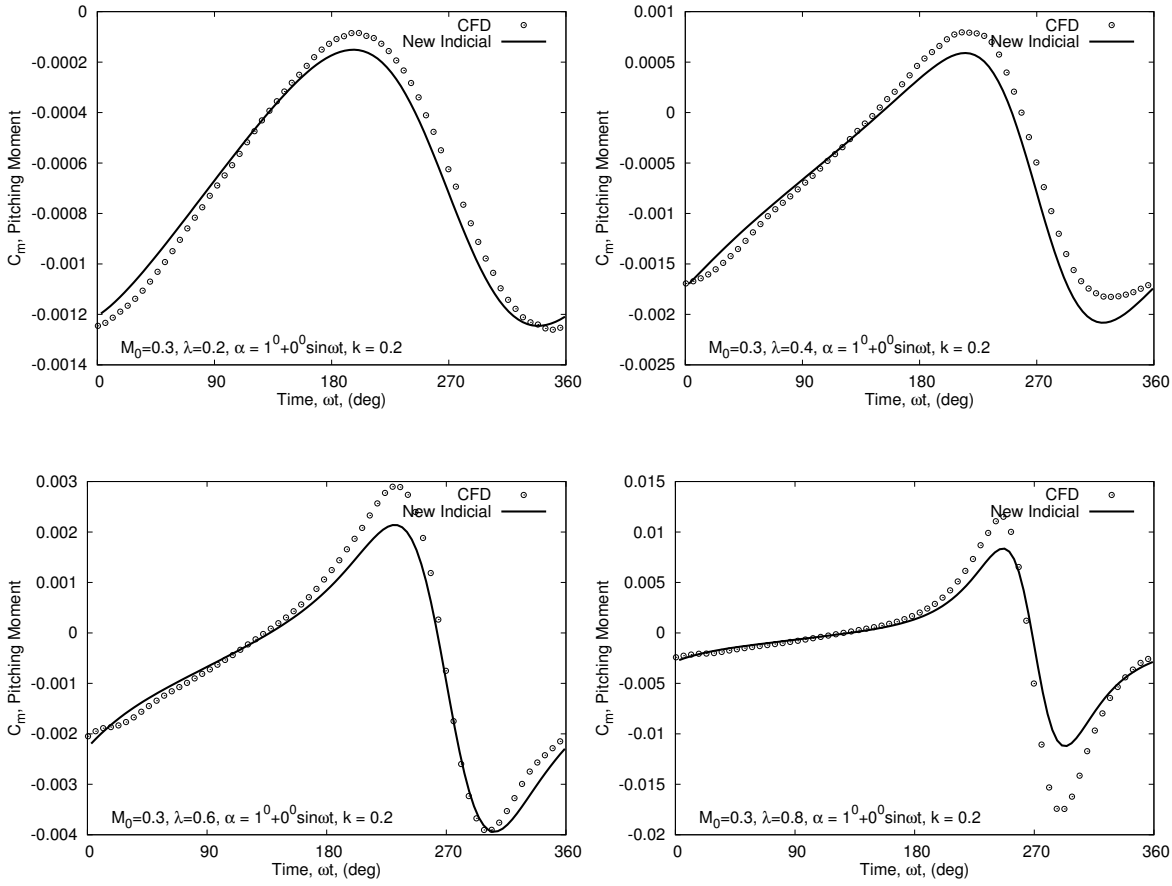

Figure 3.7: Variation of pitching moment for constant angle of attack and oscillating free-stream Mach number for $M = 0.3(1+\lambda\sin\omega t)$, $k = 0.2$, $\alpha = 1^\circ$.

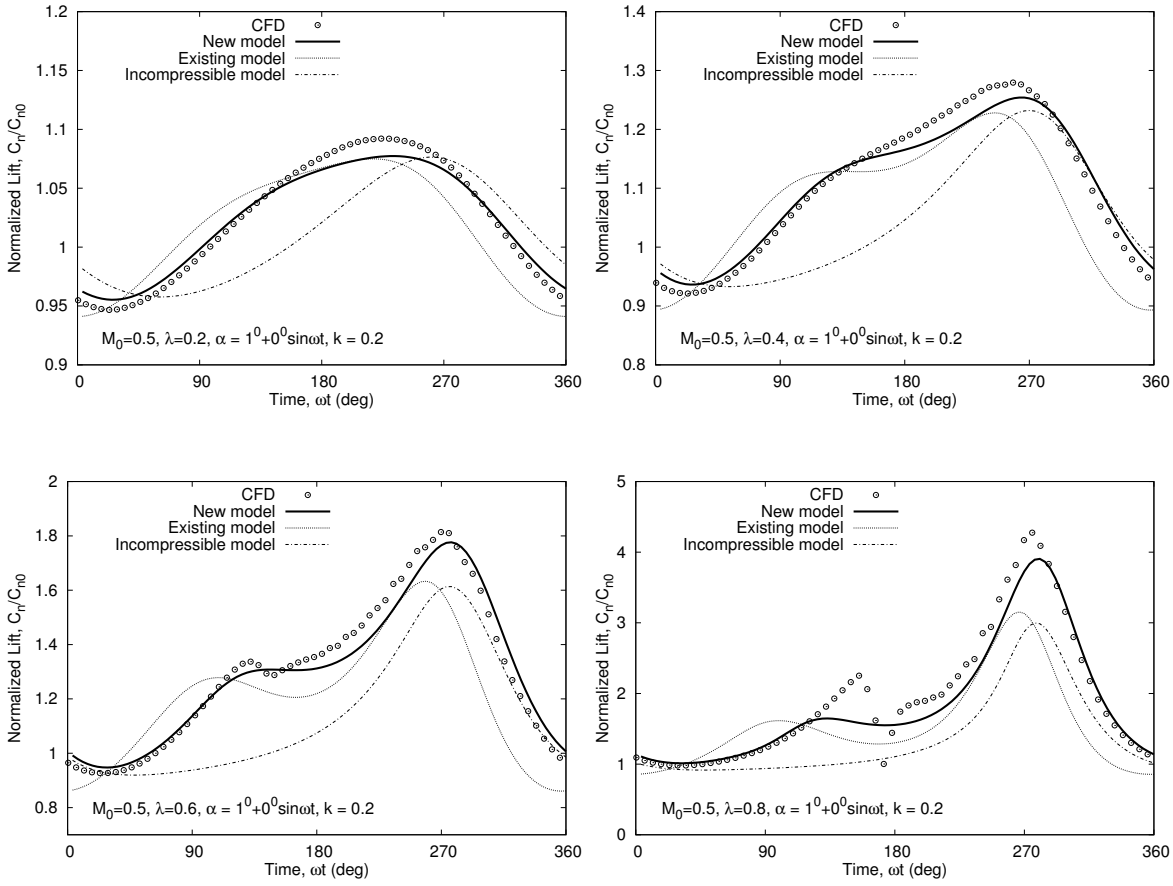

Figure 3.8: Variation of lift coefficient for constant angle of attack and oscillating free-stream Mach number for $M = 0.5(1+\lambda\sin\omega t)$, $k = 0.2$, $\alpha = 1^\circ$.

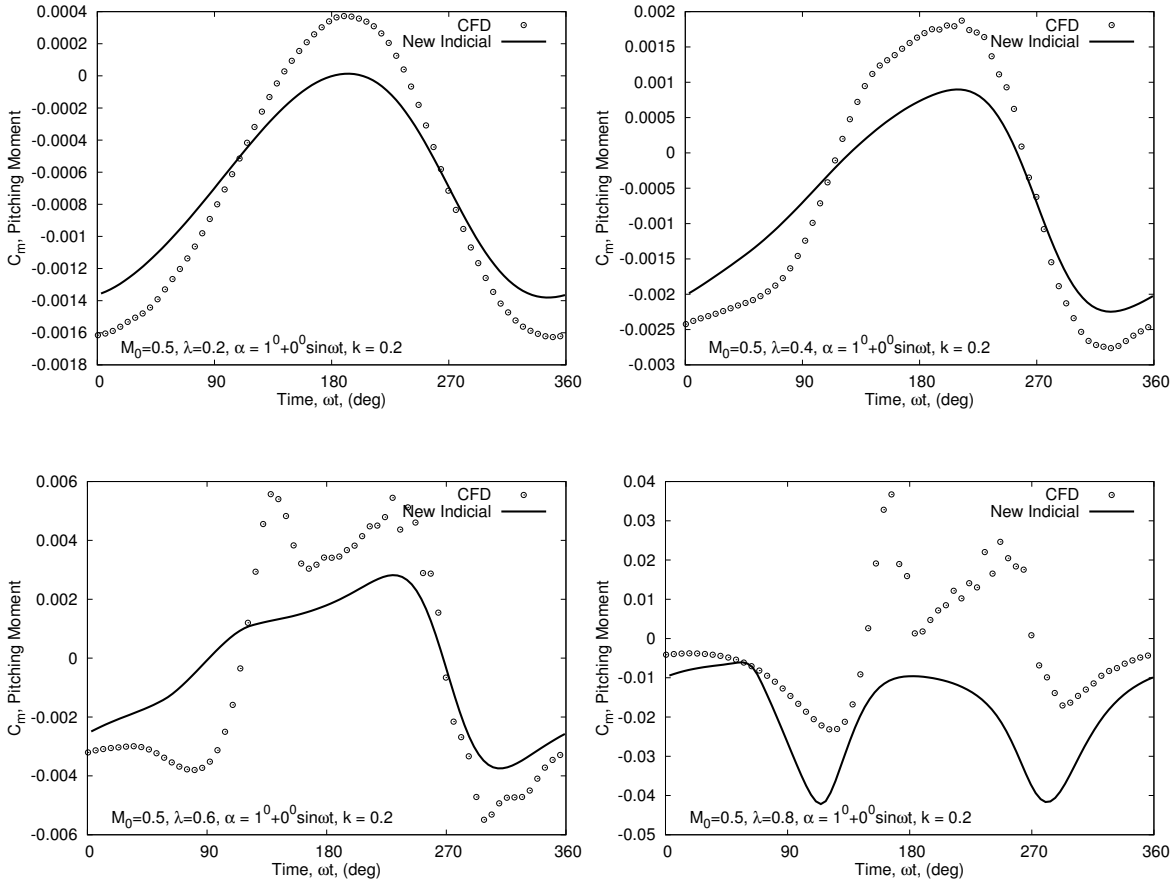

Figure 3.9: Variation of pitching moment for constant angle of attack and oscillating free-stream Mach number for $M = 0.5(1+\lambda\sin\omega t)$, $k = 0.2$, $\alpha = 1^\circ$.

ever, the incompressible model under-predicts the lift (especially in the low Mach number region). The new form of the indicial model gives excellent agreement for all values of λ. The pitching moment predictions also show good agreement with CFD (especially for $\lambda = 0.2$ and $\lambda = 0.4$) because the aerodynamic center does not change significantly at low Mach numbers.

When the Mach numbers are higher (see Figs. 3.12 and 3.13), the nature of the results is similar to the corresponding case with constant angle of attack. The inadequacy of the incompressible and the existing theories is clearly evident for $\lambda = 0.6$ and 0.8 where both of these theories under-predict the lift significantly. The new theory shows good agreement with CFD if the Mach number does not exceed the critical Mach number ($M_{\text{cr}} = 0.8$ in this case). As discussed earlier, beyond the critical Mach number the formation and movement of shocks over the airfoil surface affects the pressure distribution and makes it difficult to make accurate predictions of the lift and pitching moment using any kind of linear model. Even under such conditions, the indicial theory gives reasonable unsteady airloads predictions.

Figures 3.16, 3.17, 3.18 and 3.19 show results when the variations in Mach number and angle of attack are out of phase with each other. Again the results show excellent agreement between the indicial and CFD methods. In fact, it is observed that the predictions are actually better when there is a phase difference between the Mach number and the angle of attack variations. This is because the Mach number and angle of attack do not reach their maximum values at the simultaneously (as would be the case when there is no phase difference). This mitigates the compressibility effects associated with the formation of shocks and, therefore, makes it somewhat easier to predict the lift and

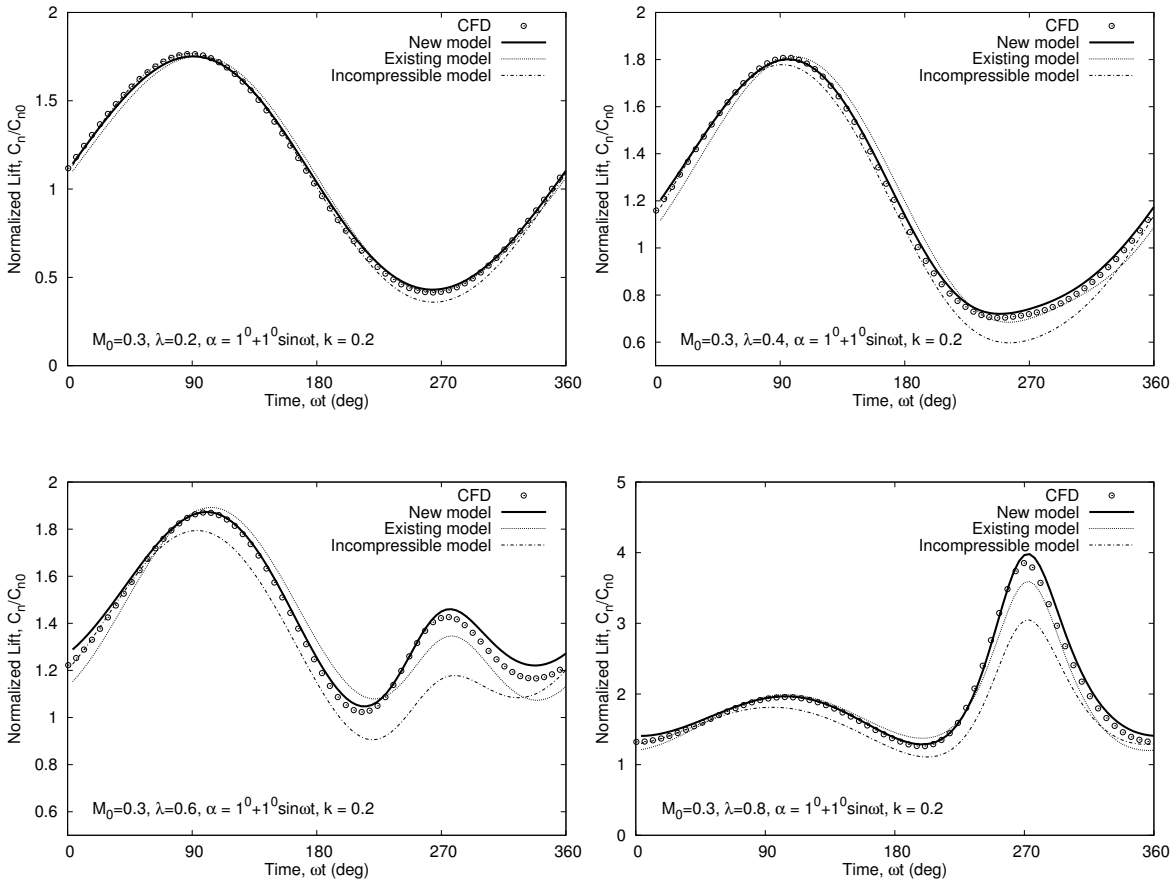

Figure 3.10: Variation of lift coefficient for combined pitching and free-stream Mach number oscillations for $M = 0.3(1+\lambda\sin\omega t)$, $k = 0.2$, $\alpha = 1^\circ + 1^\circ\sin\omega t$.

pitching moment using the indicial model. This is illustrated in the case where $M_0 = 0.65$ and $\lambda = 0.4$. Here, it is observed that when there is a phase difference of 180°, the lift predictions are better than those when there is no phase difference.

Figure 3.20 shows the chordwise pressure distributions at various instants of time. It is observed that while a shock does form, it exists only for a short period during the cycle. The jump in the lift curve around $\omega t = 190^\circ$ corresponds to the point when the shock wave reaches the leading edge of the airfoil.

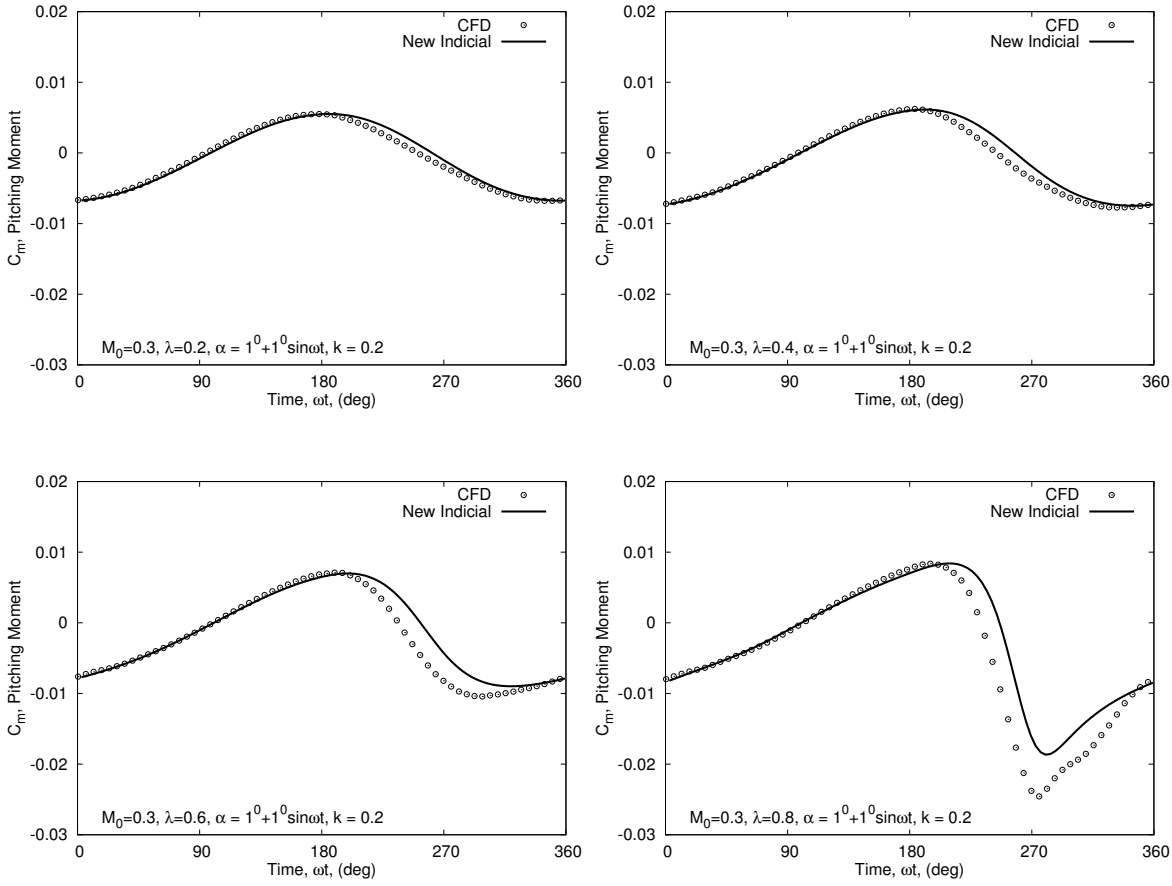

Figure 3.11: Variation of pitching moment for combined pitching and free-stream Mach number oscillations for $M = 0.3(1+\lambda\sin\omega t)$, $k = 0.2$, $\alpha = 1^\circ + 1^\circ\sin\omega t$.

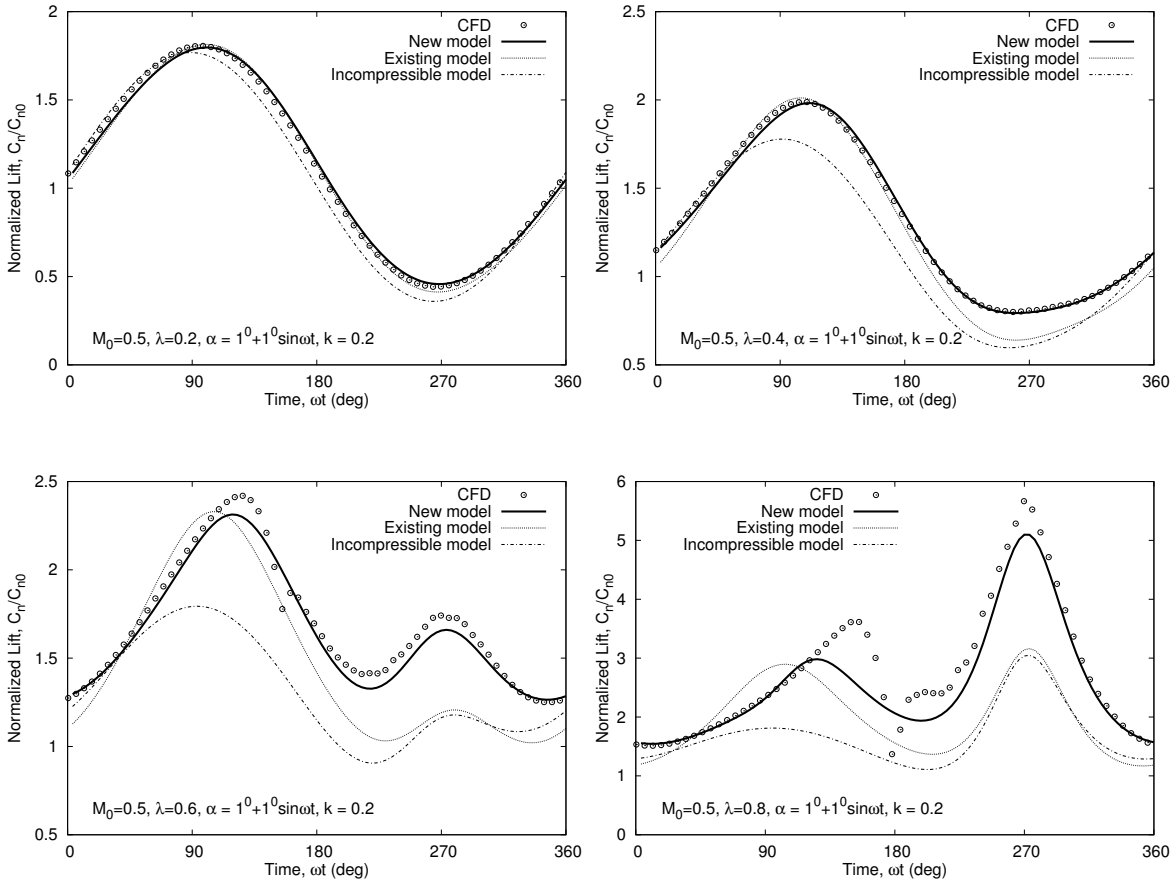

Figure 3.12: Variation of lift coefficient for combined pitching and free-stream Mach number oscillations for $M = 0.5(1+\lambda\sin\omega t)$, $k = 0.2$, $\alpha = 1^\circ + 1^\circ\sin\omega t$.

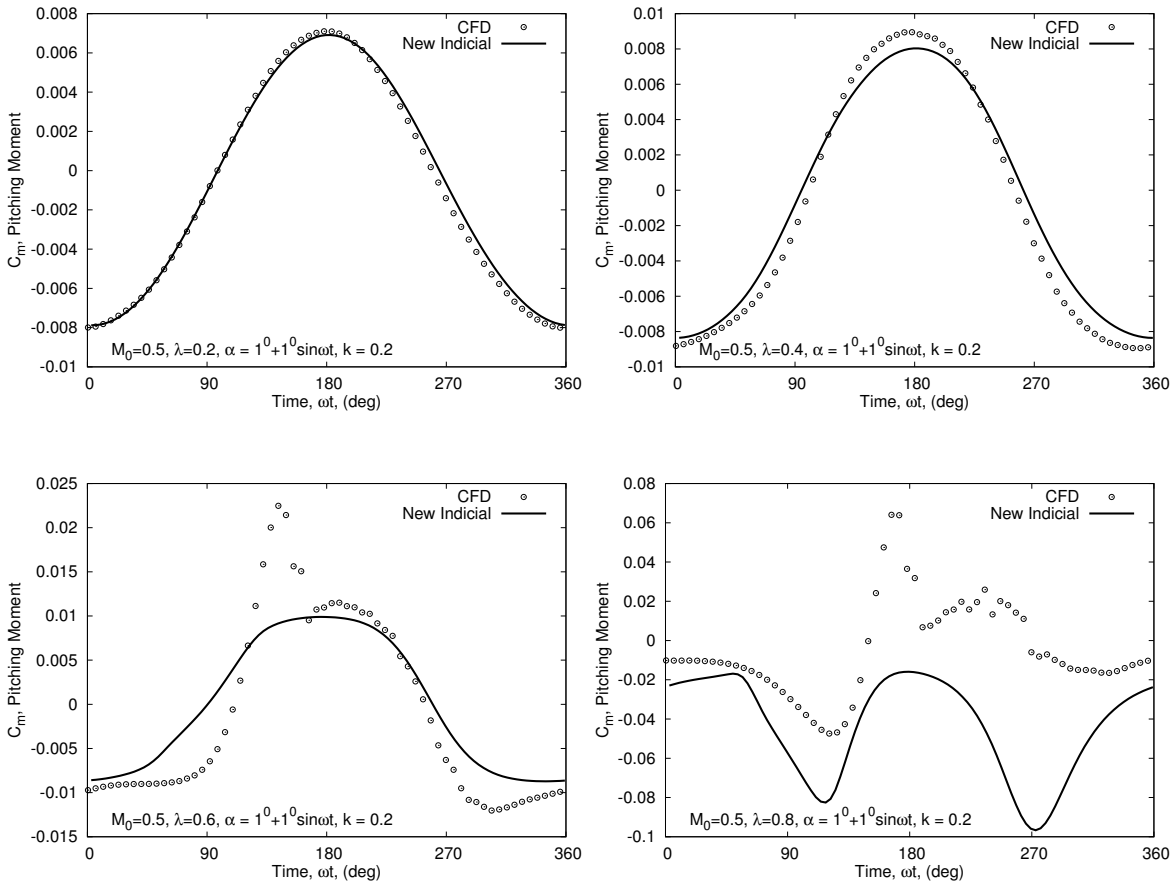

Figure 3.13: Variation of pitching moment for combined pitching and free-stream Mach number oscillations for $M = 0.5(1+\lambda\sin\omega t)$, $k = 0.2$, $\alpha = 1^\circ + 1^\circ\sin\omega t$.

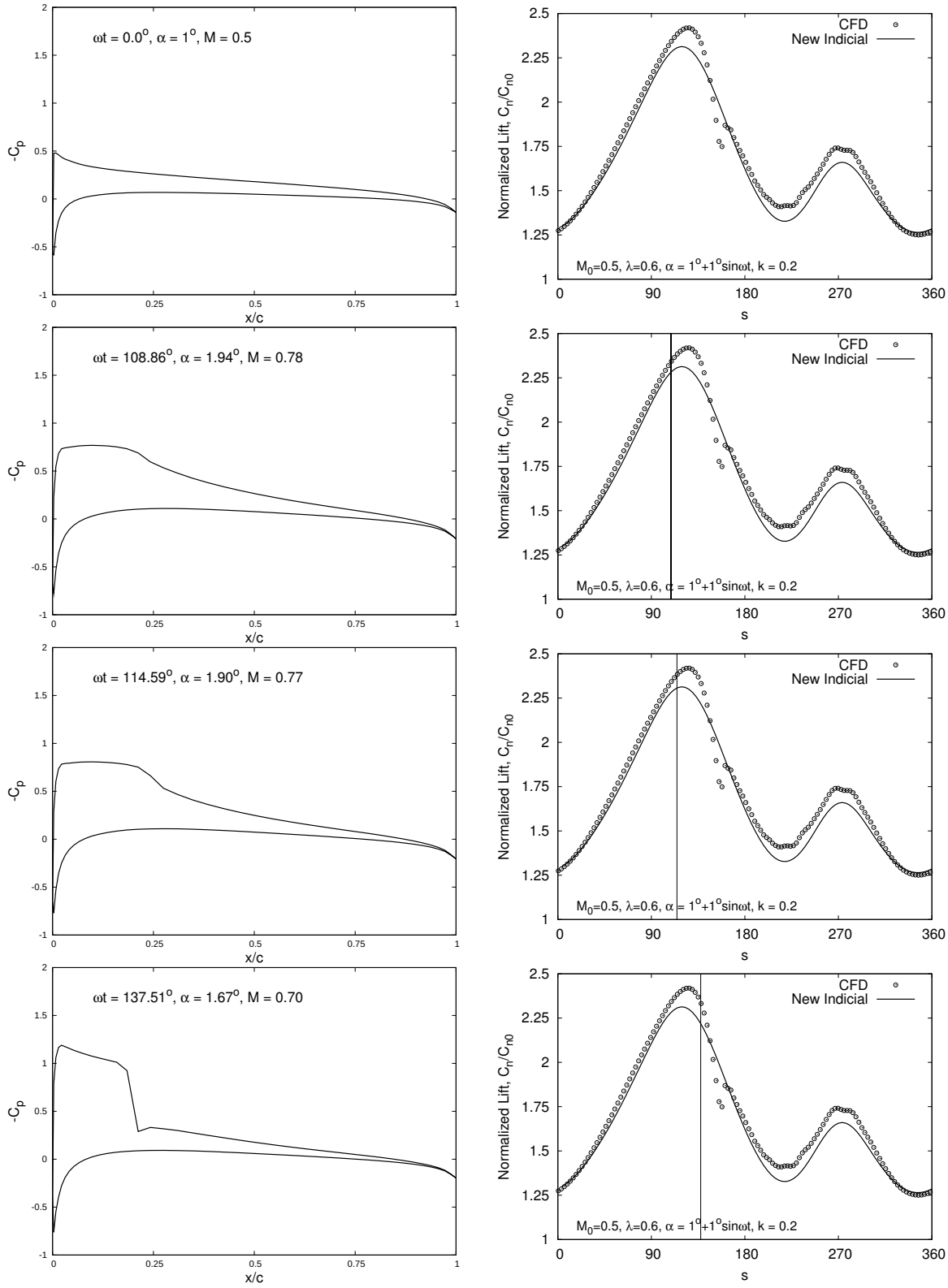

Figure 3.14: Pressure distribution over the airfoil at different times for $M = 0.5$, $\lambda = 0.6$, $\alpha = 1^\circ + 1^\circ \sin\omega t$, $k = 0.2$ $(0^\circ < \omega t < 137.5^\circ)$

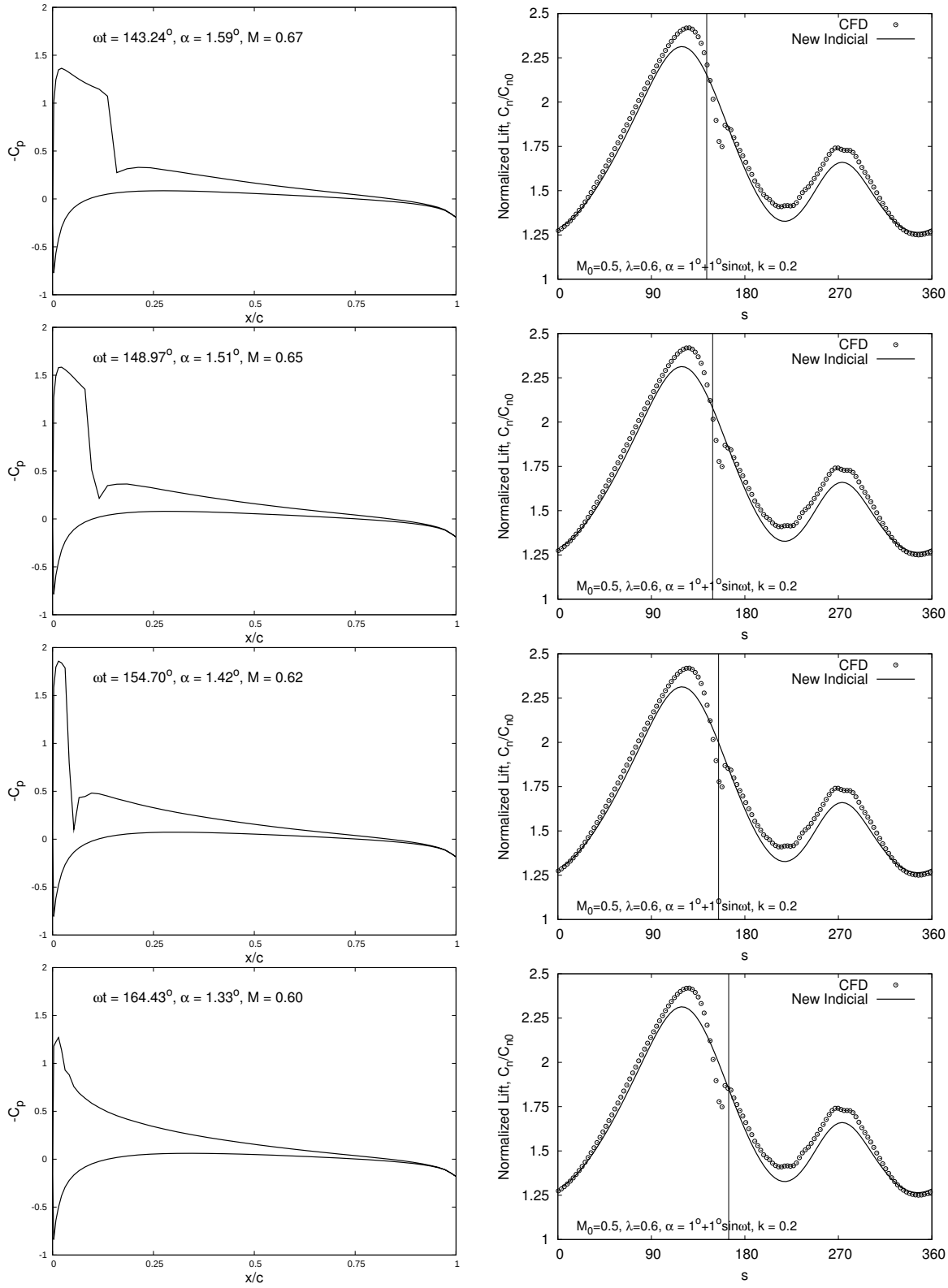

Figure 3.15: Pressure distribution over the airfoil at different times for $M = 0.5$, $\lambda = 0.6$, $\alpha = 1^\circ + 1^\circ \sin\omega t$, $k = 0.2$ $(143.24^\circ < \omega t < 164.43^\circ)$.

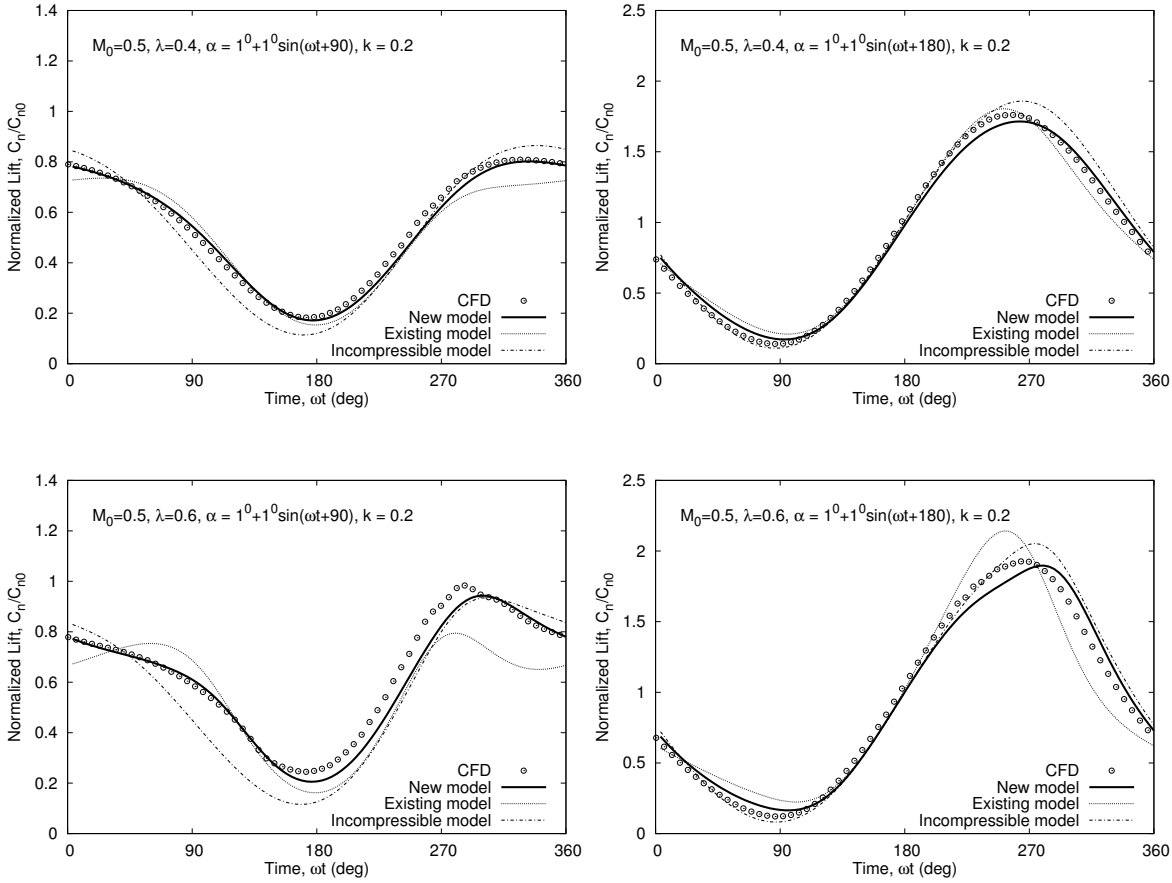

Figure 3.16: Variation of lift coefficient for out of phase pitching and free-stream Mach number oscillations.

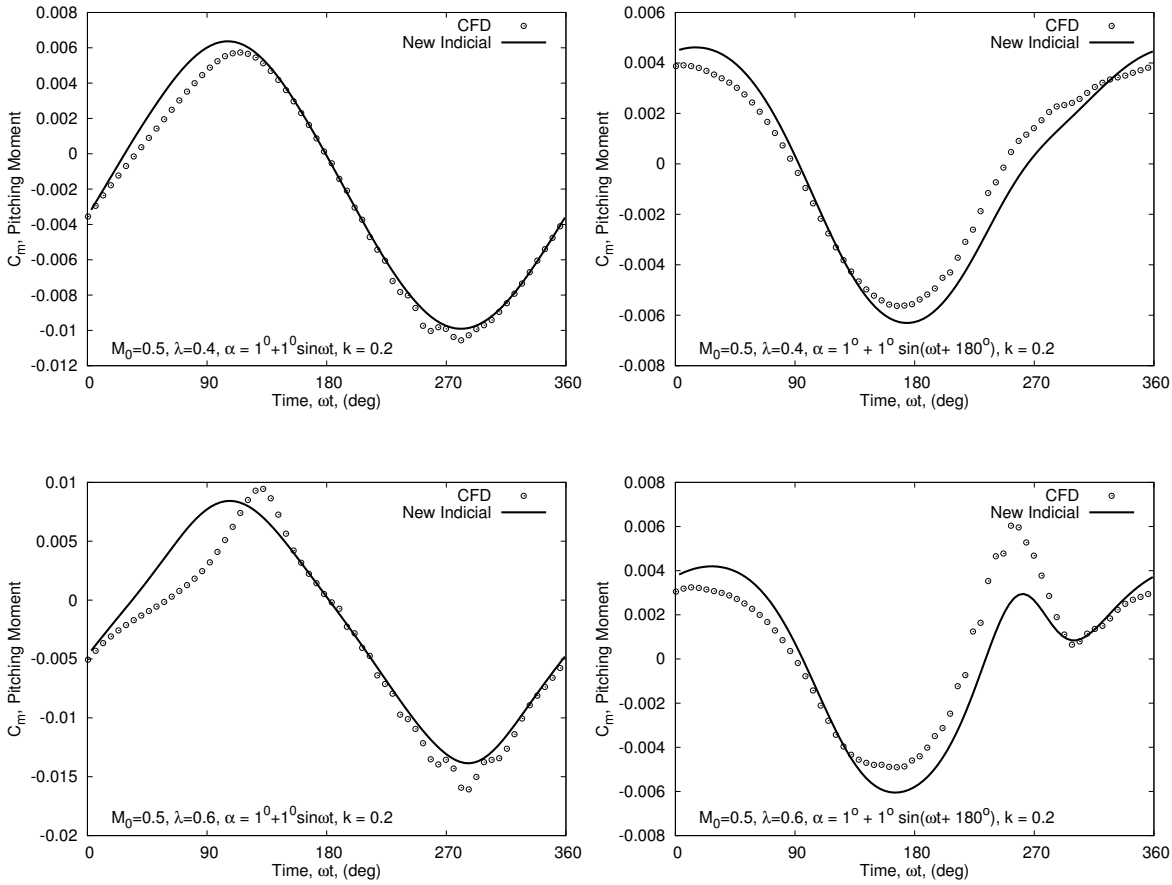

Figure 3.17: Variation of pitching moment coefficient for out of phase pitching and free-stream Mach number oscillations.

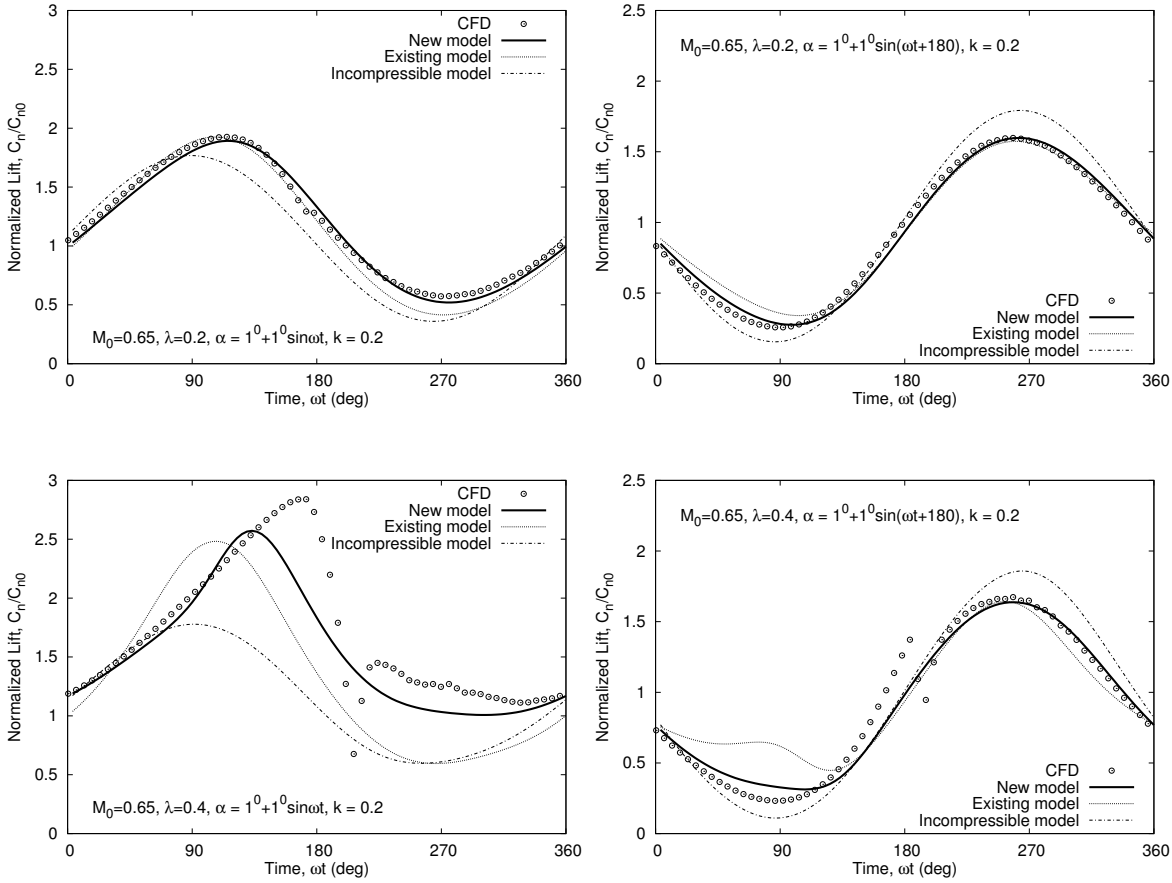

Figure 3.18: Variation of lift for out of phase pitching and free-stream Mach number oscillations.

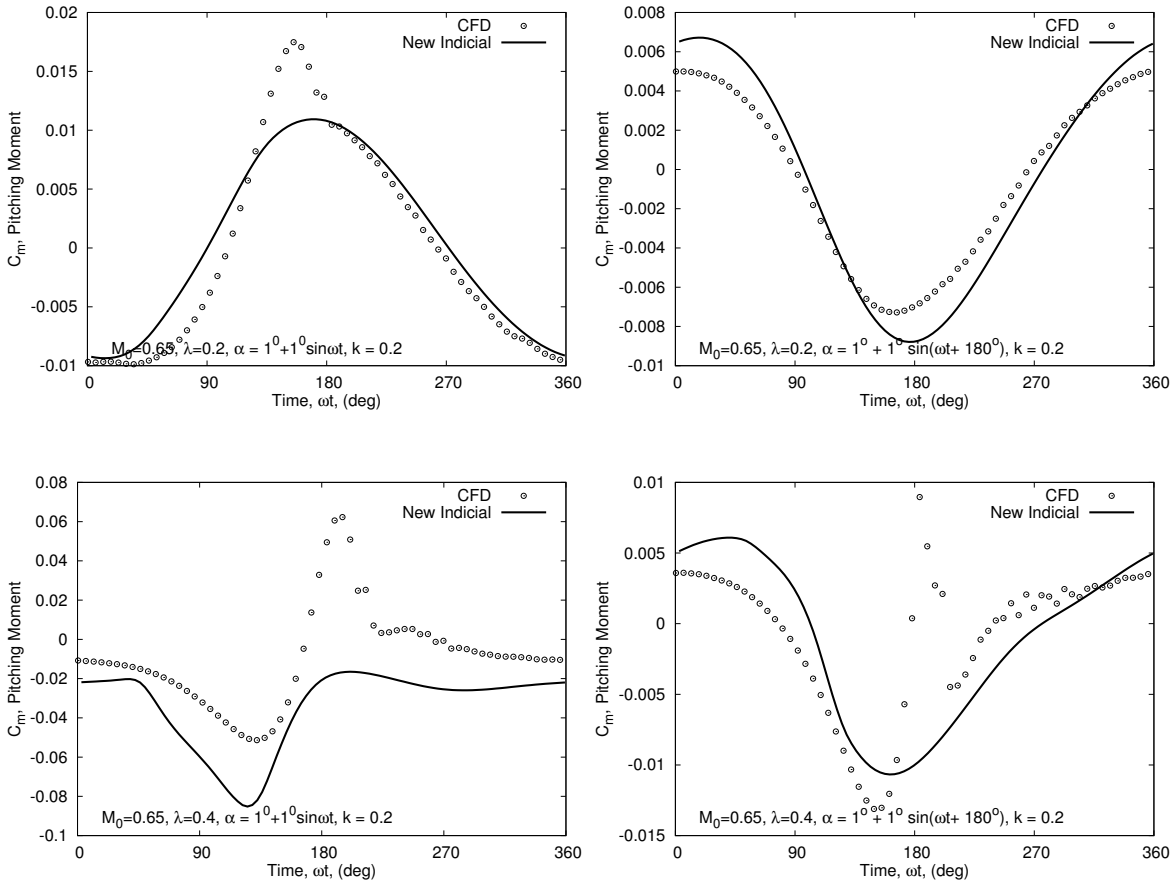

Figure 3.19: Variation of pitching moment for out of phase pitching and free-stream Mach number oscillations.

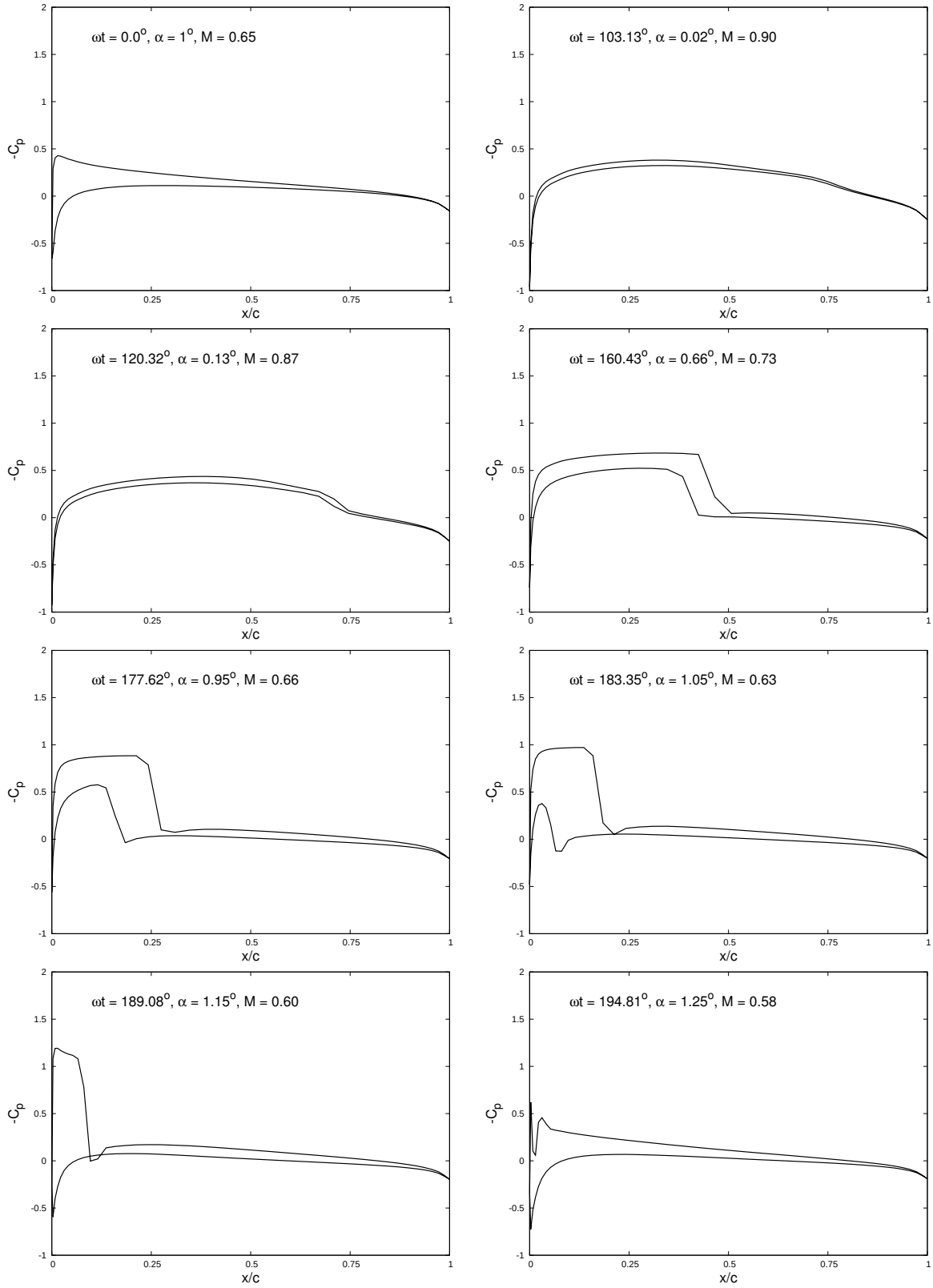

Figure 3.20: Pressure distribution over the airfoil at different times for $M = 0.65$, $\lambda = 0.4$, $\alpha = 1^\circ + 1^\circ \sin(\omega t + 180^\circ)$, $k = 0.2$.

3.4 Results for Different Reduced Frequencies

Figures 3.21, 3.22, 3.23 and 3.24 show results for different reduced frequencies of 0.05, 0.1, 0.2 and 0.4 for the conditions $M_0 = 0.5$, $\alpha_m = 1^\circ$, $\overline{\alpha} = 1^\circ$, $\lambda = 0.4$ and 0.6. For $\lambda = 0.4$, there is good agreement between the indicial method and CFD for all reduced frequencies, except for $k = 0.4$ where a phase difference is observed beyond $\omega t = 120^\circ$. For $\lambda = 0.6$ the results, in terms of general trends and predictive capability, are similar for all reduced frequencies except, again, for $k = 0.4$.

Interestingly, for $\lambda = 0.6$, shocks are formed for $k = 0.05$, 0.1 and 0.2. For $k = 0.4$, no shock is formed. However, the indicial lift predictions are actually poorer for $k = 0.4$. This is surprising because it would be expected that the absence of expected nonlinearities would make it easier to predict the airloads. One possible reason for this behavior lies in the accurate treatment of the noncirculatory terms. High reduced frequencies are associated with high noncirculatory airloads. At high reduced frequencies, the noncirculatory terms assume greater significance and, consequently, any errors in their representation could give rise to phase or amplitude changes in the lift and pitching moment predictions. Figures 3.25 and 3.26 show some additional results for reduced frequencies other than 0.2.

Figure 3.27 and 3.28 show the variation of lift and pitching moment when the angle of attack and Mach number oscillations occur at different reduced frequencies. The compressible indicial models show very good agreement with CFD results except for the $\lambda = 0.8$ case where the Mach number is as high as 0.9. It is seen that the existing indicial model and the new indicial model do not differ significantly for Mach number variations

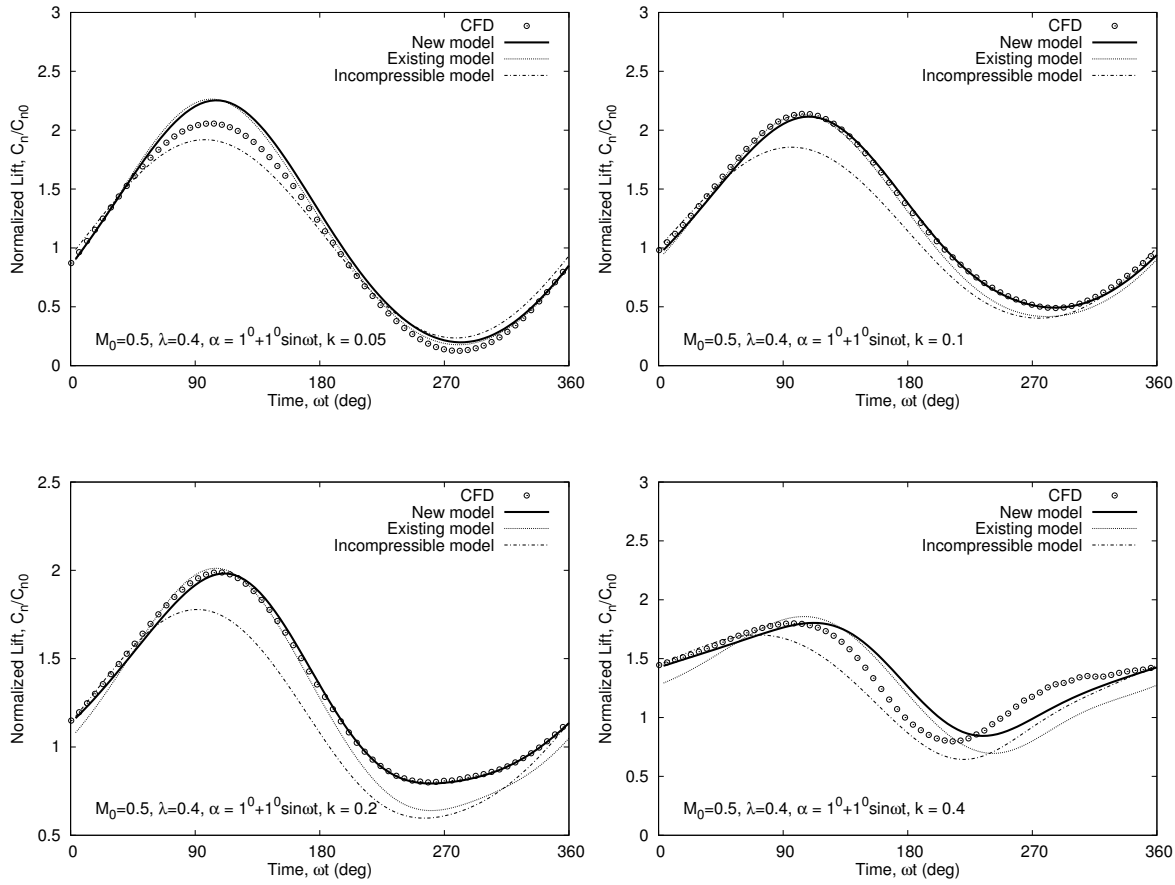

Figure 3.21: Variation of lift coefficient for different reduced frequencies ($M = 0.5(1 + 0.4\sin\omega t), \alpha = 1^\circ + 1^\circ \sin\omega t$).

at low reduced frequencies. The pitching moment predictions are also seen to be in very good agreement with the CFD results.

3.5 Simplified Approach for Pitching Moment Calculations

All the pitching moment results shown so far have been obtained by using Eq. (2.39). While this approach provides a good estimate of the pitching moment, it is computationally expensive because it involves the evaluation of two Duhamel integrals. It also requires an extensive data-set for the center of pressure as a function of both angle of at-

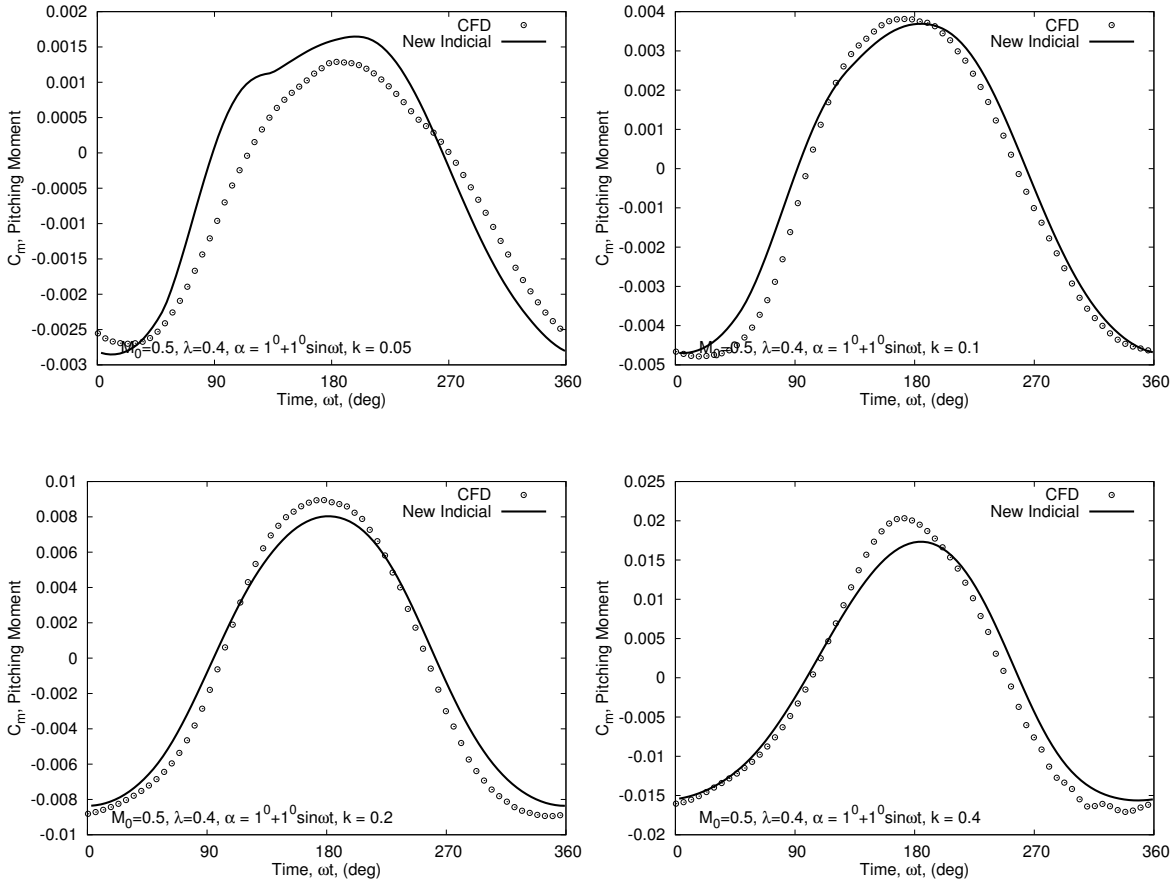

Figure 3.22: Variation of pitching moment coefficient for different reduced frequencies $(M = 0.5(1+0.4\sin\omega t), \alpha = 1^\circ + 1^\circ \sin\omega t)$.

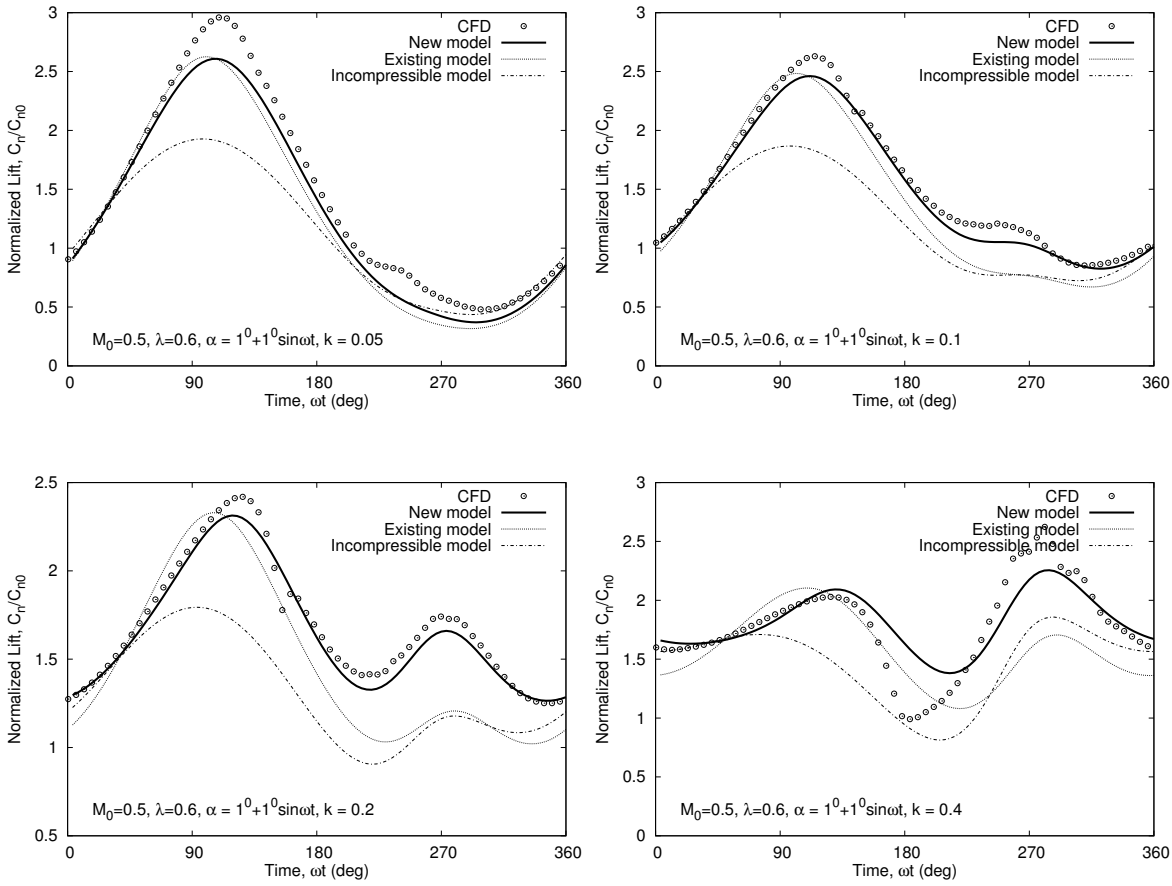

Figure 3.23: Variation of lift coefficient for different reduced frequencies ($M = 0.5(1 + 0.6\sin\omega t), \alpha = 1^\circ + 1^\circ\sin\omega t$).

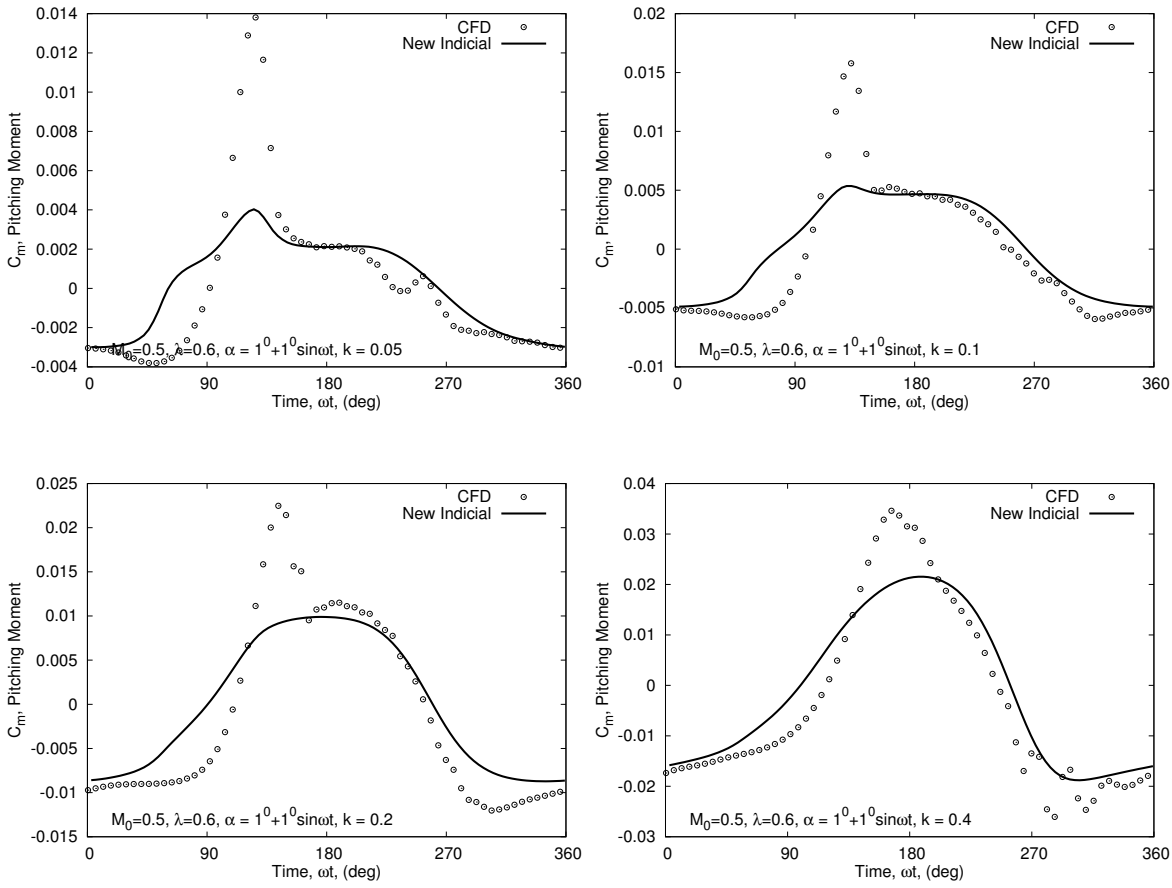

Figure 3.24: Variation of pitching moment coefficient for different reduced frequencies $(M = 0.5(1+0.6\sin\omega t), \alpha = 1^\circ + 1^\circ \sin\omega t)$.

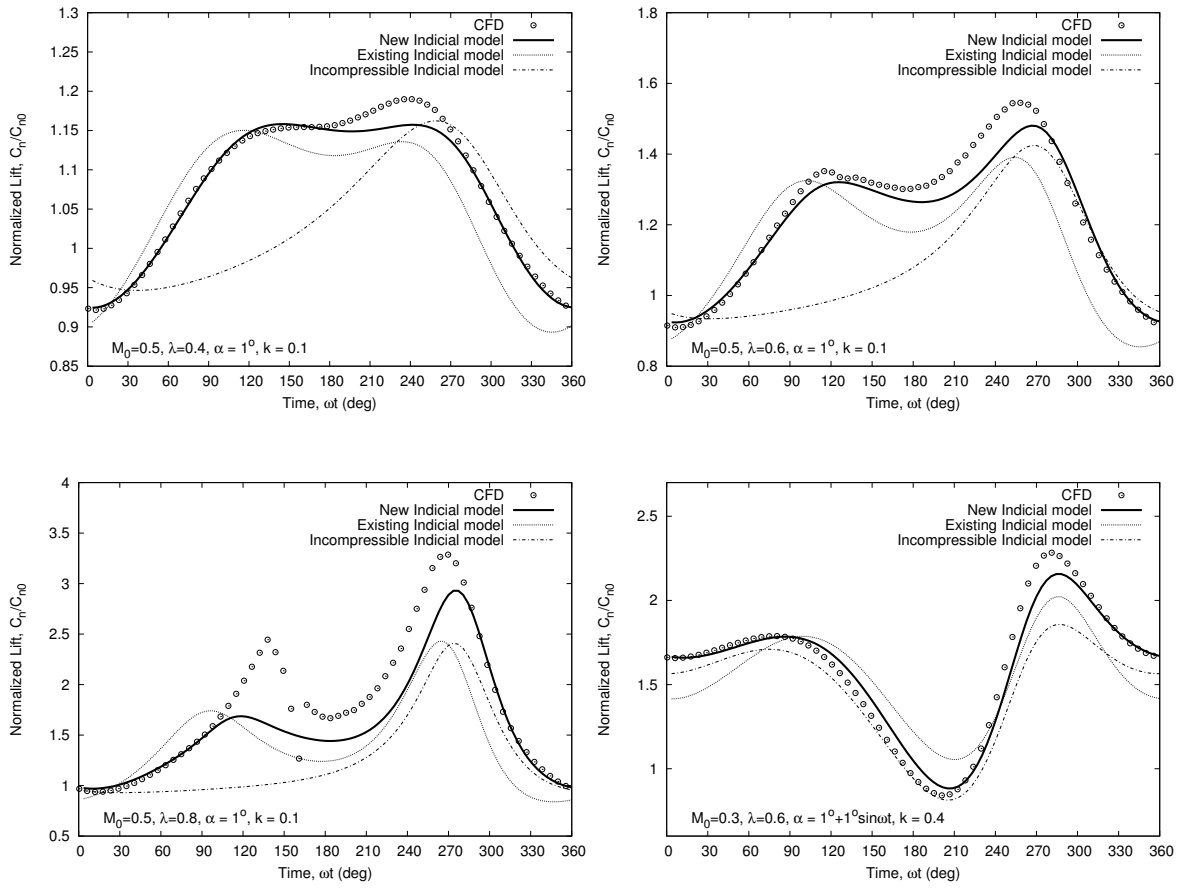

Figure 3.25: Variation of lift coefficient for different reduced frequencies ($M = M_0(1 + \lambda \sin \omega t), \alpha = \alpha_m + \overline{\alpha} \sin \omega t$).

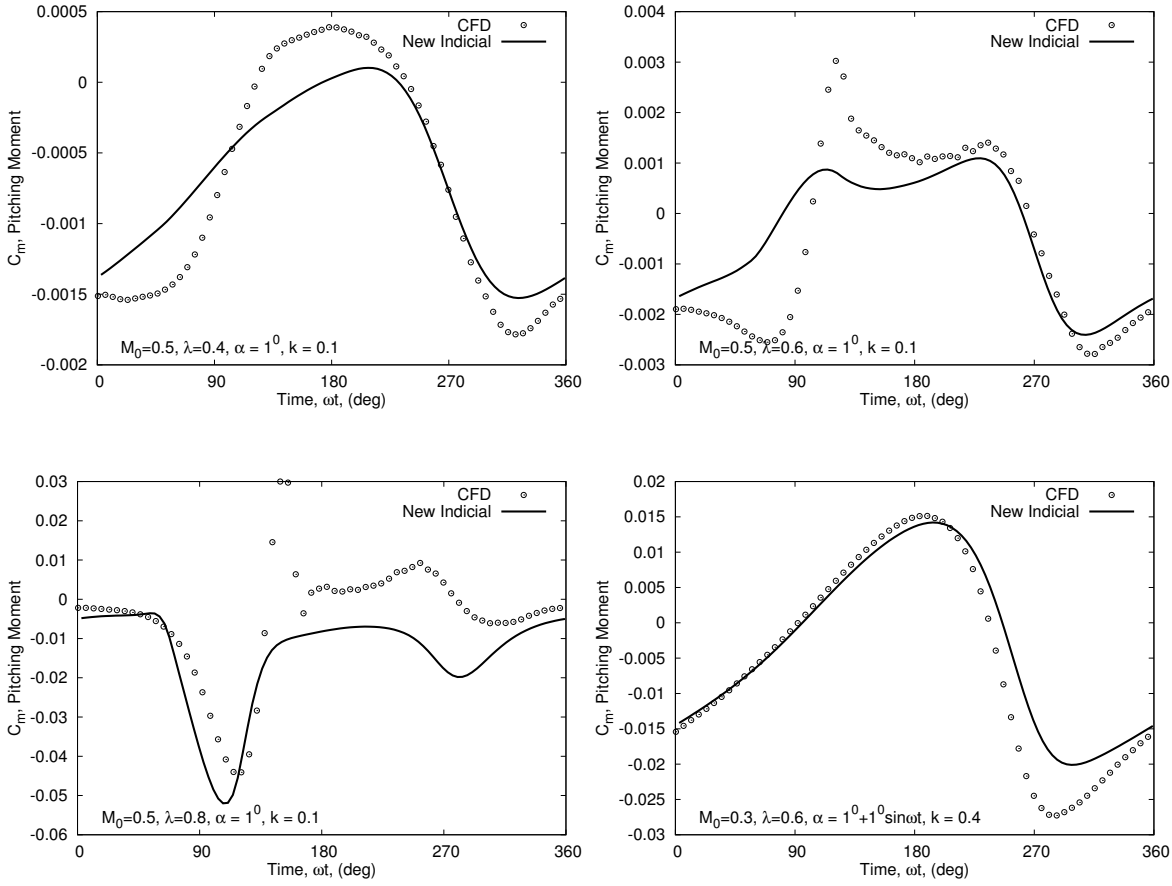

Figure 3.26: Variation of pitching moment coefficient for different reduced frequencies $(M = M_0(1+\lambda\sin\omega t), \alpha = \alpha_m + \overline{\alpha}\sin\omega t)$.

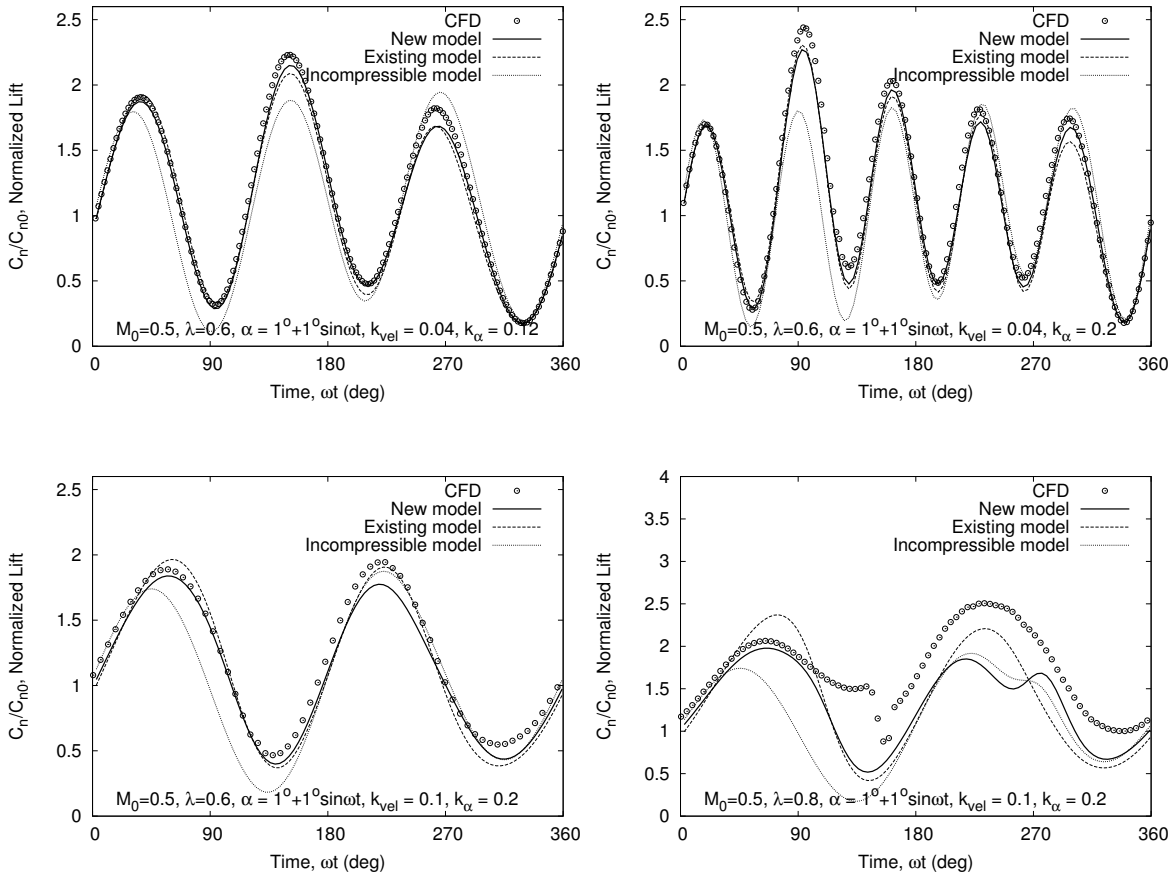

Figure 3.27: Variation of lift coefficient when Mach number and angle of attack oscillations occur at different reduced frequencies ($M = 0.5(1+\lambda\sin\omega_M t), \alpha = 1^\circ + 1^\circ\sin\omega_\alpha t$).

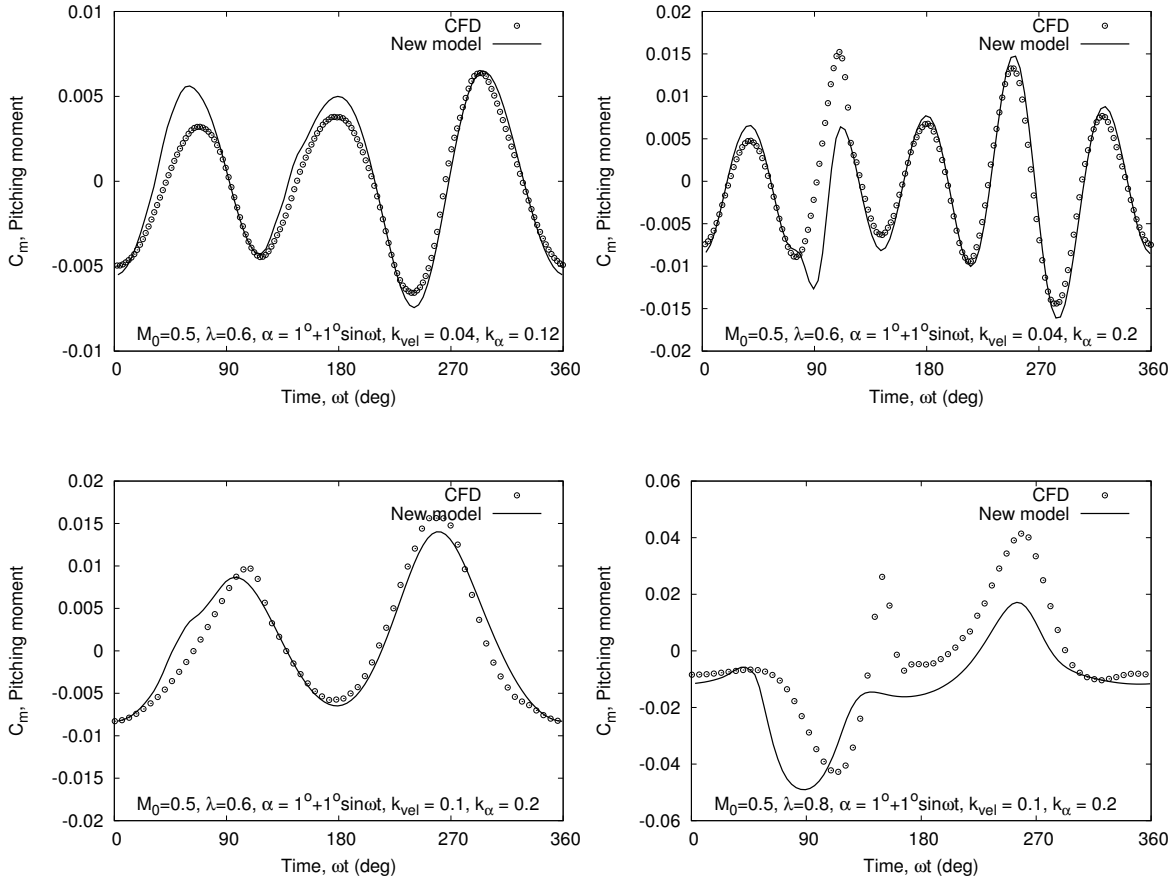

Figure 3.28: Variation of pitching moment coefficient when Mach number and angle of attack oscillations occur at different reduced frequencies ($M = 0.5(1+\lambda\sin\omega_M t), \alpha = 1^\circ + 1^\circ\sin\omega_\alpha t$).

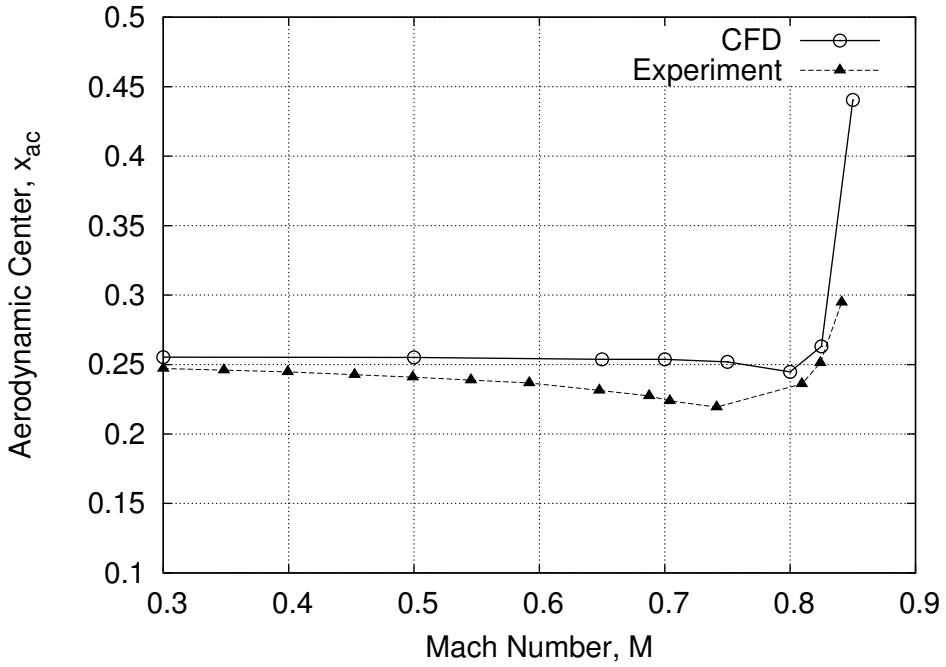

Figure 3.29: Variation in the aerodynamic center as a function of free-stream Mach number for the NACA 0006 airfoil. Data source: Riegels (Ref. 31).

tack and Mach number ($x_{cp} = x_{cp}(\alpha, M)$), which may prove difficult especially when the data is obtained experimentally. One alternative to this approach is to use the aerodynamic center, $x_{ac}(M)$, instead of the center of pressure in the unsteady pitching moment equation. Here, the circulatory lift $C_n^c(t,M)$ is assumed to be acting at the aerodynamic center and its moment about the $1/4$-chord-point is used to replace the first Duhamel integral in Eq. (2.39). Because the aerodynamic center is independent of the angle of attack, it needs to be determined from CFD or experiment only as a function of the Mach number. The simplified pitching moment equation would then be

$$\begin{aligned} C^c_{m_{1/4}}(t,M) &= C_n^c(t,M)(0.25 - x_{ac}(M)) - \\ &\quad \frac{1}{V}\left[\frac{\pi\dot{\alpha}_0 c}{8\beta_0}\phi_m^c(s,M) + \int_0^s \frac{d}{d\sigma}\left(\frac{\pi\dot{\alpha}c}{8\beta}\right)\phi_m^c(s-\sigma,M)\,d\sigma\right] \end{aligned} \tag{3.1}$$

Figure 3.29 shows the variation of the aerodynamic center as a function of the Mach

number. The differences between the CFD and experiment may be attributed to the inviscid nature of the Euler solver as well as because of the difficulties in accurately predicting the airloads using CFD or experiment at high Mach numbers. It should be borne in mind that at high subsonic Mach numbers the concept of an aerodynamic center is not strictly valid because the dependence of lift and pitching moment on α is no longer linear. Consequently one would have to use approximate values of the aerodynamic center based on the regions of α where the behavior is locally linear. Figure 3.30 compares the pitching moment results using the simplified method (aerodynamic center approach) and the original method described in Chapter 2 (the center of pressure approach). It is seen that for subcritical flows where the aerodynamic center variations are not too significant, the simplified approach gives very similar results to the original method. When the Mach numbers involved are high, the simplified approach shows significant deviations, primarily because of the inaccuracies in the estimation of the effective aerodynamic center. Under these conditions the center of pressure approach better captures the general trends in the pitching moment behavior. Nevertheless, for most subcritical flows, the simplified approach provides a good estimate of the pitching moment behavior.

3.6 Effect of Airfoil Thickness

All the results so far were obtained for a NACA 0006 airfoil. The NACA 0006 was chosen because, being a thin airfoil, it is reasonable to model its unsteady behavior based on thin airfoil theory. In particular its lift curve slope C_{n_α} can be calculated to a good degree of accuracy by using Glauert compressibility rule (i.e., $C_{n_\alpha} = 2\pi/\beta$) without having to

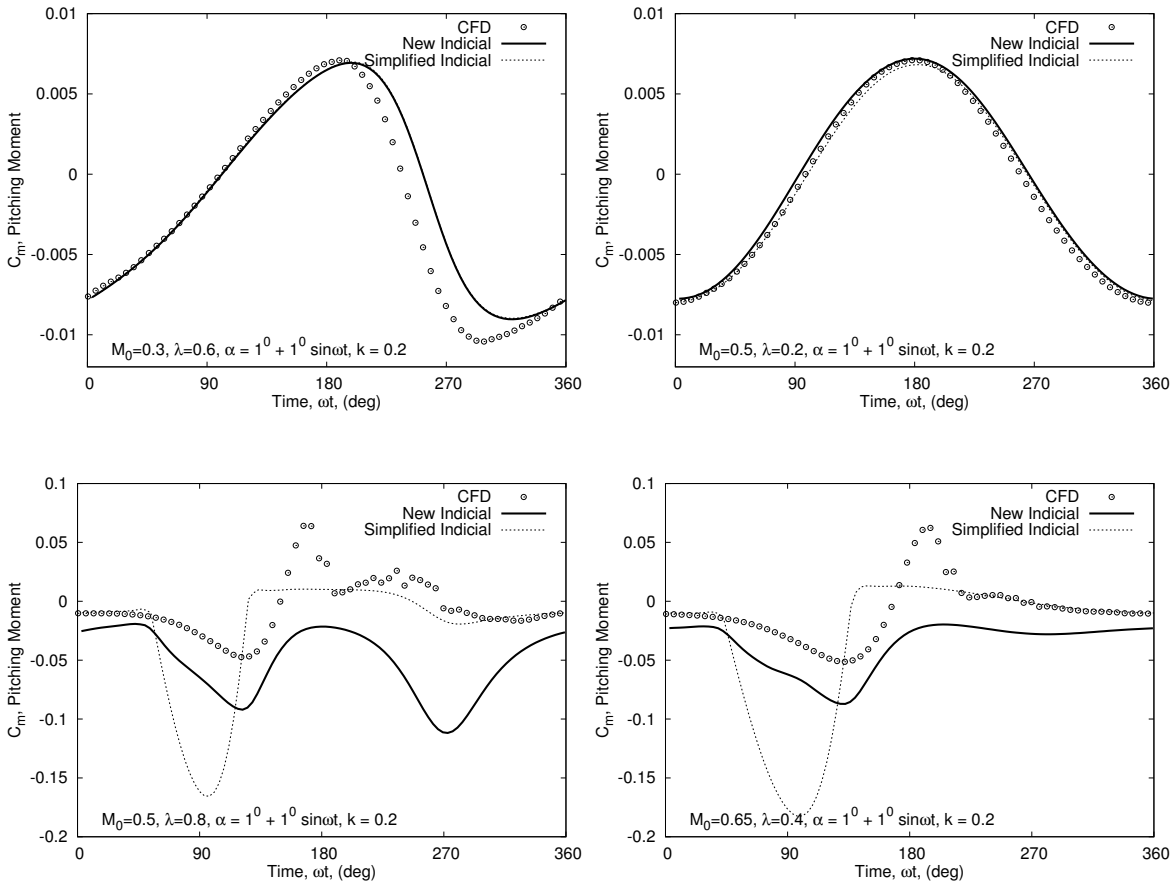

Figure 3.30: Comparison of the pitching moment coefficient using the new indicial method and its simplified version ($M = M_0(1+\lambda\sin\omega t), \alpha = \alpha_m + \overline{\alpha}\sin\omega t$).

generate a detailed database of the lift coefficient for a wide range of Mach numbers and angles of attack. However, helicopters use a wide range of airfoils for which the thin airfoil assumptions may not be fully justified. It is therefore important to investigate the sensitivity of the unsteady airloads to the effects of airfoil thickness.

In this study, four other airfoils were considered — NACA 0002, NACA 0012, NACA 00015 and the NACA 0020. Figure 3.31 and 3.32 show the unsteady airloads for the aforementioned airfoils for combined variations in angle of attack and Mach number as obtained from CFD. It is seen that while the general trends are very similar, there are some differences, especially at supercritical Mach numbers. Firstly, it is seen that there is an offset in the lift. This is to be expected because, as the thickness increases, the lift curve slope, C_{n_α}, changes and no longer follows the Glauert compressibility rule. In Fig. 3.31 it is seen that for NACA 0015 and NACA 0020, the nonlinear effects characterized by the abrupt changes in the lift are present even for $\lambda = 0.4$. Similarly, in Fig. 3.31, there are no sudden changes in the lift curve for the NACA 0002 airfoil, indicating the absence (or lessening) of the nonlinear effects that are present for the other airfoils. This is because, as the thickness increases the critical Mach number is lowered (i.e., for the NACA 0012, NACA 0015 and NACA 0020, the critical Mach number is lowered, whereas for NACA 0002, it increases).

To modify the indicial method to better predict the unsteady airloads for other airfoils it is necessary to:

- Calculate the indicial coefficients for that particular airfoil. The indicial coefficients used in this work were obtained for the NACA 0006 airfoil.

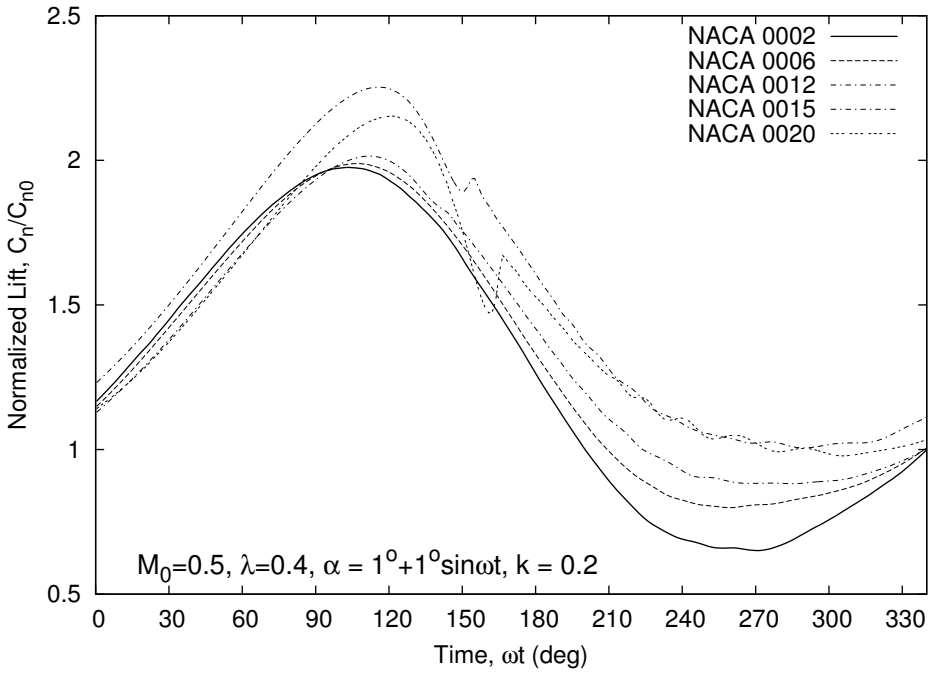

Figure 3.31: Variation of lift for different airfoils for $M = 0.5(1 + 0.4\sin\omega t), \alpha = 1^\circ + 1^\circ \sin\omega t$.

- Develop a look-up table for the lift coefficient for a wide range of Mach numbers and angles of attack for that airfoil.

Some of these issues are discussed in Chapter 4.

3.7 Effect of Viscosity

The effect of viscosity on the unsteady airloads is another important issue. Generally, the Reynolds numbers typically encountered by helicopter blades are in the range of 1 to 10 million. The flow field under these conditions is generally turbulent and proper care should be taken to model the turbulence effects. In the present work, the Baldwin–Lomax model (Ref. 34) was used. Figure 3.33 shows the variation of lift for combined variations in angle of attack and Mach number for $Re = 10^6$. It is seen that the results are fairly

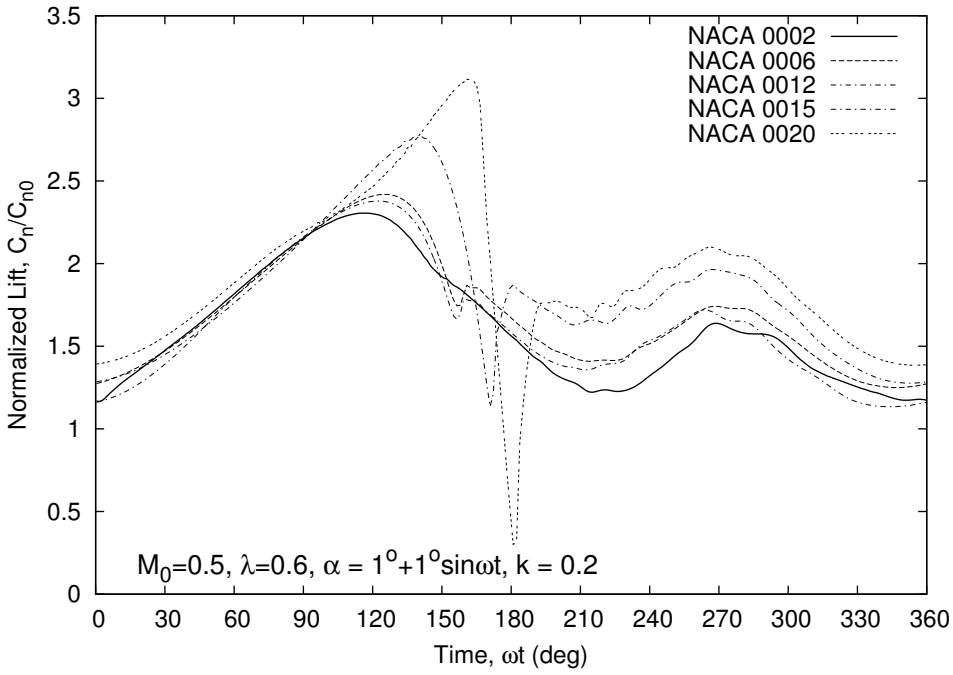

Figure 3.32: Variation of lift for different airfoils for $M = 0.5(1 + 0.6\sin\omega t), \alpha = 1^\circ + 1^\circ \sin\omega t$.

similar to the equivalent cases when run in the Euler mode.

3.8 Sensitivity of the Results to Time-step Size

A proper choice of the time-step size is important for both accuracy and computational efficiency. While a small time-step size would provide greater predictive accuracy, it can increase the computational cost for the same problem. This is true for both CFD and the indicial method. For most of the computations carried out in this work, the CFD calculations were carried out at a normalized time-step size of 0.025. Figure 3.34 shows the effect of time-step size on the unsteady lift predictions. It is seen that the results for $\Delta t = 0.025$ and 0.0125 are almost indistinguishable. Furthermore for $\Delta t = 0.05$ the results are almost identical except for a small amplitude reduction in the high Mach number

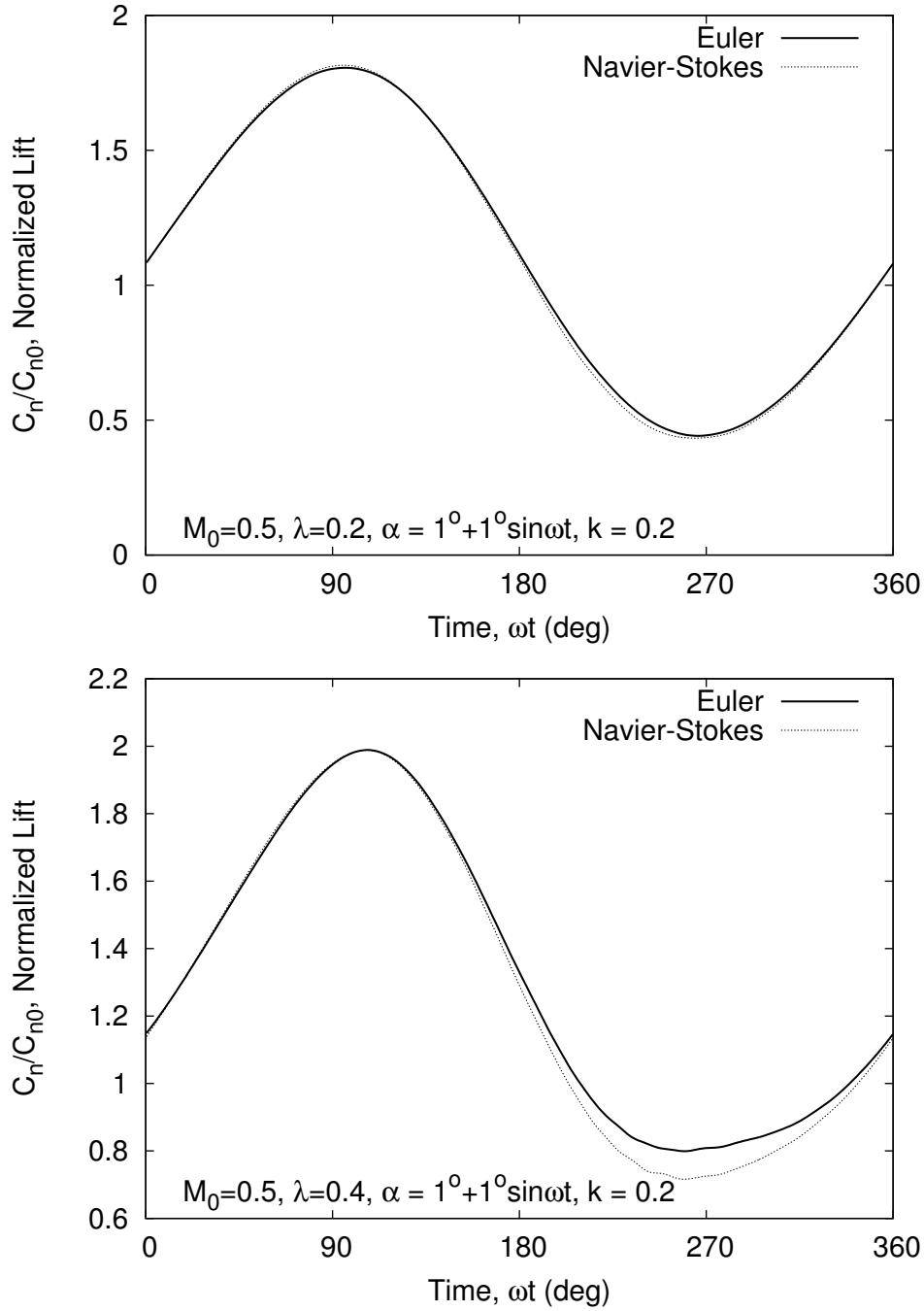

Figure 3.33: Effect of viscosity on the unsteady airloads.

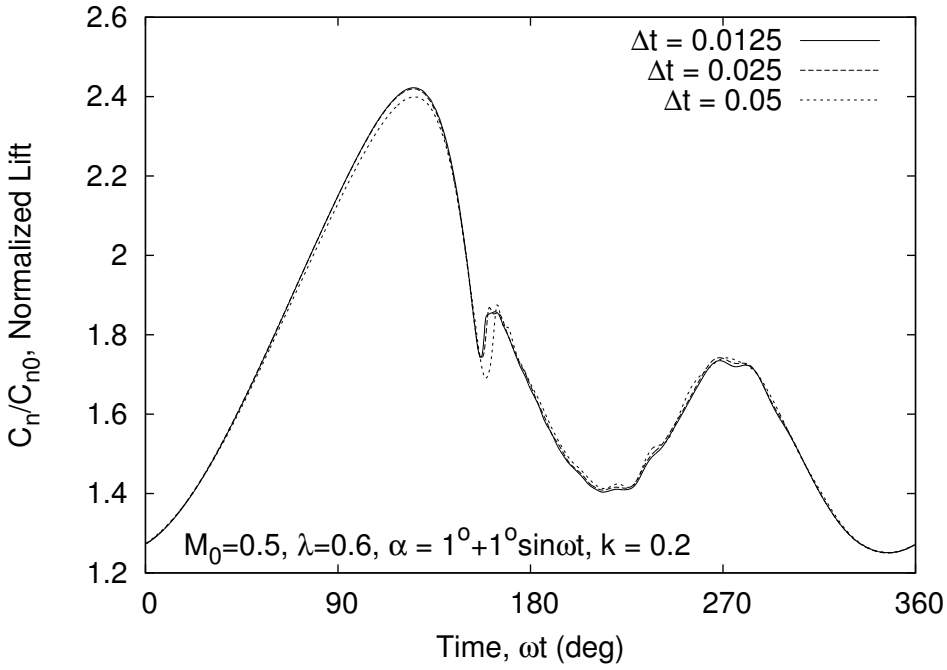

Figure 3.34: Effect of time-step size on CFD lift predictions.

regime and a phase difference in the region where the shock is formed.

A proper choice of the time-step size for the indicial method is important because the computational times can decrease drastically when the number of time-steps are reduced (recall that the exact algorithm is $O(N^2)$). In this work, the results were obtained for 500 time-steps because this gives accurate results for all the cases. For lower Mach numbers, the number of time-steps per cycle can be further reduced with negligible losses in accuracy. For other time-steps (100, 250, etc.) the results are very similar to the results with 500 time-steps, with some deviations towards the end of the cycle (see Fig. 3.35).

3.9 Grid Resolution

The grid resolution is an important issue for any CFD computation. In the present work, most of the CFD calculations were obtained for a 241×53 C-grid. To be valid, the

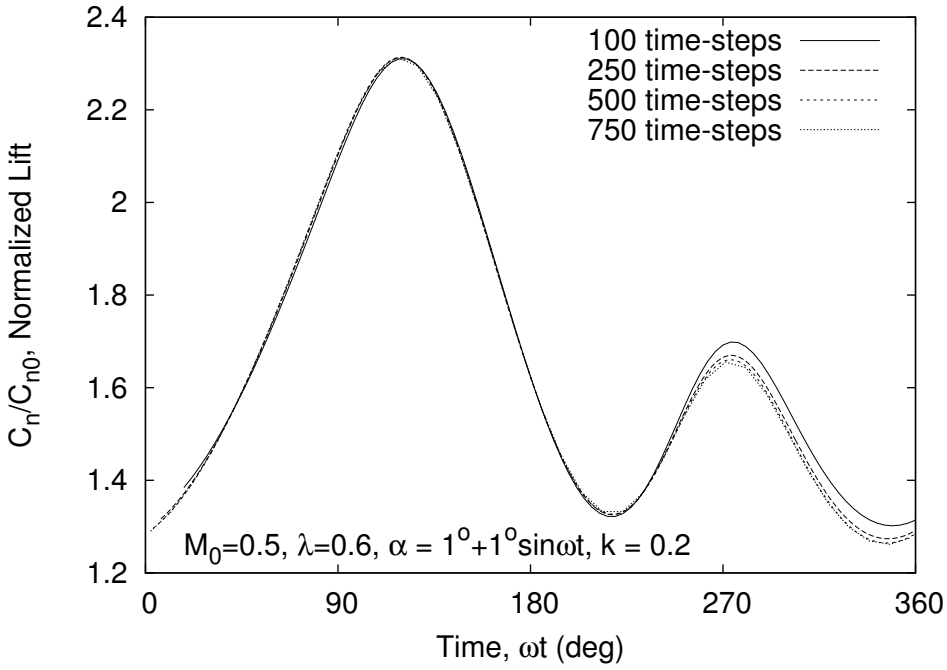

Figure 3.35: Effect of time-step size on indicial lift predictions.

CFD results should be grid-independent. Figure 3.36 compares the lift variation for grid-resolutions of 241×53 with that for 291×53. As seen in the figure the differences are negligible. Figure 3.37 compares the lift variation for grid-resolutions of 241×53 with that for 241×41. Again, the results are very similar, except for some small differences in the low Mach number region.

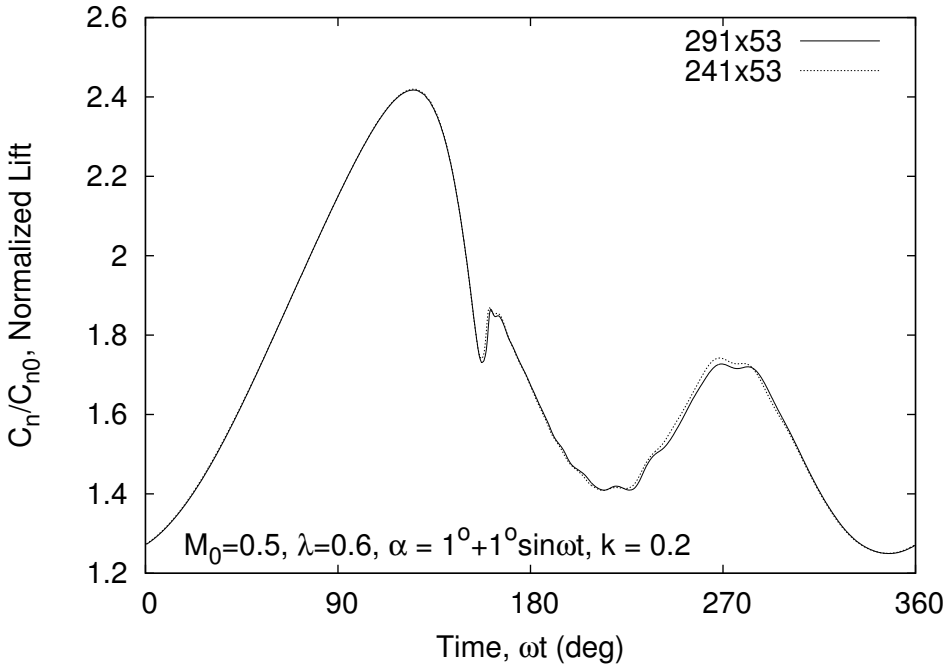

Figure 3.36: Effect of chord-wise grid resolution.

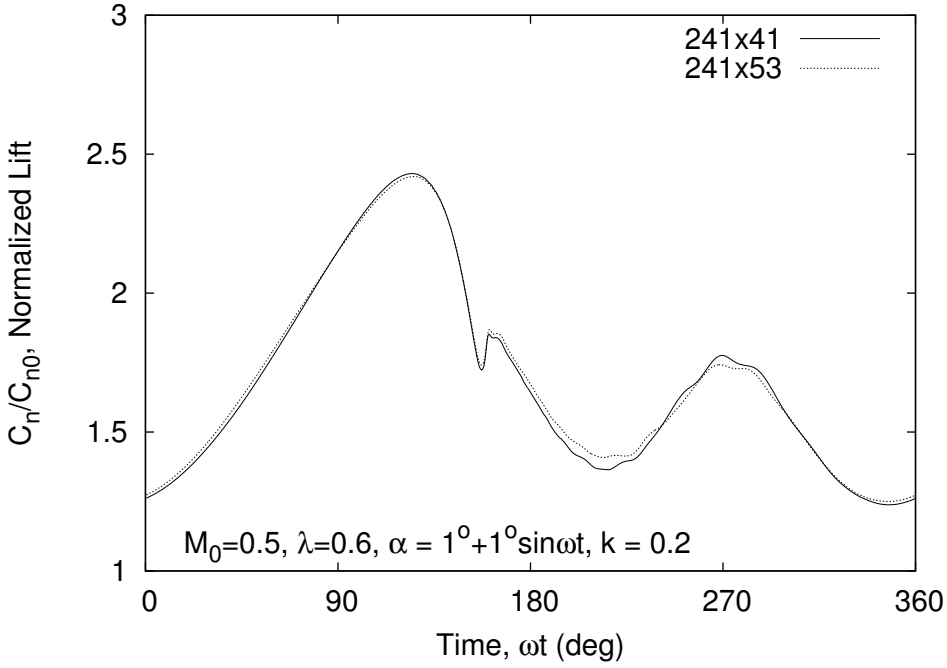

Figure 3.37: Effect of grid resolution normal to the chord.

Chapter 4

Conclusions and Future Work

This thesis has described the development of an indicial based unsteady airfoil theory for compressible flows with a variable free-stream Mach number. The method extends the incompressible indicial method to the treatment of compressible flows with combined pitching and Mach number variations. Overall, the results show that the new compressible indicial model is very effective in predicting the unsteady lift and pitching moment if the Mach numbers involved are below the critical Mach number.

4.1 Conclusions

The following conclusions have been drawn from the study:

1. The incompressible indicial method was found to provide good estimates of airloads if compressibility effects are small ($M < 0.3$). For Mach numbers greater than 0.3, the effects of compressibility on the unsteady airloads becomes increasingly important, and the incompressible method fails to capture these effects.

2. The existing compressible indicial model, while providing better predictions than the incompressible model, gives rise to large amplitude and phase errors for non-steady Mach number variations.

3. The new model provides very good estimates of the unsteady airloads for subcritical

flows. Both the indicial lift and moment predictions show close agreement with CFD results.

4. For supercritical flows, the compressible indicial model does not capture certain nonlinear effects associated with the formation and movement of shock waves over the airfoil surface. While the method does provide a reasonable estimate of the lift coefficient for supercritical flows, further refinement of the model is needed for better estimates of the pitching moment.

5. At higher reduced frequencies ($k > 0.4$), some phase differences were observed between the indicial and CFD results. These may be attributed to the approximations in the modeling of the noncirculatory terms, which are significant at high reduced frequencies.

6. The effect of airfoil thickness on the unsteady airloads was studied for a NACA 0002, NACA 0006, NACA 0012, NACA 00015 and NACA 0020 airfoils. The results show that while the general trends are similar for all the airfoils, some differences arise in the form of : a small offset in the unsteady airloads, which arises because the lift curve slope C_{n_α} and the indicial coefficients are different for different airfoils; and a decrease in the critical Mach number with an increase in airfoil thickness.

7. Three numerical approaches for solving the Duhamel integral are described — a recurrence algorithm, an exact algorithm and a new pseudo-recurrence algorithm. The recurrence algorithm offers nearly five orders of magnitude reduction in computational time over CFD, but gives rise to inaccuracies for varying Mach number

flows. The exact algorithm is computationally more expensive, but provides accurate solutions to the indicial formulation. The new algorithm, which combines the positive features of the exact and the recurrence algorithms, is shown to provide the same degree of accuracy as the exact algorithm at a lower computational cost.

4.2 Future Work

While the new indicial model has been shown to function well for a wide range of flow conditions, it is also seen that the theory has limitations at higher (supercritical) Mach numbers and higher reduced frequencies. The predictive capability of the indicial model can be further enhanced by identifying those elements in the model that give rise to deficiencies and improving upon them. One possible step in this direction lies in the treatment of the lift curve slope C_{n_α} and the indicial coefficients themselves.

From Eq. (2.27) and Eq. (2.44) it is seen that determination of the circulatory response requires an a priori knowledge of the lift curve slope C_{n_α}, and the indicial coefficients A_1, A_2, b_1, and b_2. Until now, a simplified approach has been used, wherein the lift curve slope was assumed to follow the Glauert rule as given by

$$C_{n_\alpha} = \frac{2\pi}{\beta} \tag{4.1}$$

and the indicial coefficients were taken to be constant and independent of Mach number and angle of attack, i.e.,

$$\begin{aligned} A_1 &= 0.3493,\ b_1 = 0.0984 \\ A_2 &= 0.6507,\ b_2 = 0.7759 \end{aligned} \tag{4.2}$$

The results have shown that such approximations are adequate for subcritical flows for a NACA 0006 airfoil. However, this approach is not strictly valid at high subsonic Mach numbers or for thicker airfoils, as will be seen in the following sections.

4.2.1 Lift Curve Slope

The indicial method can be extended to provide a more accurate prediction of the unsteady airloads by using CFD to calculate the lift curve slope at different angles of attack and Mach numbers instead of using the simplified Glauert compressibility rule, which is valid only for thin, symmetric airfoils, i.e.,

$$C_{n_\alpha} = C_{n_\alpha}^{\mathrm{CFD}}(M, \alpha) \tag{4.3}$$

Figures 4.1 and 4.2 show C_n as a function of α and M using CFD and the Glauert compressibility rule. It is seen that at high Mach numbers and angles of attack the differences between CFD and linear theory are not small. Also, it must be borne in mind that for thicker airfoils the lift curve slope cannot be calculated using the Glauert rule even for low and moderately subsonic Mach numbers. This explains the need to use Eq. (4.3) over Eq. (4.1) under these conditions.

4.2.2 Indicial Coefficients

The treatment of the indicial coefficients is another important issue. It is known that the indicial coefficients are functions of Mach number and the angle of attack. Parameswaran & Baeder (Ref. 32) and Singh & Baeder (Ref. 33) have shown how the indicial aerodynamic response coefficients can be obtained from first principles using CFD (see also, Lee

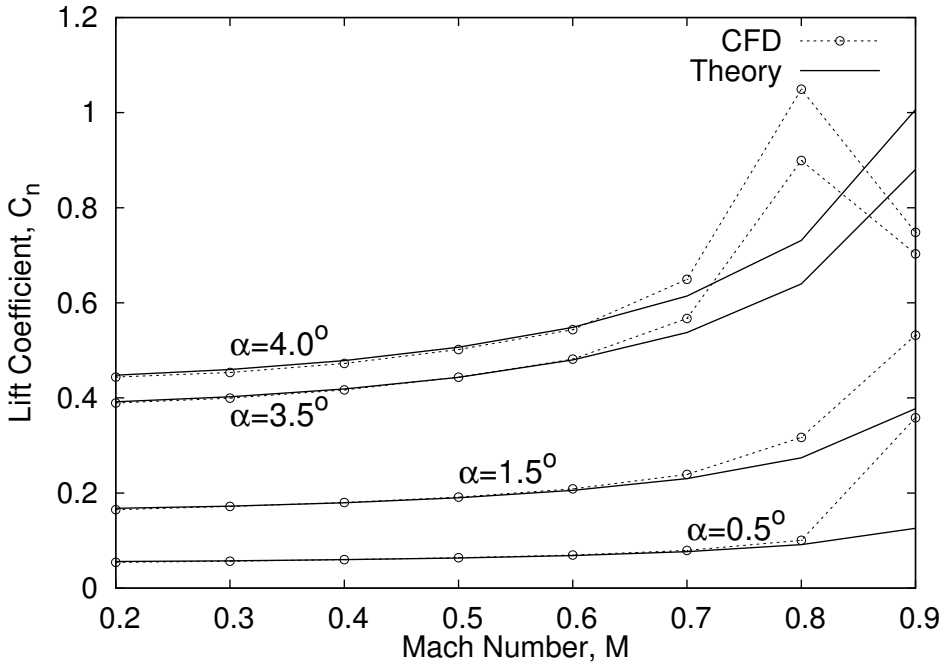

Figure 4.1: C_n vs M for different α using CFD and linear compressible theory.

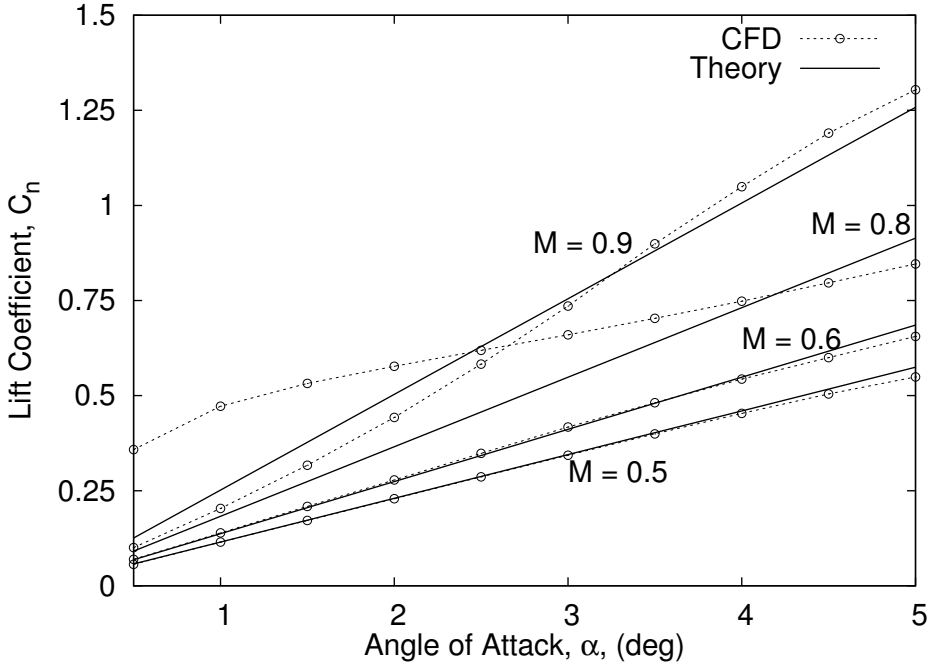

Figure 4.2: C_n vs α for different M using CFD and linear compressible theory.

et al. Ref. 24). Using this method, the indicial coefficients can be obtained for a given Mach number and angle of attack, i.e., now

$$A_1 = A_1(M,\alpha),\ b_1 = b_1(M,\alpha)$$

$$A_2 = A_2(M,\alpha),\ b_2 = b_2(M,\alpha) \tag{4.4}$$

As noted earlier, the indicial response is influenced by both C_{n_α} and the indicial coefficients. For e.g., Eq. (2.27) can be rewritten for a step forcing as

$$C_n^c(t,M) = \frac{1}{V}\left[C_{n_\alpha} w_{3/4}(s=0) + \Delta\left(C_{n_\alpha} w_{3/4}\right)\phi_n^c(s-\sigma,M)\right] \tag{4.5}$$

$$= \frac{1}{V}\left[C_{n_\alpha} w_{3/4}(s=0) + \Delta\left(C_{n_\alpha} w_{3/4}\right)\left(1 - A_1 e^{-b_1\beta^2 s} - e^{-b_2\beta^2 s}\right)\right] \tag{4.6}$$

For a step change in angle of attack, this reduces to

$$C_n^c(t,M) = \frac{1}{V}\left[C_{n_\alpha} V\alpha(s=0) + \Delta\left(C_{n_\alpha} V\alpha\right)\left(1 - A_1 e^{-b_1\beta^2 s} - e^{-b_2\beta^2 s}\right)\right] \tag{4.7}$$

$$= C_{n_\alpha}\alpha_m + C_{n_\alpha}\Delta\alpha\left(1 - A_1 e^{-b_1\beta^2 s} - e^{-b_2\beta^2 s}\right) \tag{4.8}$$

$$= C_n^{qs}(M,\alpha_m) + \Delta C_n^{qs}(1 - A_1 e^{-b_1\beta^2 s} - A_2 e^{-b_2\beta^2 s}) \tag{4.9}$$

where the superscript s denotes the quasi-steady value. Therefore, to study the effect of the indicial coefficients on the indicial response, independent of the effects of C_{n_α}, the CFD and indicial theory results must be suitably normalized (i.e., the contribution of C_{n_α} to the step response needs to be removed through normalization). This can be achieved through the following normalization procedure.

For a step forcing it is known that

$$C_n(t,M) = C_n^{nc}(t,M) + C_n^c(t,M) \tag{4.10}$$

where

$$C_n^{nc}(t,M) = \frac{4\Delta\alpha}{M}\phi_n^c(t,M) \tag{4.11}$$

$$C_n^c(t,M) = C_n^{qs}(M,\alpha_m) + \Delta C_n^{qs}(1 - A_1 e^{-b_1\beta^2 s} - A_2 e^{-b_2\beta^2 s}) \tag{4.12}$$

where the superscript *qs* denotes the quasi-steady value obtained using CFD or linear theory, i.e.,

$$C_n^{qs}(M,\alpha_m) = 2\pi\alpha_m/\beta \quad \text{or} \quad C_n^{\text{CFD}}(M,\alpha_m)$$

$$\Delta C_n^{qs} = 2\pi\Delta\alpha/\beta \quad \text{or} \quad C_n^{\text{CFD}}(M,\alpha_m+\Delta\alpha) - C_n^{\text{CFD}}(M,\alpha_m)$$

Combining Eq. (4.10) and Eq. (4.12) gives

$$C_n(t,M) = C_n^{nc} + C_n^{qs}(M,\alpha_m) + \Delta C_n^{qs}(1 - A_1 e^{-b_1\beta^2 s} - A_2 e^{-b_2\beta^2 s}) \tag{4.13}$$

Transferring $C_n^{qs}(\alpha_m,M)$ to the left-hand side of Eq. (4.13) and dividing throughout by ΔC_n^{qs} gives

$$\frac{C_n(t,M) - C_n^{qs}(\alpha_m,M)}{\Delta C_n^{qs}} = \frac{C_n^{nc}(t,M)}{\Delta C_n^{qs}} + (1 - A_1 e^{-b_1\beta^2 s} - A_2 e^{-b_2\beta^2 s}) \tag{4.14}$$

The first term in Eq. (4.14), which is a result of the noncirculatory part of the response, is a transient term and decays to zero very rapidly. The second term, which is essentially the circulatory indicial response function, $\phi_n^c(s,M)$, is the dominant term and is specified completely using only the indicial coefficients (without any contribution from C_{n_α}). Such a representation makes it easy to study the effect of Mach number on the indicial coefficients without including the effects from the lift curve slope C_{n_α}.

Figures 4.3 and 4.4 show the normalized step response for $M = 0.5$, $\alpha_m = 1^\circ$ and 2°. The results show excellent agreement between the CFD and the indicial model. At

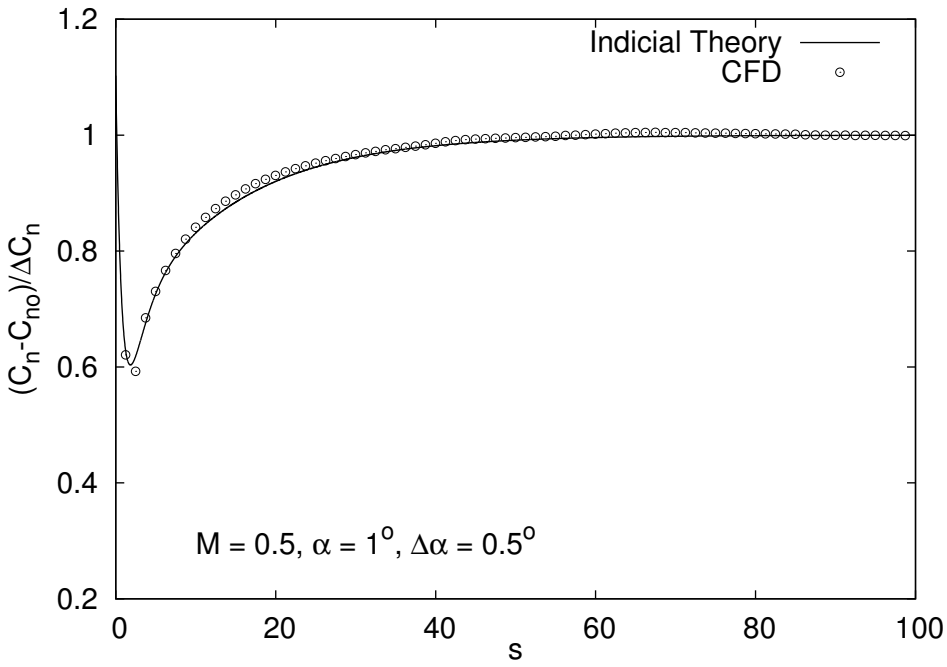

Figure 4.3: Step response for $M = 0.5$, $\alpha_m = 1^\circ$, $\Delta\alpha = 0.5^\circ$ with regular indicial coefficients.

a higher Mach number of 0.8 and $\alpha_m = 1^\circ$ (Fig. 4.5) differences arise between the CFD and indicial results. As α_m is increased to 2°, the differences become more pronounced (see Fig. 4.6). Because the lift predictions for arbitrary forcing are based on the lift response to step inputs, it would be expected that under supercritical conditions the lift predictions would also have some differences. This is confirmed by the results in the previous chapters. One way of improving the lift predictions under these conditions is to modify the indicial coefficients as a function of the Mach number and angle of attack (Notice that this is different from the β^2 scaling in the exponent of the indicial response).

Instead of assuming the indicial coefficients to be constant, as given by Eq. (4.2), they can be treated as functions of the Mach number and AoA (see Lee et al. Ref. 24).

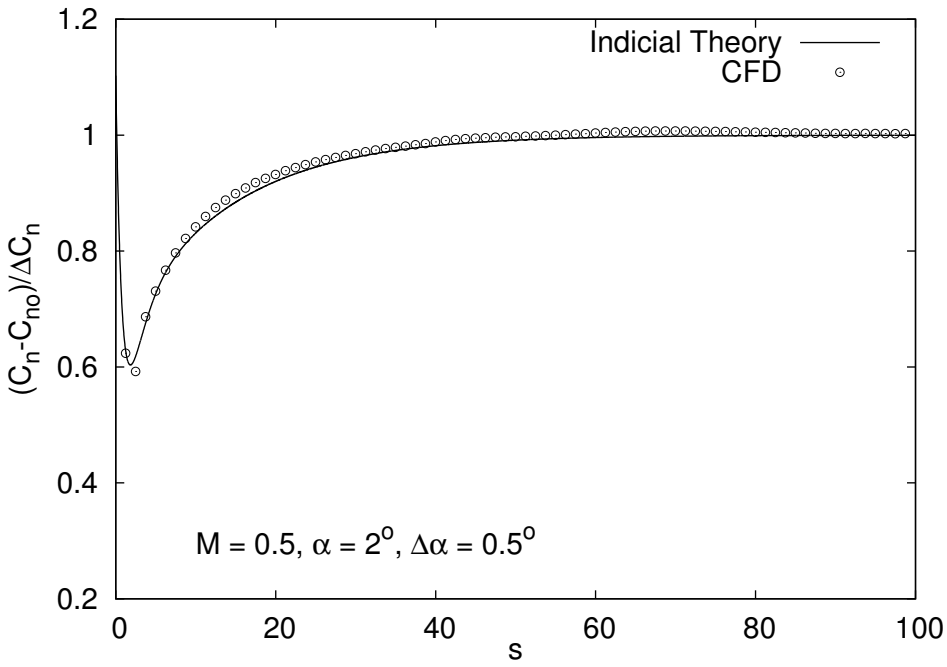

Figure 4.4: Step response for $M = 0.5$, $\alpha_m = 2^\circ$, $\Delta\alpha = 0.5^\circ$ with regular indicial coefficients.

For example, for $M = 0.8$, if the indicial coefficients are modified as

$$A_1 = 0.596,\ b_1 = 0.124$$

$$A_2 = 0.404,\ b_2 = 1.027$$

for $\alpha_m = 1^\circ$, and

$$A_1 = 0.636, \quad b_1 = 0.090,$$

$$A_2 = 0.364, \quad b_2 = 0.554$$

for $\alpha_m = 2^\circ$, then a better agreement between CFD and the indicial results is obtained (Figs. 4.7 and 4.8). From this, it may be concluded that treating the indicial coefficients A_1, A_2, b_1, b_2 as a function of Mach number and AoA could improve the unsteady airloads predictions (especially at high Mach numbers). However, it should be borne in mind that

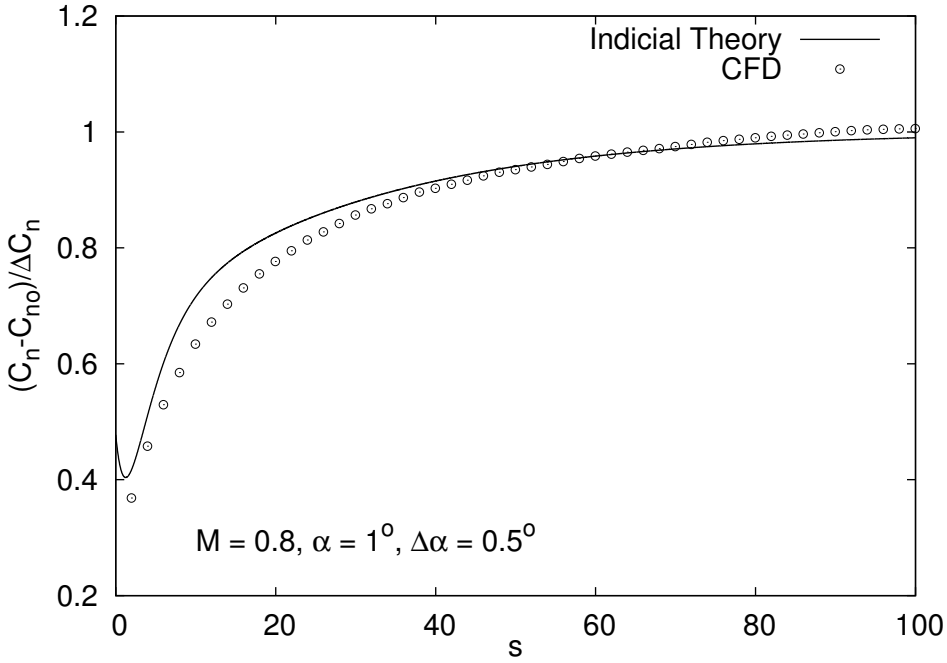

Figure 4.5: Step response for $M = 0.8$, $\alpha_m = 1^\circ$, $\Delta\alpha = 0.5^\circ$ with regular indicial coefficients.

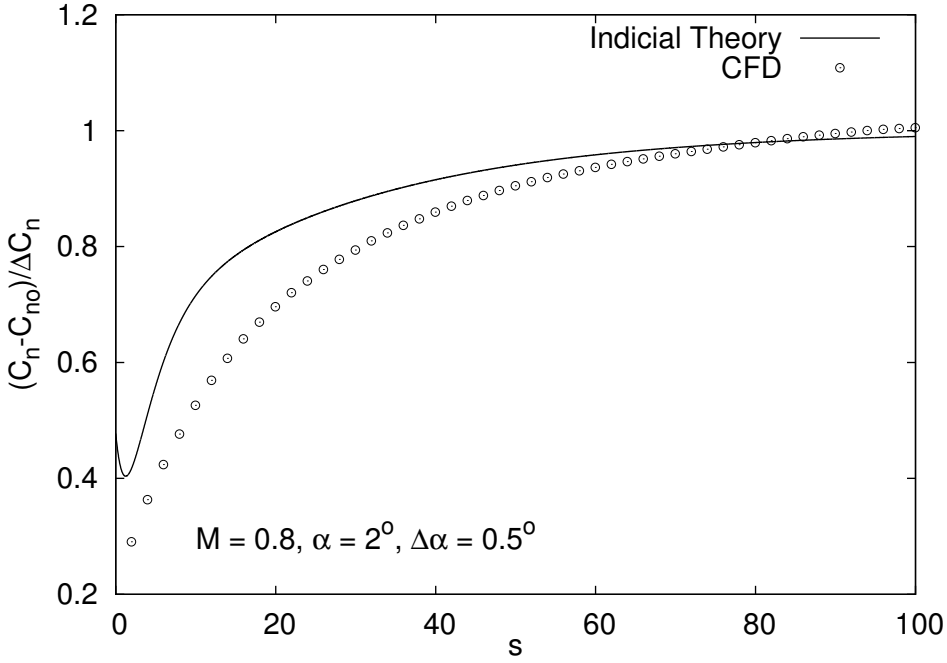

Figure 4.6: Step response for $M = 0.8$, $\alpha_m = 2^\circ$, $\Delta\alpha = 0.5^\circ$ with regular indicial coefficients.

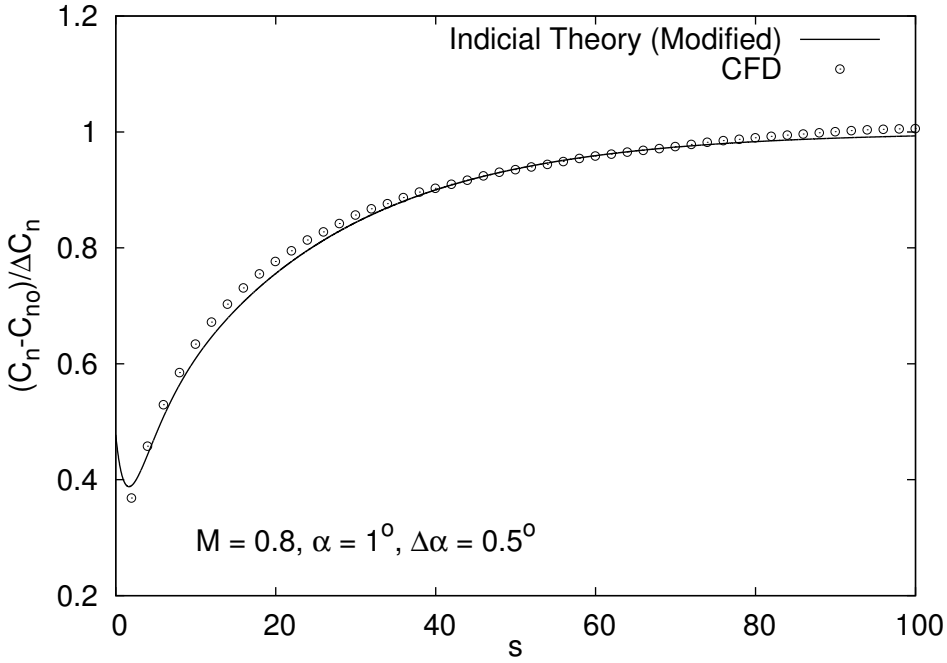

Figure 4.7: Step response for $M = 0.8$, $\alpha_m = 1^\circ$, $\Delta\alpha = 0.5^\circ$ with modified indicial coefficients.

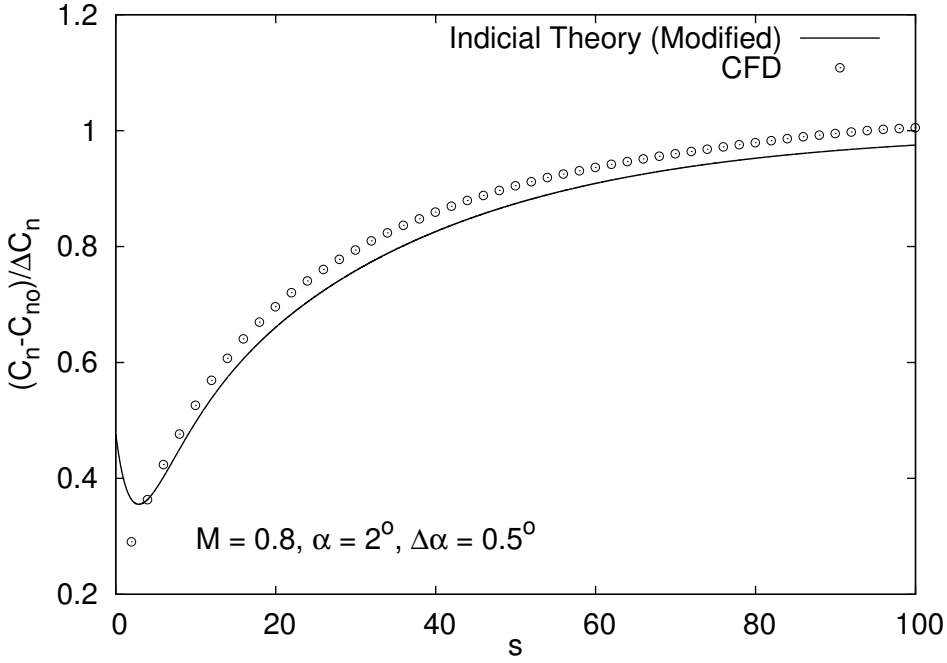

Figure 4.8: Step response for $M = 0.8$, $\alpha_m = 2^\circ$, $\Delta\alpha = 0.5^\circ$ with modified indicial coefficients.

using the modified indicial method based on CFD data involves an additional computational overhead for calculating the lift curve slope and the indicial coefficients at each time step. It also requires a significant prior computational investment to develop a database for C_{n_α} and the indicial coefficients for a wide range of flow conditions. Another drawback with this method is that separate data sets have to be obtained for different airfoils. Thus, while the modified approach has the potential to offer better results, it comes at a higher computational overhead. This cost can be justified depending requirements and constraints placed on the level of analysis in which it is to be used.

It should be remembered that treating the indicial coefficients and lift curve slope as functions of angle of attack and Mach number based on CFD data does not make the scheme non-linear. This is because the indicial responses are still superposed and, therefore, always assumes linearity. Therefore the approach would not be expected to capture strictly nonlinear phenomena. What this approach does do is that by using the CFD responses from a nonlinear regime it offers a better prediction system in this regime even though the method itself is linear.

4.2.3 Enhancements to the Numerical Algorithm

It was shown in Chapter 2 that for flows with time-varying Mach numbers, a modified recurrence algorithm needs to be used. It was seen that this involves a proper choice of the parameter m, which determines the number of time-steps that need to calculated exactly. It was seen that the optimum choice of m depends on the Mach number regime (M_0), as well as the amplitude of Mach number oscillations (λ). The higher the values of M_0 and λ, the higher the value of m for a given error tolerance.

As noted in Table 1.1, the value of M_0 and λ is different at different radial locations of the rotor. Therefore inorder to compute the airloads efficiently, it would be necessary to use different values of m at different radial locations. Towards this end it would be useful to examine several issues such as:

- Study the error behavior of the modified recurrence algorithm and develop ways to estimate it based on the flow conditions and the numerical solution parameters.
- Develop ways to to obtain the optimum value of m for a given blade section based on some error criteria.
- Investigate ways to dynamically change the value of m at a particular blade section based on the flow conditions while also keeping track of the errors involved in the airloads prediction.

It would also be useful to extend the numerical algorithm to make it second and third order accurate because this would allow an increase in time-step size and thereby reduce the computational time. This could prove particularly beneficial for the exact/modified algorithm because its computational time is inversely proportional to the square of the time-step size.

Appendix

Calculation of Indicial Coefficients

The compressible indicial response to a step change in forcing is obtained from CFD and represented in functional form as a two-term exponential series. The parameters used to specify the indicial response function are known as indicial coefficients. Because the accuracy of the indicial prediction system is based on the accuracy of the indicial response function, extraction of the indicial coefficients used to specify the indicial response function from CFD results is extremely important. This appendix briefly describes the procedure involved in extracting the indicial coefficients from CFD data (see Ref. 1 and Ref. 24).

In the earlier chapters it was shown how the indicial response to a step change in forcing (say angle of attack) is modeled as consisting of a circulatory and noncirculatory components, i.e.,

$$C_n(t,M) = C_n^c(t,M) + C_n^{nc}(t,M) \tag{A.1}$$

The circulatory and noncirculatory parts are functionally represented as

$$\begin{aligned} C_n^c(t,M) &= C_{n_\alpha}\Delta\alpha\,\phi_n^c(s,M) && \text{(A.2)}\\ &= C_{n_\alpha}\Delta\alpha\left(1 - A_1\exp(-b_1\beta^2 s) - A_1\exp(-b_1\beta^2 s)\right) && \text{(A.3)}\\ C_n^{nc}(t,M) &= \frac{4\Delta\alpha}{M}\phi_{n_\alpha}^{nc}(s,M) && \text{(A.4)}\\ C_n^{nc}(t,M) &= \frac{4\Delta\alpha}{M}\exp\left(\frac{-s}{T_{n_\alpha}}\right) && \text{(A.5)} \end{aligned}$$

where,

$$T_{n_\alpha} = \frac{4Mk_\alpha}{2(1-M) + 2\pi M^2 \beta (A_1 b_1 + A_2 b_2)} \tag{A.6}$$

From the above equations, we note that once the indicial coefficients A_1, A_2, b_1 and b_2 are known, the circulatory and noncirculatory lift responses are completely specified. Notice that T_{n_α} is itself a function of the aforementioned coefficients, and need not be calculated separately. To obtain the values of the indicial coefficients, an optimization algorithm is used by treating the CFD results as the "exact" solution. A 4-element vector can be defined that consists of the indicial coefficients, i.e.,

$$\mathbf{x}^T = (A_1, A_2, b_1, b_2) \tag{A.7}$$

The vector in Eq. (A.7) must be chosen to minimize the difference between the functional approximation to the indicial response, $C_n(t)_{\text{ind}}$, and the CFD results, $C_n(t)_{\text{CFD}}$. To do this, an objective function $J(\mathbf{x})$ can be defined in terms of a residual sum of squares as

$$J(\mathbf{x}) = \sum_{m=1}^{N} \left(C_n(t_m)_{\text{ind}} - C_n(t_m)_{\text{CFD}}\right)^2 \tag{A.8}$$

where N is the number of discrete points at which the CFD result is known. The determination of the indicial coefficients then becomes a nonlinear programming problem of minimizing $J(\mathbf{x})$ in the parameter space $\mathbf{x}$ subject to the constraints

$$A_1, A_2, b_1, b_2 > 0 \tag{A.9}$$

and the equality constraint

$$\sum_{n=1}^{N} A_n = 1 \tag{A.10}$$

It is advisable to calculate the indicial coefficients based on the CFD data for a Mach number that is sufficiently below the critical Mach number (say 0.5). This is done so as to

ensure the absence of any nonlinear phenomena such as shock waves. After the indicial coefficients are obtained at a particular subsonic Mach number, the indicial response for all other subcritical Mach numbers can be obtained by using the scaling factor β^2 as seen in Eq. (A.3).

BIBLIOGRAPHY

[1] Leishman, J. G., *Principles of Helicopter Aerodynamics,* Cambridge University Press, New York, 2000, Chapter 10.

[2] Bisplinghoff, R. L., Ashley H., and Halfman, R. L., *Aeroelasticity*, Addison-Wesley, 1955.

[3] Beddoes, T. S., "Practical Computation of Unsteady Lift," *Vertica*, Vol. 8, No. 1, 1984, pp. 55–71.

[4] Leishman, J. G., "Validation of Approximate Indicial Aerodynamic Functions for Two-Dimensional Subsonic Flow," *Journal of Aircraft*, Vol. 25, No. 10, 1987, pp. 914–922.

[5] Leishman, J. G., and Nugyen, K. Q., "A State-Space Representation of Unsteady Aerodynamic Behavior," *AIAA Journal*, Vol. 28, No. 5, May 1990, pp. 836–845.

[6] Leishman, J. G., "Indicial Lift Approximations for Two–Dimensional Subsonic Flow as Obtained from Oscillatory Measurements," *Journal of Aircraft*, Vol. 30, No. 3, 1993, pp. 340–351.

[7] Wagner, H., "Über die Entstehung des dynamischen Auftriebs von Tragflügeln," *Zeitschrift für angewandte Mathematik und Mechanik*, Band 5, 1925, pp. 17–35.

[8] Küssner, H. G., "Zusammenfassender Bericht über den instationären Auftreib von Flügeln," *Luftfahrtforschung,* Vol. 13 No. 3, pp. 914—922.

[9] von Kármán, Th., and Sears, W. R., “Airfoil Theory for Non-Uniform Motion,” *Journal of the Aeronautical Sciences*, Vol. 5, No. 10, Aug. 1938, pp. 379–390,

[10] Sears, W. R., “Operational Methods in the Theory of Airfoils in Nonuniform Motion,” *Journal of the Franklin Institute*, Vol. 230, July 1940, pp. 95–111.

[11] Theodorsen, T., “General Theory of Aerodynamic Instability and Mechanism of Flutter,” *NACA Report 496*, 1935, pp. 413–433.

[12] Greenberg, J. M., “Airfoil in Sinusoidal Motion in a Pulsating Stream,” NACA TN No. 1326, 1946

[13] Kottapalli, S. B. R., “Drag on an Oscillating Airfoil in Fluctuating Free Stream,” Ph.D. Thesis, Georgia Institute of Technology, 1977.

[14] Isaacs, R. , “Airfoil Theory for Flows of Variable Velocity,” *Journal Aeronautical Sciences*, Vol. 12, No. 1, 1945, pp. 113–117.

[15] van der Wall, B. and Leishman, J. G., “On the Influence of Time-Varying Flow Velocity on Unsteady Aerodynamics,” *Journal of the American Helicopter Society*, Vol. 39, No. 4, October 1994, pp. 25–36.

[16] Mazelsky, B., “Determination of Indicial Lift and Moment of a Two-Dimensional Pitching Airfoil at Subsonic Mach Numbers from Oscillatory Coefficients with Numerical Calculations for a Mach Number of 0.7,” NACA TN2613, 1952

[17] Mazelsky, B. and Drischler, J. A., “Numerical Determination of Indicial Lift and Moment Functions of a Two-Dimensional Sinking and Pitching Airfoil at Mach Numbers 0.5 and 0.6,” NACA TN2739, 1952

[18] Mazelsky, B., “On the Noncirculatory Flow about a Two-Dimensional Airfoil at Subsonic Speeds,” *Journal of the Aeronautical Sciences*, Vol. 19, No. 12, pp. 848—849, 1952.

[19] Tyler, J. C., and Leishman, J. G., “An Analysis of Pitch and Plunge Effects on Unsteady Airfoil Behavior,” *Journal of the American Helicopter Society*, Vol. 37, No. 3, July 1992, pp. 69–82.

[20] Leishman, J. G., “Unsteady Lift of an Airfoil with a Trailing-Edge Flap Based on Indicial Concepts,” *Journal of Aircraft*, Vol. 31, No, 2, March-April, 1994, pp. 288–297.

[21] Hariharan, N., and Leishman, J. G., “Unsteady Aerodynamics of a Flapped Airfoil in Subsonic Flow by Indicial Concepts,” *Journal of Aircraft*, Vol. 33, No. 5, Sept./Oct. 1996, pp. 855–868.

[22] Leishman, J. G., “Subsonic Unsteady Aerodynamics Caused by Gusts and Vortices Using the Indicial Method,” *Journal of Aircraft*, Vol. 33, No. 5, Sept./Oct. 1996, pp. 869–879.

[23] Leishman, J. G., “Unsteady Aerodynamics of Airfoils Encountering Traveling Gusts and Vortices,” *Journal of Aircraft*, Vol. 34, No. 6, Nov.-Dec. 1997, pp. 719–729.

[24] Lee, D., Leishman, J. G., and Baeder, J. D., “A Nonlinear Indicial Method For the Calculation of Unsteady Airloads,” 59th *Forum of the American Helicopter Society*, Phoenix, Arizona, May, 2003.

[25] Srinivasan, G. R., Baeder, J. D., Obayashi, S., and McCroskey., W. J., “Flowfield of a Lifting Rotor in Hover: A Navier-Stokes Simulation,” *AIAA Journal*, Vol. 30, No. 10, Oct. 1992, pp. 2371–2378.

[26] Sitaraman, J., Baeder, J. D., and Iyengar, I.S., “On the Field Velocity Approach and Geometric Conservation Law for Unsteady Flow Simulations,” Paper No. 2003-3835, 16th *AIAA Computational Fluid Dynamics Conference*, Orlando, Florida, June 2003

[27] Jones, R. T., “Operational Treatment of the Non-Uniform Lift Theory in Airplane Dynamics,” NACA Technical Note 667, 1938.

[28] Jones, R. T., “The Unsteady Lift of a Wing of Finite Aspect Ratio,” NACA Report 681, 1940.

[29] Lomax, H., “Indicial Aerodynamics,” *AGARD Manual of Aeroelasticity*, Part II, Chapter 6, 1968.

[30] Lomax, H., Heaslet, M. A., Fuller, F. B., and Sluder, L., “Two and Three Dimensional Unsteady Lift Problems in High Speed Flight,” NACA Report 1077, 1952.

[31] Riegels, F. W., *Aerofoil Sections — Results from Wind-Tunnel Investigations and Theoretical Foundations*, Butterworths, London, 1961

[32] Parameswaran, V., and Baeder, J. D., “Indicial Aerodynamics in Compressible Flow – Direct Calculations,” *Journal of Aircraft*, Vol. 34, No. 1, 1997, pp. 131–133.

[33] Singh, R., and Baeder, J. D., “The Direct Calculation of Indicial Lift Response of a Wing Using Computational Fluid Dynamics,” *Journal of Aircraft*, Vol. 35, No. 4, 1997, pp. 465–471.

[34] Baldwin, B. S., and Lomax, H., “Thin-Layer Approximation and Algebraic Model for Separated Turbulent Flows,” AIAA Paper 78-257, Jan. 1978.